POMA – A Zonal Model for Airflow and Temperature Distribution Analysis

Yi Lin

A Thesis

in

The Department

of

Building, Civil and Environmental Engineering

Presented in Partial Fulfillment of the Requirements for the Degree of Master of Applied Science at Concordia University
Montreal, Quebec, Canada

June 1999

0-612-43649-7

ABSTRACT

POMA – A Zonal Model for Airflow and Temperature Distribution Analysis

Yi Lin

A zonal model is a new kind of numerical model to simulate the airflow and temperature distribution within a room by means of personal computers. It is an intermediate model between multizone and Computational Fluid Dynamics (CFD) model. Compared to multizone models, zonal models can provide engineers with an estimated view of airflow and temperature distribution within a room, which cannot be predicted by multizone models. Zonal models have advantages over CFD models in their simple use. time-saving characteristics and satisfactory precision.

In this thesis, a thorough review of zonal models is presented. Based on the review work. the development of a new zonal model, **P**ressurized z**O**nal **M**odel with **A**ir diffusers (**POMA**), for the analysis of airflow and temperature distribution within a room was proposed. POMA model overcomes some limitations of the previous zonal models.

There are two kinds of ventilation situations, i.e. natural and forced ventilation, which POMA can handle. In the forced ventilation, to specify the supply airflow conditions, a new method which takes advantage of the existing diffuser characteristic equations was proposed. This method is proven to be applicable.

POMA was applied to four case studies in two kinds of ventilation strategies, i.e. natural ventilation and forced ventilation. POMA's predictions were then compared with measurements and/or Computational Fluid Dynamics (CFD) model predictions. A good agreement between the predictions of POMA and CFD model and/or measurement results demonstrates POMA is a practical tool for the analysis of airflow and temperature distribution within a room.

ACKNOWLEDGMENT

I would like to express my greatest gratitude to my supervisor, Dr. F. Haghighat, for his continued guidance, financial support, encouragement and patience through all the phases of this research.

Extended thanks go to Dr. A.C. Megri, for his lively and fruitful discussions regarding this research.

My debt to Dr. Zheng Jiang is difficult to express. Thanks to her for providing the CFD results and for her endless advice and constant encouragement, not only in my work and study, but also in my life. Without her generous help this report would not be the same.

My sincere appreciation to Dr. Yan Huo for his valuable discussions and suggestions regarding CFD and computer problems.

My friends and colleagues from around the world that I met here in Montreal, and those in Hainan and Beijing, thank you for your love and help.

Finally, but certainly not least, my deepest appreciation to my family, and especially to my mother and brother, who have been so supportive and loving.

Table of Content

List of Figures

List of Tables

Nomenclature

A area of boundary, (m^2)

A_0 effective area of diffuser, $A_0=C_d*A_c$, (m^2)

C_d discharge coefficient, set to 0.8 based on experiments

Cp Specific heat of air, (1005 W/kg K)

F_i function i,

F entire vector of functions Fi.

h convective heat transfer coefficient, (W/m^2K)

H_0 width of jet at outlet or at vena contracta, (m)

J Jacobian matrix,

K coefficient of power law, usually taken as 0.83, ($m/s\ Pa^n$)

K_I centerline velocity constant depending on outlet type and discharge pattern,

L depth of the zone, (m)

n flow exponent, usually taken as 0.5,

m airflow rate across horizontal boundary, (kg/s)

m_{0-H}^{normal} mass flow rate modeled as that across normal boundary, (kg/s)

m_{0-Zn} mass flow rate from 0 to Z_n on vertical boundary, (kg/s)

m_{Zn-H} mass flow rate from Z_n to H on vertical boundary, (kg/s)

m_{ij} rate of mass flow from zone i to zone j, (kg/s)

m_{source} rate of mass supplied by source in zone, (kg/s)

m_{si} mass source in zone I, (kg/s)

m_{sink} rate of mass removed from zone, (kg/s)

M_i mass in zone i, (kg)

P pressure, (Pa)

ΔP pressure difference, (Pa)

P_0 pressure in zone 0, (Pa)

P_1 pressure in zone 1, (Pa)

P_{middle} pressure at the middle point of zone (Pa)

P_{ref} reference pressure, (Pa)

q heat flow rate, (W)

q_{ij} rate of heat energy from zone i to zone j, (W)

q_{source} rate of heat energy supplied by the source in zone, (W)

q_{sink} rate of heat energy removed from zone. (W)

Q_i heat energy in zone i, (J)

r radial distance of point under consideration from centerline of jet, (m)

$r_{0.5}$ radial distance in same cross-sectional plane from axis to the point where velocity is one-half centerline velocity, i.e. $V=0.5V_x$, (m)

R gas constant for air, (287.055 J/kg K)

t time variable, (s)

T temperature of zone (K)

$\Delta T_{wall\text{-}zone}$ temperature difference between wall surface and zone, (K)

$\Delta T_{zone\text{-}zone}$ temperature difference between two adjacent zones, (K)

V velocity across the boundary at the certain distance r, (m/s)

Vol volume flow rate, (m^3/s)

V_x centerline velocity, (m/s)

V_0 average initial velocity at discharge, (m/s)

V_x centerline velocity in the same cross-sectional plane, (m/s)

X distance to the diffuser face on the jet centerline, (m)

x_i unknown factors,

$\mathbf{X}$ entire vector of values x_i

ρ_{zone} air density of the zone, (kg/m^3)

ρ_{flow} air density of the zone from which the air flows in, (kg/m^3)

$\rho_{0\text{-}Zn}$ density of airflow from 0 to Z_n, (kg/m^3)

$\rho_{Zn\text{-}H}$ density of airflow from Z_n to H, (kg/m^3)

λ convergence step in Newton-Raphson,

ε sign of flow direction, of which absolute value is 1,

Chapter 1

Introduction and Literature Review

1.1 Introduction to Airflow and Temperature Distribution

Nowadays, many people working in the office or in a commercial building often complain about the poor air climate conditions. Too high or too low temperatures always cause the occupants to feel uncomfortable. Sometimes even in the same building or in the same office, occupants feel differently depending on their locations. These problems are usually caused by poor airflow and temperature distribution within buildings.

Airflow and thermal distribution within buildings has attracted international attention. either at a research level or industry level. There are several international conferences regarding this issue, such as the Air Infiltration and Ventilation Center (AIVC) conference, the International Conference on Air Distribution in Rooms (ROOMVENT). In 1992, experts from twelve countries have worked together on a project entitled "Airflow Patterns within Buildings (Annex 20)" under the auspice of the International Energy Agency (IEA) to evaluate the performance of airflow models and to establish their viability as design tools. The legal text (IEA, 1989), which defines Annex 20's objectives, tasks and responsibilities, states:

> "Research attention has recently been given to the patterns of air circulation within rooms and through buildings, to ensure that fresh air supply and pollutant removal requirements are effectively obtained without undue use of energy resources".

From the text above, it is obvious that the airflow and temperature distribution within buildings is very important. It is necessary to accurately predict the airflow and thermal distribution. This will aid engineers to design, diagnose and analyze ventilation systems of buildings.

As stated by many researchers, predicting and assessing the airflow and temperature distribution can be achieved by two main methods: experimental investigation and numerical prediction (Huo, 1997) (Moser, 1991) (Nielsen, 1989). Both of these two methods have their disadvantages and advantages.

The full-scale or model experiments usually can provide measurement data of very high quality. But they are expensive and time consuming. The cost of a single experiment is in the range from US$3,000 to US$20,000 (Nielsen, 1989). More expensive full-scale experiments may involve actual decorating, furnishing and interior fittings so that the owner, architect and consultants can experience the environments at a very early stage.

Furthermore, it is difficult to get the information on the sensitivity of parameters in experimental investigations.

As discussed by Nielsen, there was a trend of using numerical models to simulate the airflow using computers in recent years. due to the quick development of computer technology (Nielsen, 1989).

In 1991, Moser stated some of the benefits of numerical simulation, which are listed in the following (Moser, 1991).

- Information is available in all points of the flow field (on computational grid).
- Any desired variable of the physical model can be output and plotted: Air velocity and its fluctuations, temperature, concentrations of contaminants and humidity, etc.
- Sensitivity tests and parameter variations are easy to do, and computed trends should be even more reliable than absolute values of variables.

In conclusion, computer modeling and simulation is one of the most powerful tools currently available to analyze the indoor air pattern.

Generally, two kinds of numerical models are used extensively to simulate airflow and thermal distribution within buildings, i.e. the multizone model and the Computational Fluid Dynamics (CFD) model.

1.2 Review of MultiZone Models

The multizone model is a simplified model. It is a common tool for calculating air and contaminant exchange between rooms of a building and between building and outdoors. One of the first multizone models developed was the BSRIA-model LEAK which was published in 1970 by Jackman (Feustel, 1998). There are a lot of papers describing multizone airflow models, such as Jackman (1970), Herrlin (1987), Feustel and Smith (1989), Walton (1989) and Megri (1993). A survey and comparison of nine multizone models was carried out by Haghighat in 1989 (Haghighat, 1989). In 1992, Feustel reported 50 different programs in his extensive survey of multizone airflow models (Feustel and Dieris, 1992).

In multizone airflow models, a network approach is applied. This approach takes a room within a building as one zone that is connected to others by openings between rooms and openings to outside. Uniform and instant mixing is assumed for each zone so that there are homogeneous pressure, temperature and contaminant concentrations in each zone (Haghighat, 1989). The connections, i.e. the flow paths between rooms, are described by functional relationships between mass flow and pressure difference. A system of algebraic equations derived from contaminant mass balance in each zone is then set up. The solution of these equations leads to the explicit data of pressure. mass flow rate and concentrations of contaminants, etc, in each zone. Temperature is used as a known input for the calculation of the mass flow between two zones (Schalin, 1992).

The multizone model has the advantage of user friendliness in terms of problem definition, straightforward internal representation and calculation procedure. It is easy to use and has a low computation cost. The advantage of multizone model is that it allows the prediction of bulk flows through the whole building as caused by wind, temperature differences, and/or mechanical systems. However, it does not provide detailed information about temperature and airflow distribution within a room due to its simplified approach.

In practice, the temperature, contaminant concentration and other parameters may vary in the space. A detailed knowledge of indoor environmental parameters is important in many cases such as the temperature and contaminant concentration which vary largely due to a local pollutant source or heat source in the room. As discussed above, the main limitation of a multizone model is its capability to provide this kind of detailed knowledge. Normally, such detailed knowledge can be obtained by means of the CFD model.

1.3 Review of Computational Fluid Dynamics (CFD) models

CFD can provide users with the detailed knowledge of airflow pattern, temperature and contaminant distributions within a room. This method has been highly recognized in air movement analysis (Huo, 1997). Nielsen has shown that the predictions of CFD models agree with the measurements in the simulation of rooms with different ventilation systems, i.e. mixing ventilation in small rooms, displacement ventilation, and air movement in large areas. The CFD model was also demonstrated to be a potential tool to predict and model time dependent distribution in enclosed spaces (Nielsen, 1989).

In a CFD approach to predict the airflow pattern in a single room, the room is divided into a large number of cells (typically about 10,000) (Schalin, 1992). For each cell transport equations for mass, momentum, energy, turbulence quantities and concentrations of contaminants are solved. Variables solved for this application are pressure, air velocity, temperature and contaminant concentrations.

Despite the richness of the results in terms of detailed information regarding the flow and temperature field within a room, CFD suffers from the huge user effort in terms of problem definitions and computation efforts. Users of CFD have to exert a great effort in defining the boundary conditions. It is too complicated to be used by non-specialists. CFD software nowadays, including the very good commercial software, is relatively difficult to use. It regularly takes about half a year for the user to feel comfortable with the software (Chen and Jiang, 1992).

As widely known, the running of a CFD simulation could be very time consuming (Huo, 1997). It will take many hours, up to days to do a simulation of a room. The computer resources required for running a CFD is really critical. The computers are supposed to have large memory space and advanced CPU with high capabilities. Usually a powerful workstation is required for the implementation of CFD.

Furthermore, CFD software is very expensive. It is too expensive for the users to buy the whole software. Usually users of CFD will only pay for the license of the software for a certain period of time, such as one or two years.

In 1995, Rodriguez and Allard pointed out three reasons for the impracticability of including CFD in detailed building simulation codes (Rodriguez and Allard, 1995):

- CFD models are stand-alone packages which are extremely difficult to be integrated within the time scheme of detailed building thermal models.
- They are too time-consuming.
- The user of detailed building simulation programs is not usually interested in the excessively discretized results that can be obtained from a CFD.

Due to the inherent shortcomings of CFD, it is difficult to practically integrate CFD model within general building simulation. Some researchers have tried to integrate CFD into multizone models but the results were not satisfactory. For instance, in 1989, Nielsen presented a new method for linking CFD detailed airflow pattern results with a multizone model. Though the results were good, this method was only suited for applications to cases in which detailed air knowledge in a few rooms or only one specific room is required (Nielsen, 1989).

1.4 Review of Zonal Models

1.4.1 Development of Zonal Models

Satisfying the ever-increasing demand of evaluating local thermal comfort and indoor air quality in various zones of a building gives rise to a need of an intermediate approach between CFD and multizone models. The intermediate approach is expected to have the capabilities of providing the detailed knowledge of airflow and temperature distribution within a room with satisfying precision. Moreover, it should be a simplified model. Thus it can be easy to use and will not suffer from the high computation cost of CFD models, with the compensations of tolerable errors.

The zonal model is developed to meet these requirements of the intermediate approach. It is a simplified model which can provide some global indications of temperature and velocity profiles, it is relatively easy for the user to define the problem, and is easily incorporated into building design software.

In 1992, Allard and Inard carried out a thorough survey and evaluation of currently available zonal models. The pioneer works were presented and discussed extensively. The review pointed out the usefulness of zonal model in order to get a quick estimate of the nonisothermal behavior of a room with heating or ventilation systems. Furthermore, the existing comparisons with CFD or real-scale experiments show that the zonal models are able to predict, with reasonable accuracy, airflow rates and heat transfers within a room.

The term, "zonal model", was first proposed by Lebrun in his Ph.D thesis in 1970 (Allard and Inard, 1992). Since the idea of zonal models is so new and promising, various research teams continue to develop this kind of model under the generic name of zonal model (Allard and Inard, 1992). Among those pioneers, (Allard and Inard, 1992), (Howarth, 1980), (Inard, Bouia and Dalicieux, 1996), (Laret, 1980), (Wurtz, 1995) and (Togari et al, 1993) have made contributions to this area.

1.4.2 General Structure of Zonal Models

In a zonal model, a room is divided into a number of n well-mixed isothermal macroscopic zones in which parameters such as temperature and contaminant concentrations are assumed to be uniform. There are interzonal mass and thermal flows between zones. The air in the room is assumed to be inviscid. In each zone, the principle of mass and energy conservation must be obeyed. They can be written as:

$$\frac{dM_i}{dt} = \sum_{j=1}^{n} m_{ij} + m_{source} + m_{\sin k} \quad (1\text{-}1)$$

$$\frac{dQ_i}{dt} = \sum_{j=1}^{n} q_{ij} + q_{source} + q_{\sin k} \quad (1\text{-}2)$$

Where,

M_i : mass in zone i, (kg)

m_{ij} : rate of mass flow from zone i to zone j, (kg/s)

m_{source} : rate of mass supplied by the source in zone, (kg/s)

m_{sink} : rate of mass removed from zone, (kg/s)

Q_i : energy in zone i, (J)

q_{ij} : rate of energy transfer from zone i to zone j, (W)

q_{source} : rate of energy supplied by the source in zone, (W)

q_{sink} : rate of energy removed from zone, (W)

t : time variable, (s)

Compared to CFD models, zonal models have the same principle of modeling but are simplified in two aspects:

- The grid in zonal models is not as dense as that in CFD. Usually, there are only limited number of macroscopic zones in zonal models, such as $6\times1\times10$ zones (Inard et al, 1996).
- Turbulence is not taken into account.
- Momentum conservation is implicitly taken into account, for example in Power law. However, in some zonal models, momentum conservation is not taken into account.

The accuracy errors caused by these simplifications could be compensated by the low computational costs and simplicity of being used, as long as the zonal model could provide a satisfying prediction of the global view of the indoor pattern.

1.4.3 Review of Existing Zonal Models

I. Laret's Analytical Model

This model was a steady-state model developed by Laret (1980) to predict the temperature stratification in a room with a convective heating system located at the lower corner of the room. The room is divided into 4 zones, the ceiling, the floor, the central zone, and the plume, as shown in Figure 1.1. Energy and mass balance equations for each zone were set up. Assuming the mass flow variation is independent of the altitude within the plume, Laret proceeded with the integration of this set of equations, which gave the mean temperature of each zone and consequently the thermal stratification in the room. (Allard and Inard, 1992)

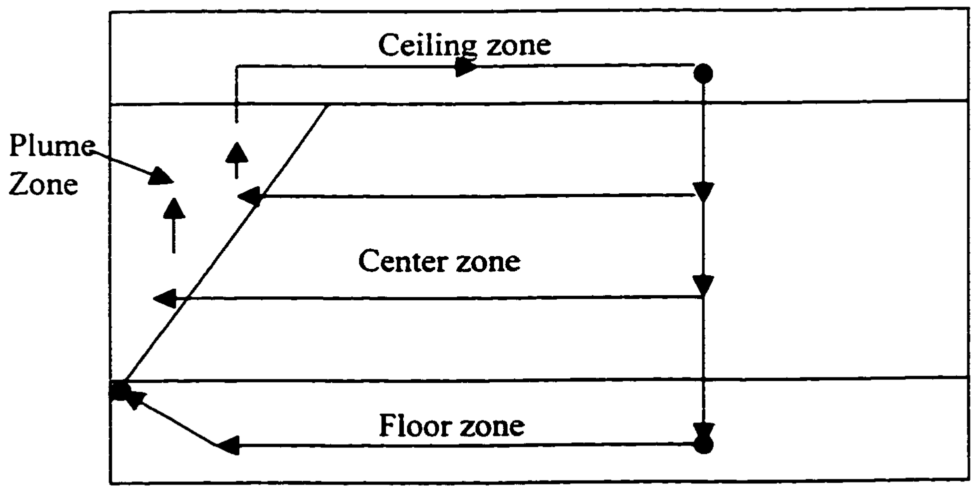

Figure 1.1 Configuration of a Analytical Model

II. Howarth's Two Zone Model

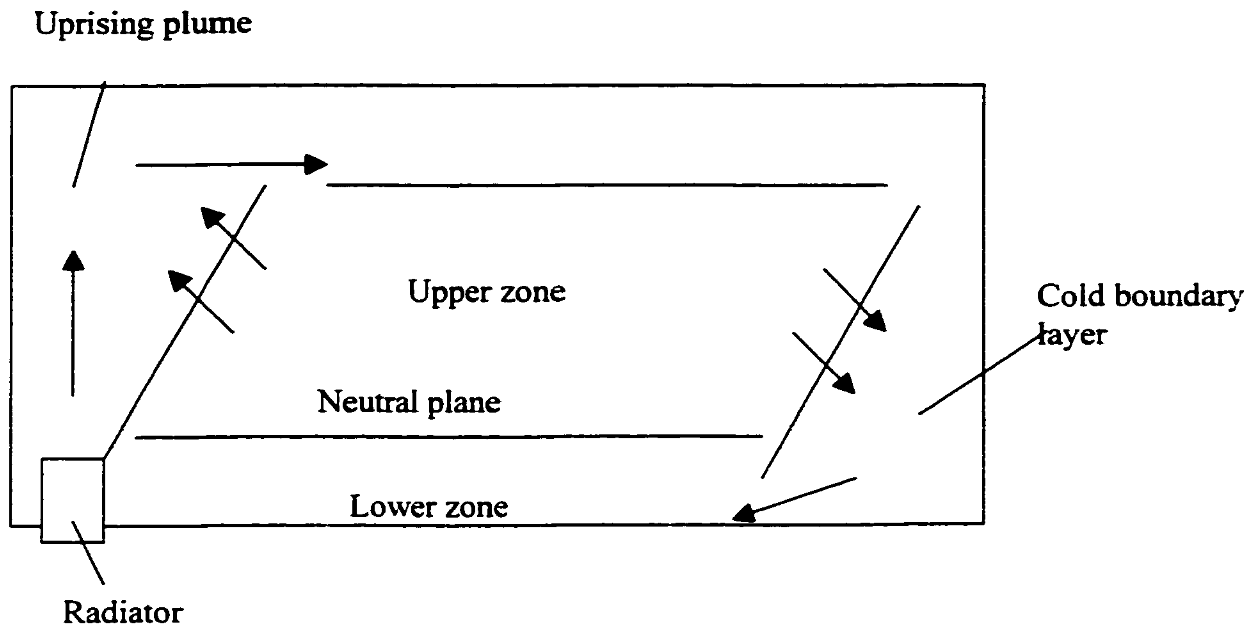

Figure 1.2 Configuration of a Two Zone Model

This model was developed by Howarth (1980) to predict the temperature stratification in a room heated by a radiator under the steady state condition. The room was divided into two zones, upper zone and lower zone, with a plume above the radiator and a cold boundary layer developed along the cold opposite wall. The mass flux across the border of the upper zone and lower zone, the neutral plane, was assumed to be zero. Hence, at the height of the neutral plate, the uprising mass flow rate in the plume is equal to the mass flow rate going down in the cold boundary layer.

In this model, Howarth calculated the heat exchanged between the air and different walls using empirical equations. The characteristics of plume and cold boundary layers as well as the coefficients were obtained from experimental results.

Inard and Buty (1991) improved Howarth's model by integrating the conductive and radiative heat exchange, and they also used experimental results to evaluate the mass flow rate in the plume and in the cold boundary.

III. Inard's Five Zone Model

Inard developed Five Zone model that mainly deals with the prediction of temperature stratification in a room, heated by a radiator or a convector at the corner of the room under a steady state condition (Inard, 1988).

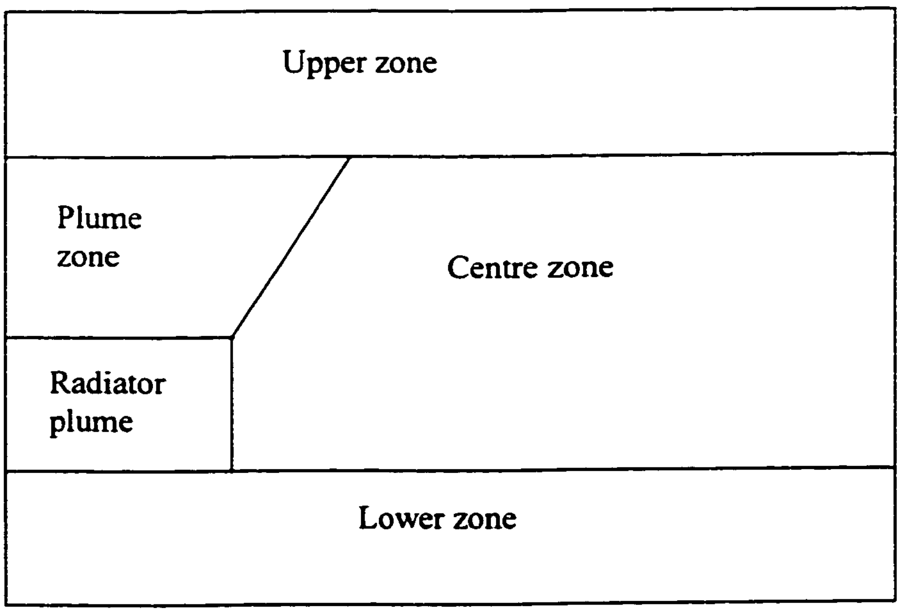

Figure 1.3 Configuration of a Five Zone Model

Based on the knowledge of airflow pattern acquired from previous experimental studies, the room was split into five zones, as shown in Figure 1.3. The convective heat exchange coefficients, radiator convective heat power and thermal resistance value were given as inputs to the model. The mass flow rates between plume and upper zone (G_{up}) and between plume and radiator (G_{ppl}) were characterized by two empirical equations obtained from experiments.

$$G_{ppl} = 9.10^{-3} C_p [\frac{(T_{ra} - T_l)}{R_{rac}} / L_{ra}]^{\frac{1}{3}} (H_{ra} + 0.1 - Z_0) L_{ra} \qquad (1\text{-}3)$$

$$G_{up} = 9.10^{-3} [(\frac{T_{ra} - T_l}{R_{rac}} - \frac{T_p - T_{gl}}{R_{glc}} - \frac{T_p - T_{tr}}{R_{trc}}) / L_{ra}]^{\frac{1}{3}} (Height - Z_0) L_{ra} \qquad (1\text{-}4)$$

Where, the subscripts of temperature (T), ra, l, p, and gl, represent radiator, lower zone, plume and glazing, respectively. The subscripts of thermal resistance (R), rac, glc and trc, represent radiator convective, glazing convective and trail convective thermal resistance. The system of equations was set up by combining these two equations with mass and energy balance equations for each zone. The solution of this system of equations provides the temperature in each zone and the mass flux across the boundary between two zones.

IV. Twelve Zone Model

The intended capability of this model was to predict the transient behaviour of a room heated by different methods (Inard and During, 1994). For each heating system, there was an individual dynamic model. The geometry of zones is varied accordingly.

Other than the mass and energy balance equations for each zone, experimental results were used to evaluate the mass flow rates in the plume and boundary layer so that the equations could reach a unique solution. For all the heating systems used, the model has been compared with experiments both in steady state and transient condition. The agreement between experimental and numerical results are satisfactory (Inard and During, 1994).

In the previous zonal models, i.e. Analytical Model, Two Zone Model, Five Zone Model and Twelve Zone Model, they were developed for specific applications and the pre-knowledge of airflow pattern within a room is required in order to define the geometry of zones. Moreover, it is noted that the definition of zones in these models is so coarse that the horizontal air temperature variation cannot be obtained except air in plumes.

V. BTHEBES Model

This unsteady-state model was used to simulate a room heated by a Gas Heat Pump (GHP) blowing from the ceiling (Gschwind et al, 1996). Many boundary conditions such as radiation and convection as well as heat conduction through walls were solved simultaneously.

In order to relieve users' effort in defining the geometry of zones, Gschwind divided the room into 22 zones in a different approach other than previous zonal models. The geometry of zones was defined automatically by the software depending on the condition of jet (orientation and speed), as shown in Figure 1.4. The air exchanges between zones were assumed to consist of exchanges due to the plume generated along the wall surfaces, exchanges due to the forced convection from the heating jet, and exchanges due to the natural convection between air zones. These exchanges were modeled as a function of the temperature of zone air and solid surface using semi-empirical laws.

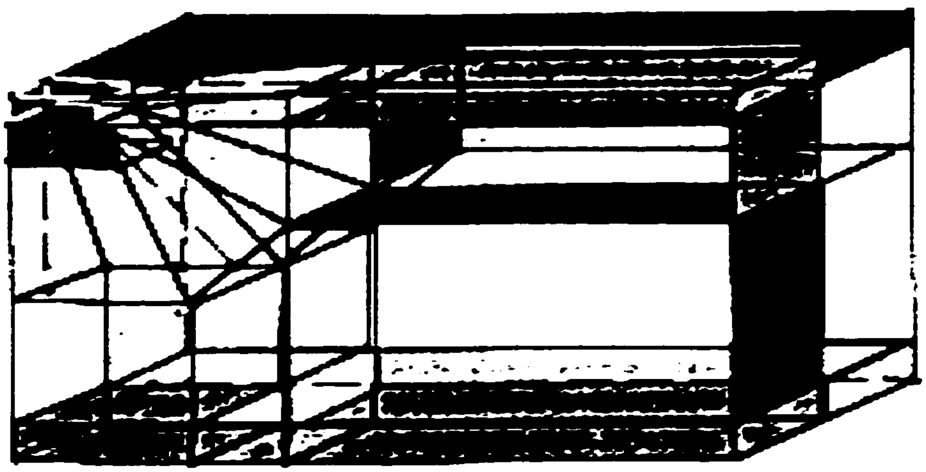

Figure 1.4 Configuration of a BTHEBES model (Gschwind et al, 1996)

Based on mass and energy balance, the temperature distribution in 22 zones was solved by the application of the Gear-Adams method. The experimental validation of BTHEBES demonstrated this model could give an accurate transient simulation of the room heated by GHP. The computation time was rather short, about one minute on a workstation for simulating air temperature variation in one minute after GHP starts. The model, however, underestimated the mixing of jet with the ambient air (Gschwind et al, 1996). In addition, since the configuration of zones is too complicated, the results of BTHEBES are difficult to understand and be used by engineers.

VI. Inard's Pressure Zonal Model

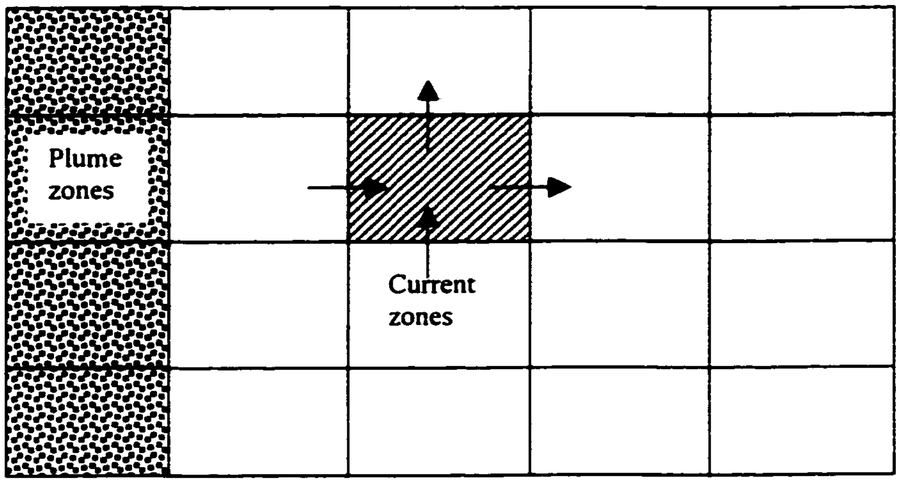

Figure 1.5 Configuration of a Pressure Zonal Model

In 1996, Inard used the pressure variables to represent the airflow between zones (Inard et al, 1996). Actually the idea of the introduction of pressure factors should be attributed to Bouia (1991). In this model, the room was divided into several zones in parallelepipedic geometry. Two kinds of zones were identified, i.e. the current or low velocity zone and the driving flow zone. The main difference between this model and other zonal models is that in this model the mass flow in the current zone was represented in terms of pressure.

The mass flow on the vertical boundary between two current zones is expressed as:

$$m_{ij} = \varepsilon_{ij} \sqrt{2\rho_j} C_d A_{ij} \left| P_j - P_i \right|^{1/2} \tag{1-5}$$

Where, ε_{ij}, of which absolute value is 1, makes the sign of flow direction.

C_d is discharge coefficient value, set to 0.8 based on experiments,

ρ is density of air,

A is area of boundary,

P is pressure of zone,

While on the horizontal border between two current zones, it is expressed as:

$$m_{ij} = \varepsilon_{ij} \sqrt{2\rho_j} C_d A_{ij} \left| (P_j - P_i) - \frac{1}{2}(\rho_i g h_i - \rho_j g h_j) \right|^{1/2} \tag{1-6}$$

In the driving flow zones, the mass flow rates across the borders within the driving flow zones and those borders between the driving flow zone and the current zone were described by driving flow behavior laws. Three kinds of flows are introduced.

1) Wall anisothemal horizontal jet

$$\frac{m(x)}{m_0} = k_1 \left(\frac{x}{b_0}\right)^{\alpha} \tag{1-7}$$

2) Wall thermal plume derived from a local heat source

$$m(z) = k_2 Q(z)^{1/3} (z - z_0)^{\beta} \tag{1-8}$$

3) Thermal boundary layer.

$$m(z) = k_3 \Delta T^{1/3} z \tag{1-9}$$

Pressure and temperature in each zone were obtained by solving a set of non-linear mass and energy balance equations. The model was validated by comparing its prediction with experimental results that were carried out in the CETHIL's (Centre de Thermique de l'INSA de Lyon) MINIBAT test cell for two types of flow, natural convection and mixed convection.

Pressure Zonal Model is promising in that the definition of zones is flexible and does not depend on the airflow pattern within the room. However, the driving forces such as jet and heat source were modeled by different kinds of empirical equations, which were based on experiments and did not have the general application field.

1.5 Objectives of This Research

From the several zonal models specified above, we can see great efforts have been made in the development of zonal models. Validated with measurement or CFD model, these zonal models have been proven to be able to predict the temperature distribution and mass flow within a room, with little computation effort. It was demonstrated that the zonal model is a practical tool to fill the gap between the CFD and multizone model.

The main limitations of the existing zonal models are:

1). The previous knowledge of airflow pattern is required to define the geometry of zones, 2). These models cannot predict the temperature variation at horizontal level except Pressure Zonal Model, and

3). They have been developed for specific applications.

The objective of this research is to develop a general-purpose zonal model that can predict the airflow pattern and temperature distribution within a room. The zonal model should be general in the following aspects:

- The definition of zones should be general. It does not require the previous knowledge of airflow pattern within the room. The number and the geometry of zones should be flexible and simple so that the users can obtain the indoor thermal environment knowledge to the certain extent which they want.
- The modeling of the driving forces will not depend on experimental results. It should be modeled in a general way so that the zonal model can be applied to all kinds of driving forces.

In addition, the zonal model is supposed to be easy to use and computationally efficient.

Chapter 2

Description of POMA

2.1 Introduction

Pressurized z**O**nal **M**odel with **A**ir diffusers (**POMA**) gives the airflow in terms of the pressure factors and assumes that the pressure is hydrostatically distributed in a zone instead of being uniform.

Different zonal models use various empirical formulas to model the driving force such as an air diffuser jet and thermal plume. These empirical models were only applicable to the specific driving force. Since the air diffuser equations in ASHRAE Fundamentals are generally applicable to various air diffusers, we integrated these characteristic equations into POMA in order to describe the air diffuser boundary conditions. As to the thermal plume, we ignore the specific equations for them and model the zones within them as the normal ones.

Furthermore, in POMA, in order to couple the jet plume with the normal zones, we identified an intermediate boundary, as will be described in detail later.

POMA uses the power law to describe the airflow as used by Wurtz (Wurtz et al, 1996). In addition to that, jet characteristic equations are integrated into POMA to deal with the forced ventilation. Moreover, POMA uses a powerful numerical solver to improve the density of the grids up to 37×13, as will be shown in the case studies in Chapter 5. Other than that, we validated POMA with experimental results (Allard et al, 1987) and with the CFD results (Jiang, 1998).

2.2 Basic Assumptions

In POMA, the room is divided into a limited number of macroscopic zones with homogeneous thermal property defined by horizontal and vertical grids. Thus the boundaries of zones are either horizontal or vertical, except for the wall surface. For each zone, a number of assumptions have been made:

1). The air is inviscid.

2). The air temperature and density are uniform. That means, the density of the air, ρ, refers to the density at the middle point of the zone. It can be calculated by Ideal Gas Law (Hutcheon et al, 1989),

$$P_{middle} = \rho_{zone} RT \tag{2-1}$$

Where,

P_{middle}: pressure at middle point of zone (Pa)

ρ_{zone}: air density of zone, (kg/m^3)

R: gas constant for air, (287.055 J/kg K)

T: air temperature of zone, (K)

This approximate approach has been demonstrated to be sufficient for many practical purposes. (Hutcheon et al, 1989)

3). There is an independent reference pressure at the bottom of each zone. The air pressure in the zone is assumed to be hydrostatically distributed based on this reference pressure.

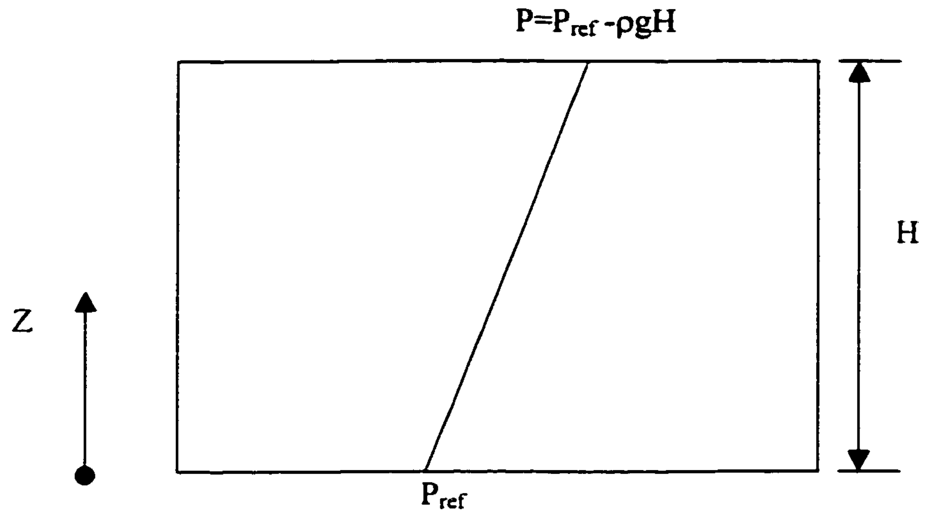

Figure 2.1 Pressure Assumption in a Zone

In Figure 2.1,

$$P = P_{ref} - \rho_{zone} g Z \tag{2-2}$$

Where,

Z: height of point considered, (m)

P: pressure at the height of Z, (Pa)

P_{ref}: reference pressure at the bottom of zone, (Pa)

H: height of zone, (m)

g : gravitational acceleration, (m/s^2)

So that, in Equation (2-2),

$$P_{middle} = P_{ref} - \rho_{zone} g \frac{H}{2} \tag{2-3}$$

4). The principle of conservation of mass and energy must be obeyed in each zone.

Mass Balance:

$$\frac{dM_i}{dt} = \sum_{j=1}^{n} m_{ij} + m_{source} + m_{\sin k} \tag{1-1}$$

Energy Balance:

$$\frac{dQ_i}{dt} = \sum_{j=1}^{n} q_{ij} + q_{source} + q_{\sin k} \tag{1-2}$$

Since, in this thesis, we are only concerned with rooms in a steady state condition, the time derivatives of the M_i and Q_i are zero. Consequently the mass and heat balance can be expressed as:

$$0 = \sum_{j=1}^{n} m_{ij} + m_{source} + m_{\sin k} \tag{2-4}$$

$$0 = \sum_{j=1}^{n} q_{ij} + q_{source} + q_{\sin k} \tag{2-5}$$

5). In POMA, the radiation component is ignored so that the heat flow is a combination of convection along wall surfaces and the heat carried by mass flow, as will be explained in the following sections.

6). Three kinds of boundaries are identified in the room (see Figure 2.2), i.e.

- Normal boundary: the boundary without the influence of the driving force (jets), i.e. boundaries between zone 1 and 2, 1 and 6, 6 and 7, etc.
- Jet boundary: the boundary totally within the plume of the jet, i.e. boundaries between zone 2 and 3, 3 and 4, 3 and 8, etc.
- Mixed boundary: the boundary on the border of plume, i.e. boundaries between zone 2 and 7, 7 and 12, 4 and 9, etc.

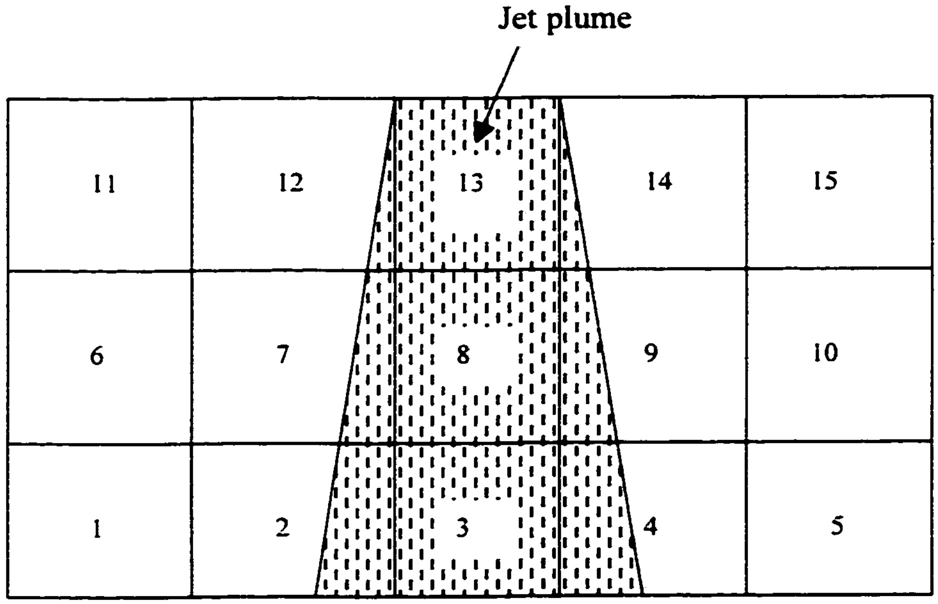

Figure 2.2 Configurations of Different Boundaries

2.3 Modelling of the Airflow across Normal Boundaries

There are three kinds of normal boundaries in POMA. These are horizontal air-to-air boundary, vertical air-to-air boundary and wall surface boundary. On the wall surface, we assume that the wall is impenetrable so that there is no airflow across the wall surface. Thus we only need to model the air-to-air boundaries.

The key point in zonal models is in reducing the number of unknown airflow. In pressure zonal models, the problem of reducing unknown factors is solved by the introduction of pressure factors. The number of unknown airflows is reduced by representing airflow in terms of a pressure difference. Varied pressure zonal models distinguished themselves in their different methods of representing airflow to pressure difference.

Power Law is applied to calculate the airflow across the boundary between the normal zones:

$$Vol = K\Delta P^n A \tag{2-6}$$

Where,

Vol: volume of flow rate, (m^3/s)

ΔP: pressure differece, (Pa)

K: coefficient of power law, usually taken as 0.83, ($m/s\ Pa^n$)

A: area of boundary, (m^2)

n: flow exponent, usually taken as 0.5.

2.3.1 Airflow across Horizontal Boundary

2.3.1.1 Basic scheme

The airflow across the horizontal boundary between two adjacent zones is modeled by means of Power Law, Equation 2-6. In order to calculate the mass flow, it is imperative to know the pressure difference across the boundary. As shown in Figure 2.3, supposing there are two reference pressures, P_{ref0} and P_{ref1}, in zone 0 and zone 1 respectively, the pressure difference across the boundary, ΔP, is:

$$\Delta P = |P_1 - P_0| \tag{2-7}$$

Where, subscripts 0 and 1 refer to zone 0 and zone 1, respectively, and

$$P_1 = P_{ref1} - \rho_1 g H_1 \tag{2-8}$$

$$P_0 = P_{ref0} \tag{2-9}$$

Substitute into Equation (2-7),

$$\begin{aligned} \Delta P &= |P_{ref1} - \rho_1 g H_1 - P_{ref0}| \\ &= |\Delta \mathrm{P}_{\mathrm{ref}} - \rho_1 g H_1| \end{aligned} \tag{2-10}$$

In which, subscript ***ref*** means reference,

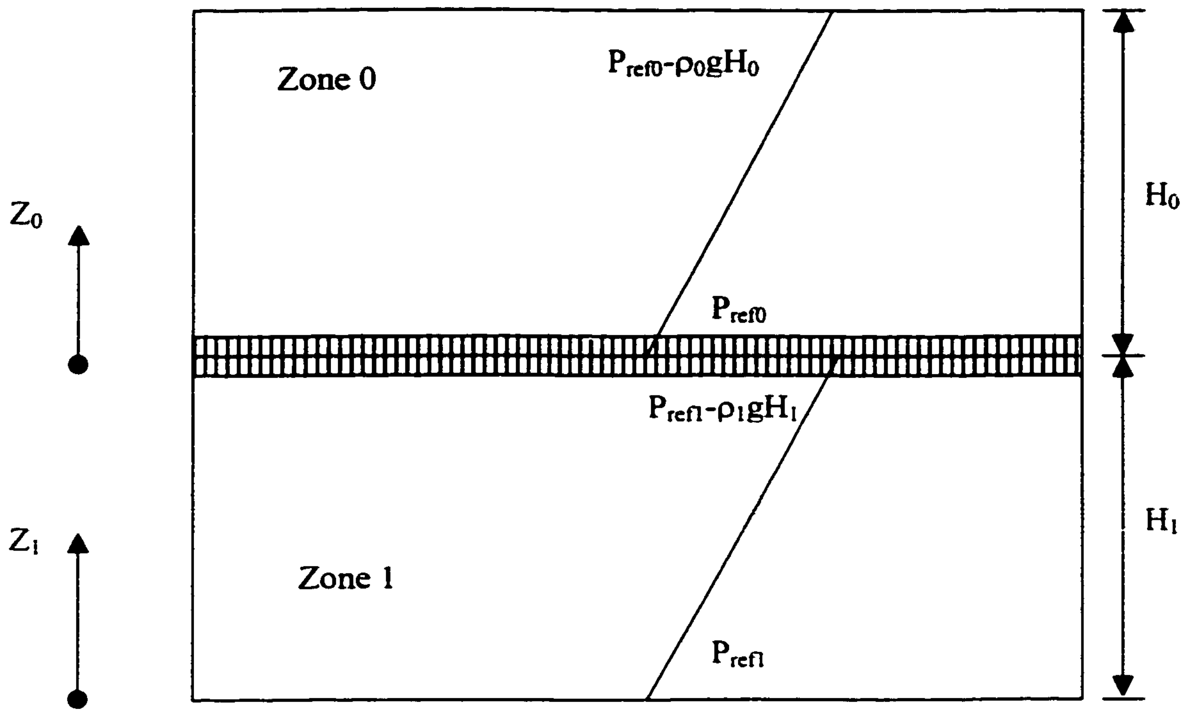

Figure 2.3 Modeling of Horizontal Boundary

Substituting Equation (2-10) into Equation (2-6), the mass flow is:

$$\begin{aligned} m &= \rho_{flow} AK\Delta P^n \\ &= \rho_{flow} AK\left|\Delta P_{ref} - \rho_1 g H_1\right| \end{aligned} \tag{2-11}$$

Where,

m: airflow rate across horizontal boundary (kg/s)

ρ_{flow} :density of zone from which air flows in. (kg/m^3)

It is noted that, since density is a function of temperature, from Equation (2-11), we can conclude that,

$$m = func(\Delta P_{ref}, T) \tag{2-12}$$

2.3.1.2 All of the possibilities

Supposed that the airflow is calculated for zone 0, in the mass balance, Equation (2-4), it is assumed that the mass flow is positive if the air flows into the zone 0, and it is negative if the air flows out of the zone. The direction of the flow depends on whether the pressure difference on the both side of the boundary (ΔP) is positive or negative.

There are two possibilities of the position of zone 0, either on the top of zone 1 or under zone 1.

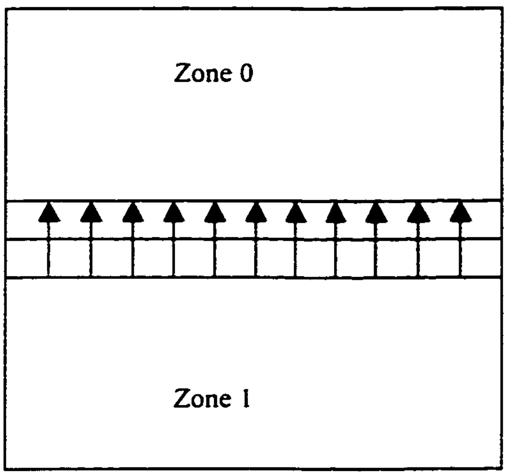

Figure 2.4 Flow situation when zone 0 on the top of zone1, and if $(P_{ref1} - P_{ref0}) - \rho_1 g H_1 \geq 0$

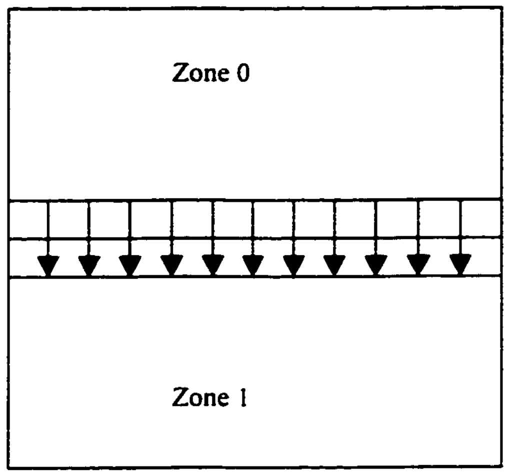

Figure 2.5 Flow situation when zone 0 on the top of zone1, and if $(P_{ref1} - P_{ref0}) - \rho_1 g H_1 < 0$

If the zone 0 is on the top of the zone 1,

and if the pressure under the boundary is larger than that above the boundary, i.e. $(P_{ref1} - P_{ref0}) - \rho_1 g H_1 \geq 0$, as shown in Figure 2.4

$$m = \rho_1 AK\left|(P_{ref1} - P_{ref0}) - \rho_1 g H_1\right|^n \qquad (2\text{-}13)$$

else if the pressure under the boundary is less than that above the boundary

i.e. $(P_{ref1} - P_{ref0}) - \rho_1 g H_1 < 0$, as shown in Figure 2.5

$$m = -\rho\, A\, K\left|(P_{ref1} - P_{ref0}) - \rho_1 g H_1\right|^n \qquad (2\text{-}14)$$

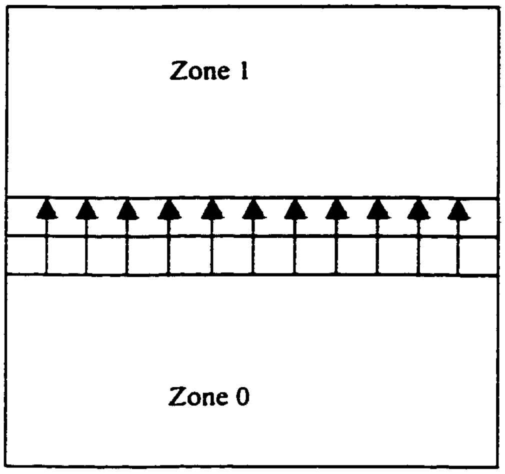

Figure 2.6 Flow situation when zone 0 is under zone 1, and if $(P_{ref1} - P_{ref0}) + \rho_0 g H_0 \geq 0$

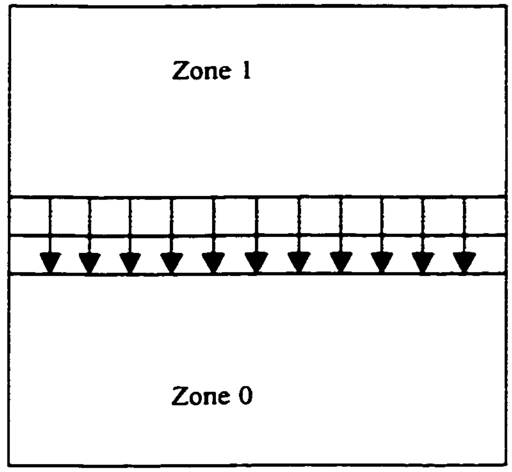

Figure 2.7 Flow situation when zone 0 is under zone 1, and if$(P_{ref1} - P_{ref0}) + \rho_0 g H_0 < 0$

Else if the zone 0 is under the zone 1,

And if the pressure under the boundary is larger than that above the boundary.

i.e. $(P_{ref1} - P_{ref0}) + \rho_0 g H_0 \geq 0$. as shown in Figure 2.6

$$m = \rho_1\, A\, K\left|(P_{ref1} - P_{ref0}) + \rho_0 g H_0\right|^n \qquad (2\text{-}15)$$

else if the pressure under the boundary is less than that above the boundary.

i.e. $(P_{ref1} - P_{ref0}) + \rho_0 g H_0 > 0$, as shown in Figure 2.7

$$m = -\rho_0 A K\left|(P_1 - P_0) + \rho_0 g H_0\right|^n \qquad (2\text{-}16)$$

2.3.2 Airflow across Vertical Boundary

2.3.2.1. Basic scheme

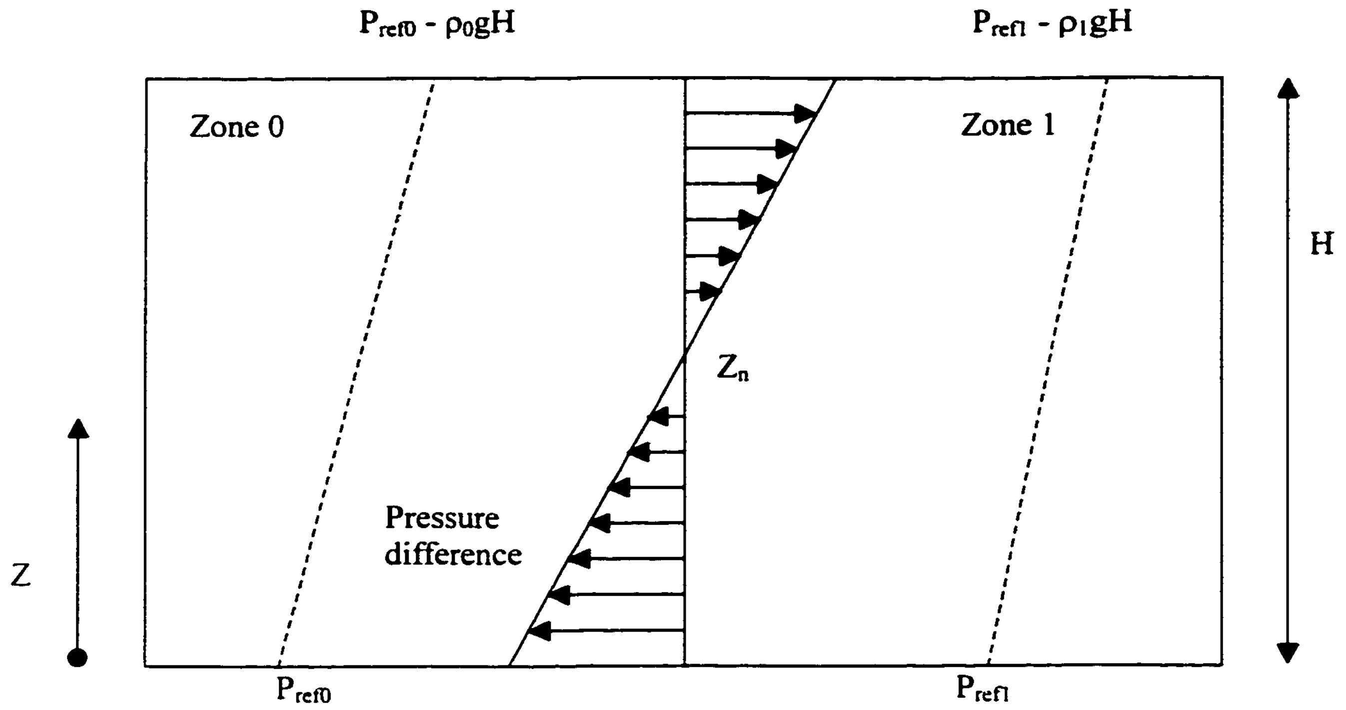

Figure 2.8 Modeling of Vertical Boundary

We assume on the vertical boundary that there is a neutral plane (Z_n), at the height of which the pressure difference between both sides of boundary is zero.

At the height of the neutral plane, the pressures in zone 0 and zone 1 is:

$$P_0 = P_{ref\,0} - \rho_0 g Z_n \tag{2-17}$$

$$P_1 = P_{ref\,1} - \rho_1 g Z_n \tag{2-18}$$

The pressure difference is,

$$\begin{aligned}\Delta P &= (P_1 - P_0) \\ &= (P_{ref1} - \rho_1 g Z_n) - (P_{ref0} - \rho_0 g Z_n) \\ &= (P_{ref1} - P_{ref0}) - (\rho_1 g Z_n - \rho_0 g Z_n)\end{aligned} \tag{2-19}$$

Since at the height of neutral plane, ΔP is equal to zero, we get

$$\Delta P_{ref} = (P_{ref1} - P_{ref0}) = \Delta\rho g Z_n \tag{2-20}$$

$\Rightarrow$

$$Z_n = \frac{\Delta P_{ref}}{\Delta\rho g} \tag{2-21}$$

Where,

$$\Delta\rho = \rho_1 - \rho_0 = \frac{P_{ref1}}{R T_1 + g\dfrac{H}{2}} - \frac{P_{ref0}}{R T_0 + g\dfrac{H}{2}} \tag{2-22}$$

Then, at a certain height of Z, the pressure difference across the boundary is:

$$\begin{aligned}\Delta P &= (P_1 - P_0) \\ &= (P_{ref1} - \rho_1 g Z) - (P_{ref0} - \rho_0 g Z) \\ &= \Delta P_{ref} - \Delta\rho g Z\end{aligned} \tag{2-23}$$

Substitute Equation (2-21) into Equation (2-23)

$$\begin{aligned} \Delta P &= \Delta\rho g Z_n - \Delta\rho g Z \\ &= \Delta\rho g (Z_n - Z) \end{aligned} \tag{2-24}$$

Based on Power Law, Equation (2-6), the mass flow rate across the vertical boundary ($m_{o\text{-}H}$) is:

$$m_{o-H} = m_{0-Zn} + m_{Zn-H} \tag{2-25}$$

Where, $m_{0\text{-}Zn}$: mass flow rate from 0 to Z_n on vertical boundary, (kg/s), and

$m_{Zn\text{-}H}$: mass flow rate from Z_n to H on vertical boundary, (kg/s)

$$\begin{aligned} m_{0-Zn} &= \int_0^{Zn} k\, L\, \rho_{0-Zn} |\Delta P|^n dz \\ &= \int_0^{Zn} k\, L\, \rho_{0-Zn} |\Delta\rho\, g\, (Z_n - Z)|^n dz \\ &= k\, L\, \rho_{0-Zn} |\Delta\rho\, g|^n \left[\frac{|Z_n|^{n+1}}{n+1} \right] \end{aligned} \tag{2-26}$$

$$\begin{aligned} m_{Z_n-H} &= \int_{Zn}^{H} k\, L\, \rho_{Zn-H} |\Delta P|^n dz \\ &= \int_{Zn}^{H} k\, L\, \rho_{Zn-H} |\Delta\rho\, g\, (Z_n - Z)|^n dz \\ &= k\, L \rho_{Zn-H} |\Delta\rho g|^n \left[\frac{|Z_n - H|^{n+1}}{n+1} \right] \end{aligned} \tag{2-27}$$

Where,

$\rho_{0\text{-}Zn}$: density of airflow from 0 to Z_n, (kg/m^3)

$\rho_{Zn\text{-}H}$: density of airflow from Z_n to H, (kg/m^3)

L: depth of zone, (m)

Substituting Equations (2-21) and (2-22) into (2-26) and (2-27) respectively, it is noted that $m_{0\text{-}Zn}$, $m_{zn\text{-}H}$ and $m_{0\text{-}H}$ are a function of ΔP_{ref} and the temperature of the relative zones.

2.3.2.2. All of the possibilities

Since the direction of the flow is determined by the pressure difference, considering Equation (2-24),

$$\begin{aligned}\Delta P &= \Delta\rho g Z_n - \Delta\rho g Z \\ &= \Delta\rho g(Z_n - Z)\end{aligned} \tag{2-24}$$

if the flow is calculated for zone 0, there are 8 kinds of possibilities about the flow directions:

a) $\Delta\rho=\rho_1-\rho_0 < 0$

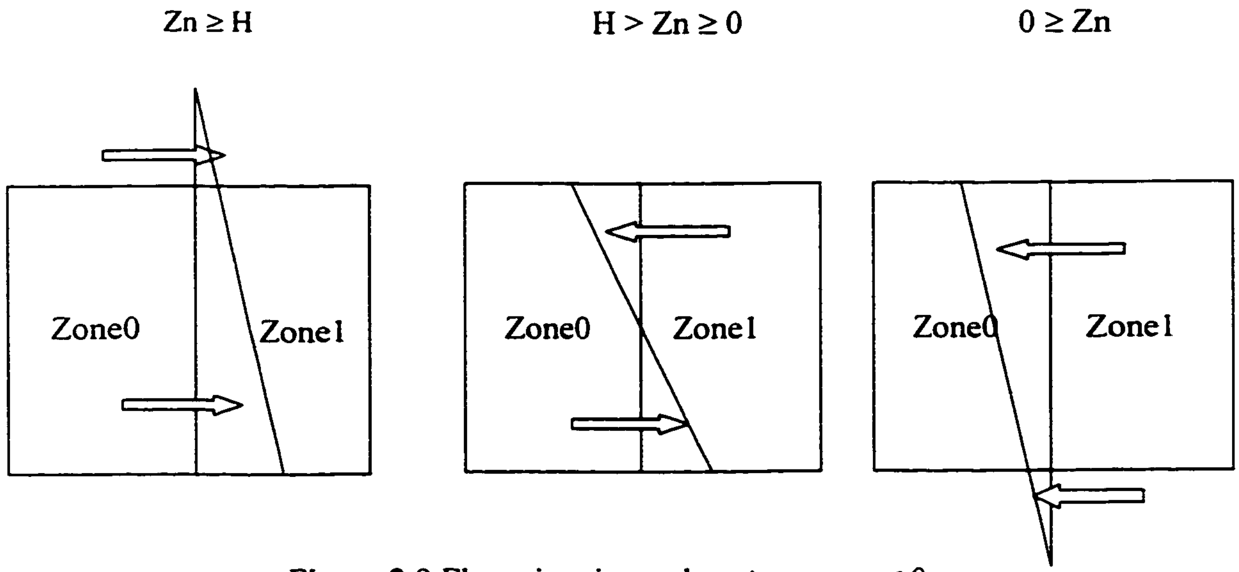

Figure 2.9 Flow situations when $\Delta\rho=\rho_1-\rho_0 < 0$

b) $\Delta\rho = \rho_1 - \rho_0 > 0$

$Zn \geq H$ $\quad$ $H > Zn \geq 0$ $\quad$ $0 \geq Zn$

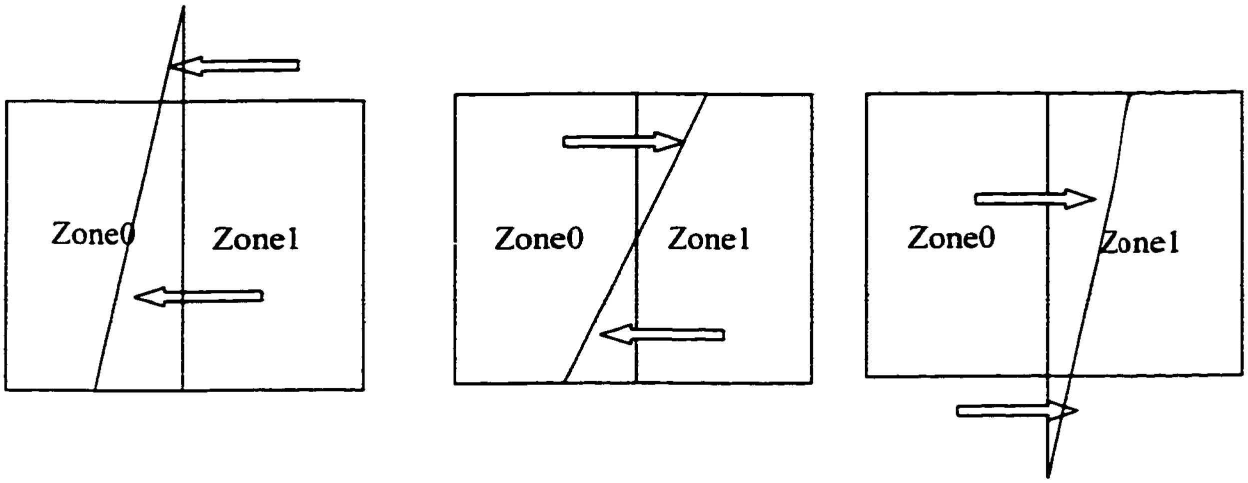

Figure 2.10 Flow situations when $\Delta\rho = \rho_1 - \rho_0 > 0$

c) $\Delta\rho = \rho_1 - \rho_0 = 0$

$\Delta P = (P_{ref1} - \rho_1 gH) - (P_{ref0} - \rho_0 gH) = P_{ref1} - P_{ref0}$

$P_{ref1} > P_{ref0}$ $\quad$ $P_{ref1} < P_{ref0}$

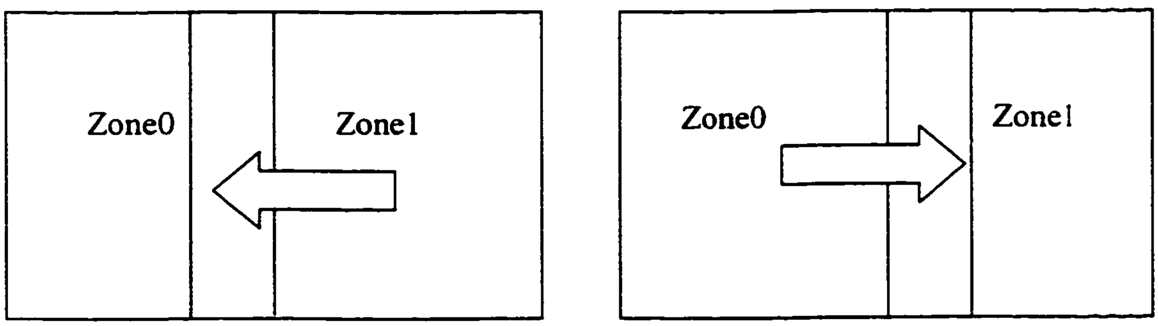

Figure 2.11 Flow situations when $\Delta\rho = \rho_1 - \rho_0 = 0$

We can express the 8 possibilities as follows:

a.1) $\Delta\rho=\rho_1-\rho_0 < 0$ and $Zn \geq H$

$$m_{0-Zn} = -k\,L\,\rho_0 \left|\Delta\rho\, g\right|^n \left[\frac{\left|Z_n\right|^{n+1}}{n+1}\right] \tag{2-28}$$

$$m_{Zn-H} = k\,L\,\rho_0 \left|\Delta\rho\, g\right|^n \left[\frac{\left|Z_n - H\right|^{n+1}}{n+1}\right] \tag{2-29}$$

a.2) $\Delta\rho=\rho_1-\rho_0 < 0$ and $H > Zn \geq 0$

$$m_{0-Zn} = -k\,L\,\rho_0 \left|\Delta\rho g\right|^n \left[\frac{\left|Z_n\right|^{n+1}}{n+1}\right] \tag{2-30}$$

$$m_{Zn-H} = k\,L\,\rho_1 \left|\Delta\rho g\right|^n \left[\frac{\left|Z_n - H\right|^{n+1}}{n+1}\right] \tag{2-31}$$

a.3) $\Delta\rho=\rho_1-\rho_0 < 0$ and $0 > Zn$

$$m_{0-Zn} = -k\,L\,\rho_1 \left|\Delta\rho g\right|^n \left[\frac{\left|Z_n\right|^{n+1}}{n+1}\right] \tag{2-32}$$

$$m_{Zn-H} = k\,L\,\rho_1 \left|\Delta\rho g\right|^n \left[\frac{\left|Z_n - H\right|^{n+1}}{n+1}\right] \tag{2-33}$$

b.1) $\Delta\rho=\rho_1-\rho_0 > 0$ and $Zn \geq H$

$$m_{0-Zn} = k\,L\,\rho_1\left|\Delta\rho g\right|^n\left[\frac{\left|Z_n\right|^{n+1}}{n+1}\right] \tag{2-34}$$

$$m_{Zn-H} = -k\,L\,\rho_1\left|\Delta\rho g\right|^n\left[\frac{\left|Z_n-H\right|^{n+1}}{n+1}\right] \tag{2-35}$$

b.2) $\Delta\rho=\rho_1-\rho_0 > 0$ and $H > Zn \geq 0$

$$m_{0-Zn} = k\,L\,\rho_1\left|\Delta\rho g\right|^n\left[\frac{\left|Z_n\right|^{n+1}}{n+1}\right] \tag{2-36}$$

$$m_{Zn-H} = -k\,L\,\rho_0\left|\Delta\rho * g\right|^n\left[\frac{\left|Z_n-H\right|^{n+1}}{n+1}\right] \tag{2-37}$$

b.3) $\Delta\rho=\rho_1-\rho_0 > 0$ and $0 > Zn$

$$m_{0-Zn} = k\,L\,\rho_0\left|\Delta\rho g\right|^n\left[\frac{\left|Z_n\right|^{n+1}}{n+1}\right] \tag{2-38}$$

$$m_{Zn-H} = -k\,L\,\rho_0\left|\Delta\rho g\right|^n\left[\frac{\left|Z_n-H\right|^{n+1}}{n+1}\right] \tag{2-39}$$

c.1) $\Delta\rho = \rho_1 - \rho_0 = 0$ (in programming, let $\Delta\rho < 1.0e\text{-}18$) and $P_{ref1} > P_{ref0}$

$$m_{0-Zn} = 0$$

$$m_{Zn-H} = k\,L\,\rho_1\left|P_{ref1} - P_{ref0}\right|^n \tag{2-40}$$

c.2) $\Delta\rho = \rho_1 - \rho_0 = 0$ and $P_{ref1} < P_{ref0}$

$$m_{0-Zn} = 0$$

$$m_{Zn-H} = -k\,L\,\rho_0 \left| P_{ref1} - P_{ref0} \right|^n \tag{2-41}$$

2.4 Modelling of the Airflow across Jet Boundary

2.4.1 Modeling of Isothermal Free Jet

2.4.1.1 Jet expansion zones

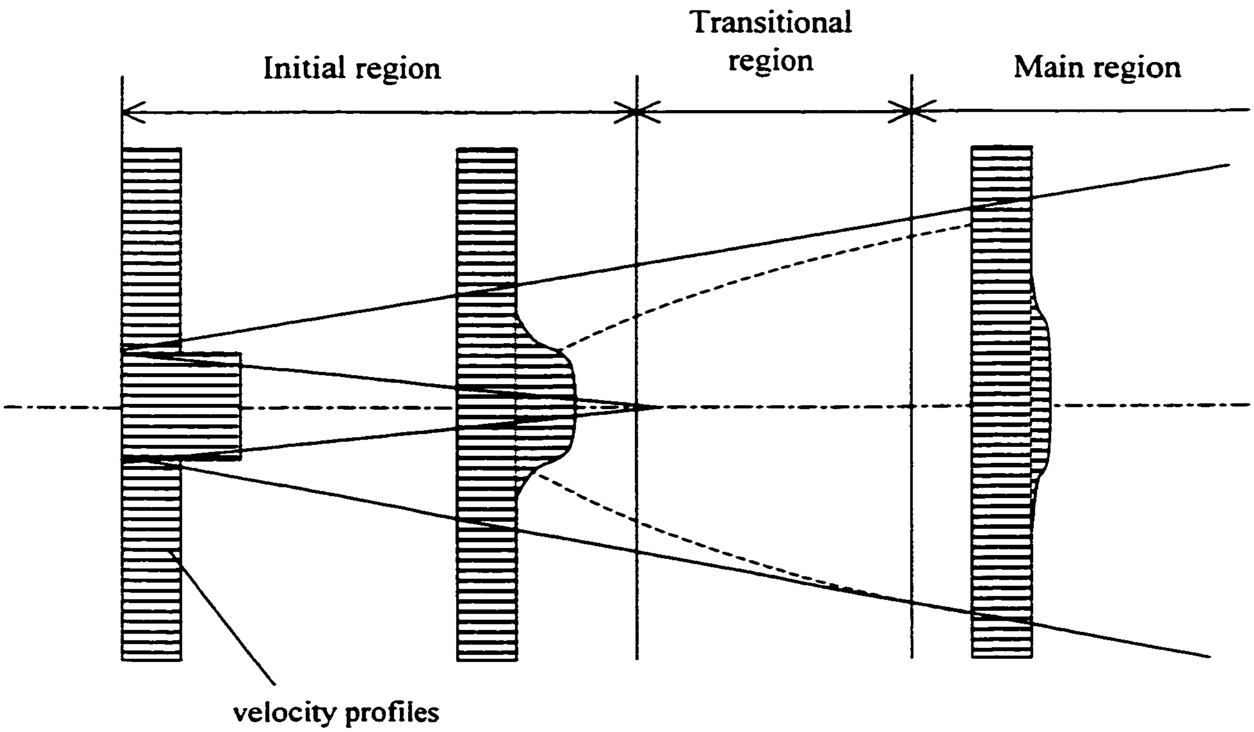

Figure 2.12 Jet expansion regions

According to ASHRAE 1993 Fundamentals Handbook, the full length of an air jet in terms of the maximum or centerline velocity and temperature differential at the cross section, can be divided into four regions, see Figure 2.12:

Region 1. Initial region: a short core region, extending about four diameters or widths from the outlet face. The maximum velocity of the air stream remains practically unchanged.

Region 2. Transition region: a short region. The centerline velocity and temperature are predictable. But no predictable velocity profiles can be obtained in this region. The length of this region depends on the type of diffuser, diffuser's aspect ratio and the initial airflow turbulence.

Region 3. Main Region: a region of fully established turbulent flow, which may be 25 to 100 equivalent air diffuser diameters (width for slot-type air diffusers). The velocity profile can be expressed by a single curve. Temperature and density differences have little effect on the cross sectional velocity profiles.

Region 4. Terminal region: a region of diffuser jet degradation, where the maximum air velocity and temperature decreases rapidly.

Since the length of region 1 and region 2 are quite short, and the macroscopic zone in zonal model is large, usually these two regions will be within the first macroscopic zone from the inlet. The first jet boundary from the inlet will be usually within the main region. Hence we ignore the velocity modeling in the initial region and the transitional region. In the case when the first jet boundary is in these two regions, the characteristic equations in the main region are applied. Moreover, in the terminal region, since the velocity is low and far from the diffuser, it will not be considered as a diffuser boundary condition.

2.4.1.2 Centerline Velocities Decay of Isothermal Free Jet

- Centerline velocity in main zone

In the main zone, maximum or centerline velocities of straight flow isothermal jets can be determined with accuracy. The centerline velocity decay of linear jets in the main zone is described by Equation (2-42), and the velocity decay of compact and radial jets is given by Equation (2-43) (ASHRAE Fundamentals, 1993):

$$\frac{V_x}{V_0} = K_1 \sqrt{\frac{H_0}{X}} \qquad (2\text{-}42)$$

$$\frac{V_x}{V_0} = K_1 \frac{\sqrt{A_0}}{X} \qquad (2\text{-}43)$$

Where,

V_x : centerline velocity, (m/s)

V_0 : average initial velocity at discharge, (m/s)

H_0 : width of jet at outlet or at vena contracta, (m)

A_0 : effective area of diffuser, (m^2)

K_1 : centerline velocity constant depending on outlet type and discharge pattern

X: distance to the diffuser face on the jet centerline, (m)

2.4.1.3 Velocity Profiles of Jets

Velocity distribution in main zone can be expressed by the Gauss error function or probability curve, which is approximated by ASHRAE Fundamentals (1993):

$$\left(\frac{r}{r_{0.5}}\right)^2 = 3.3\log\frac{V_x}{V} \tag{2-44}$$

Where,

r: radial distance of the point under consideration from centerline of jet, (m)

$r_{0.5}$: radial distance in the same cross-sectional plane from axis to point where velocity is one-half centerline velocity, i.e. $V=0.5V_x$, (m)

V_x : centerline velocity in the same cross-sectional plane, (m/s)

V: actual velocity at the point being considered.(m/s)

Experiments show that the conical angle for $0.5V_x$ and $r_{0.5v}$ is approximately one-half the total angle of divergence of a jet. The equation can be used as a good approximation for adjacent portions of regions 2 and 4. Temperature and density differences have little effect on the cross-sectional velocity profiles. (ASHRAE Fundamentals, 1993)

2.4.1.4 Angle of Divergence

Measured angles of divergence (spread) for discharge into large open spaces usually range from 20 to 24 with an average of 22°. (ASHRAE Fundamentals, 1993)

All of the equations mentioned above are developed for the main region of the diffuser jet. The parameters such as the effective supply area H_0 or A_0 and the average supply velocity V_0 can be obtained from the manufacturer's product information data. The velocity decay coefficient K_I for different diffusers can be obtained from ASHRAE Fundamentals. As long as the supply airflow rate and the supply air temperature are given, the velocity in the jet plume can be calculated using these diffuser jet characteristic equations.

2.4.2 Calculation of Airflow

2.4.2.1 Airflow across the Boundary Perpendicular to the Trajectory of the Jet

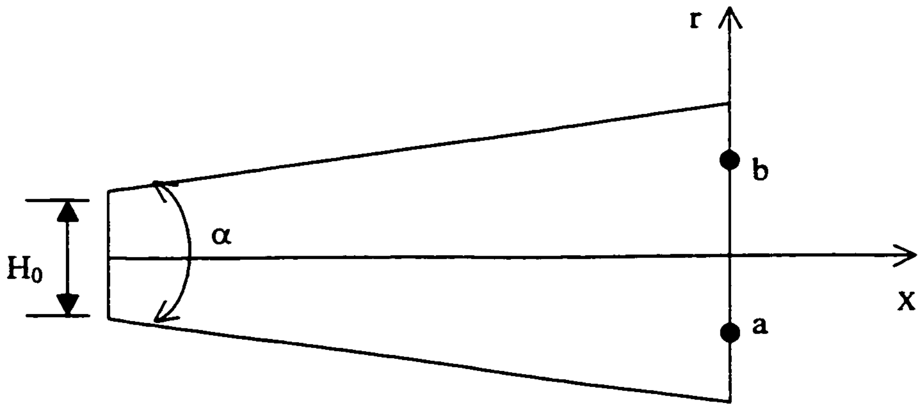

Figure 2.13 Modeling of Jet Boundary

Let us consider the jet boundary shown in Figure 2.13, which is perpendicular to the trajectory, from point a to point b, the airflow can be modeled as:

$$m = \int_0^m dm = \int_a^b \rho_{flow} V L dr \tag{2-45}$$

Where,

ρ_{flow} : density of zone from which the air flows in, (kg/m^3)

V: velocity across boundary at the certain distance r, (m/s)

L: depth of zone, (m)

We can get the velocity at certain distance, r, based on Equation (2-44)

$$V = V_x 10^{-\frac{1}{3.3}\left(\frac{r}{r_{0.5r}}\right)^2} \tag{2-46}$$

Where,

$$r_{0.5} = X \frac{tg\frac{\alpha}{2}}{2} \tag{2-47}$$

Thus, specifically, the airflow rate, m, across the jet boundary is modeled as:

$$m = \int_0^m dm = \int_a^b \rho_{flow} V_x 10^{-\frac{1}{3.3}\left(\frac{r}{xtg\frac{\alpha}{2}/2}\right)^2} Ldr \tag{2-48}$$

2.4.2.2 Airflow across the Boundary Parallel to the Trajectory

At the boundary parallel to the trajectory of the jet, the airflow across it is modeled as that across the normal boundary.

2.5 Modelling of the Airflow across Mixed Boundary.

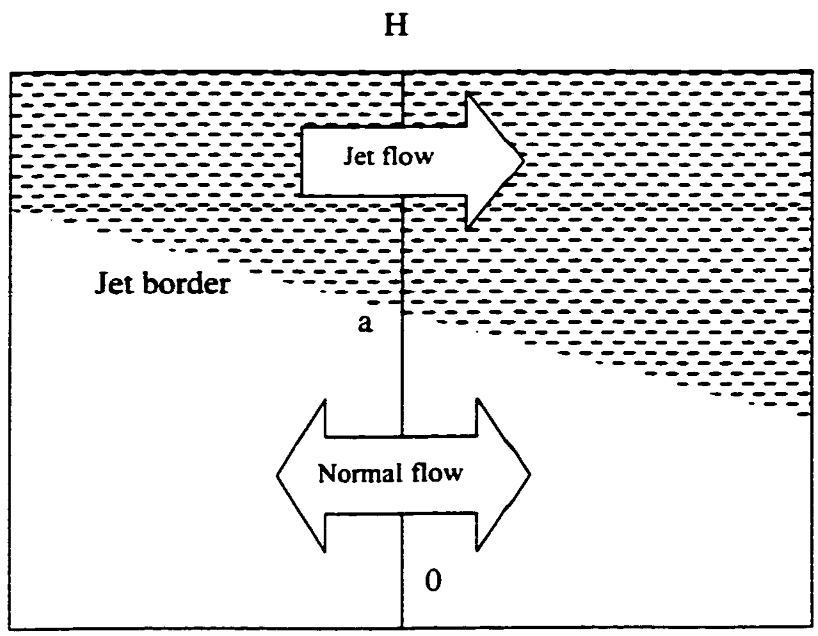

Figure 2.14 Modeling of Mixed Boundary

The airflow across the mixed boundary can be modeled as a combination of that across the jet boundary and that across the normal boundary. As shown in Figure 2.14. the partition (a-H) is within the jet region and the partition (0-a) is out of the jet region. The airflow from a to H ($m_{a\text{-}H}$) can be modeled as that across the jet boundary, by applying Equation (2-48), and the airflow from 0 to a ($m_{0\text{-}a}$), it can be modeled as the airflow across the normal boundary:

$$m_{0-a} = \frac{a}{H} * m_{0-H}^{normal} \tag{2-49}$$

Where, m_{0-H}^{normal} is the mass flow rate modeled as that across the normal boundary. (kg/s)

Consequently, the total mass flow rate across the mixed boundary m_{0-H} is:

$$m_{0-H} = m_{0-a} + m_{a-H} \tag{2-50}$$

2.6 Modelling of Heat Flow across Boundaries

Ignoring the radiation component, the heat flow is a combination of the convection and heat carried by airflow. The convection along wall surfaces is modeled by means of the Newton Cooling Law.

$$q = hA\Delta T_{wall-zone} \tag{2-51}$$

Where,

q: heat flow rate,(W)

h: convective heat transfer coefficient, (W/m^{2}K)

A: area of the wall surface, (m^2)

$\Delta T_{wall-zone}$: temperature difference between wall surface and zone air, (K)

The heat carried by mass flow is modeled as:

$$q = Cpm\Delta T_{zone-zone} \tag{2-52}$$

Where,

Cp: specific heat of air, (1005 W/kg K) (Hutcheon, 1989)

m: mass flow rate, (kg/s)

$\Delta T_{zone-zone}$: air temperature difference between two adjacent zones, (K)

Chapter 3

Numerical Solution of POMA

3.1 Global View of the Number of Equations and Unknown Factors

In the previous chapter, the modeling approach of POMA had been specified. We identified three kinds of boundaries in POMA. The mass flow and heat flow across these three boundaries were modeled to be represented in terms of pressure and temperature factors in each zone. A system of nonlinear equations based on mass and energy balance was set up.

In order to reach the solution of the problem, it is important to know exactly the number of equations and unknown factors. In the zonal model, suppose that there are n zones in the room, there should be n mass balances and n energy balances equations in the room. Many researchers have applied all of these equations in their zonal models. But unfortunately, there are only (n-1) independent mass balance equations in these n mass balance equations, and n independent energy balance equations, as will be demonstrated shortly.

3.1.1 The Simplest Case with 4 Zones

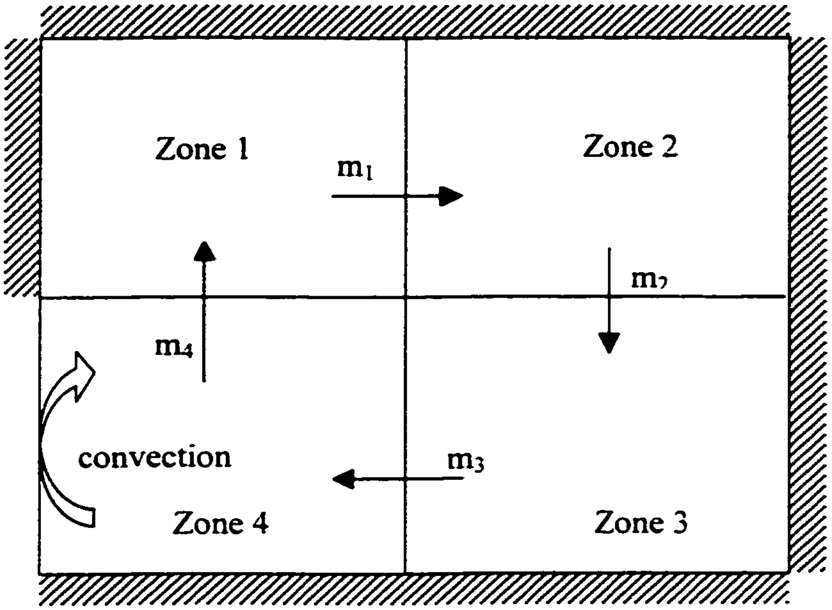

Figure 3.1 the Simplest Case with 4 Zones in the Room

Let us consider the simplest case, in which the room is divided into 4 zones. It is assumed that there is no air exchange between the room and outdoor environment, and there is no heat source in the room. All of the wall surfaces, except the left side of the zone 4, are assumed to be adiabatic.

According to mass balance in each zone, there should be 4 mass balance equations:

Zone 1: $-m_1 + m_4 = 0$ (3-1)

Zone 2: $m_1 - m_2 = 0$ (3-2)

Zone 3: $m_2 - m_3 = 0$ (3-3)

Zone 4: $m_3 - m_4 = 0$ (3-4)

Where, m_i is the mass flow across the boundary, as indicated in Figure 3.1.

Obviously, there are only 3 independent equations in these four equations. If we suppose that all of the boundaries of wall surfaces are adiabatic, which means the heat transfer is only due to the mass flow, the energy balance equations can be expressed as:

Zone 1: $-m_1T_1 + m_4T_4 = 0$ (3-5)

Zone 2: $m_1T_1 - m_2T_2 = 0$ (3-6)

Zone 3: $m_2T_2 - m_3T_3 = 0$ (3-7)

Zone 4: $m_3T_3 - m_4T_4 = 0$ (3-8)

Where, T_i is the temperature of zone i.

Considering (m_i* T_i) to be variables, there are only 3 independent equations in the above systems, i.e. (3-5) to (3-8). Hence, the number of equations is smaller than the number of the unknowns, i.e. the reference pressures and temperatures in each zone. The unique solution of the problem cannot be obtained. It is reasonable since, in the case of room with adiabatic wall surfaces, the airflow pattern is not determined. It depends on the initial flow pattern within the room.

Now suppose that the wall surface in the left boundary of zone 4 is not adiabatic, as indicated in Figure 3.1, the mass balance equations remain unchanged. Nevertheless, the energy balance equation in zone 4 will be changed to:

$$\text{Zone 4: } m_3T_3 - m_4T_4 + hA(T_{out} - T_4) = 0 \qquad (3\text{-}9)$$

Therefore, there are 4 independent energy balance equations in the room. Obviously, if all of the wall surfaces are not adiabatic, there should be also 3 independent mass balance and 4 independent energy balance equations in the room.

3.1.2 The General Case with n Zones

If we extend 4 zones to n zones in the room, assuming there may be some mass inlets and outlets in each zone, the mass balance equations are listed in the following:

$$m_{11} + m_{12} + m_{13} + \ldots + m_{1n} = m_{s1} \qquad (3\text{-}10)$$

$$m_{21} + m_{22} + m_{23} + \ldots + m_{2n} = m_{s2} \qquad (3\text{-}11)$$

$$m_{31} + m_{32} + m_{33} + \ldots + m_{3n} = m_{s3} \qquad (3\text{-}12)$$

....

$$m_{n1} + m_{n2} + m_{n3} + \ldots + m_{nn} = m_{sn} \qquad (3\text{-}13)$$

Where, m_{ij} represents the mass flow from zone j to zone i, (kg/s). It is assumed the mass flow is positive if the actual flow direction is from zone j to zone i. Otherwise, the value is negative.

m_{si} represents the mass source in the zone i. (kg/s)

According to the definition of m_{ij}, there is a relationship between m_{ij} and m_{ji}:

$$m_{ij} = -m_{ji} \tag{3-14}$$

Substituting to mass balance equations from Equation (3-10) to (3-13), we get:

$$m_{11} + m_{12} + m_{13} + \ldots + m_{1n} = m_{s1} \tag{3-15}$$

$$-m_{12} + m_{22} + m_{23} + \ldots + m_{2n} = m_{s2} \tag{3-16}$$

$$-m_{13} - m_{23} + m_{33} + \ldots + m_{3n} = m_{s3} \tag{3-17}$$

....

$$-m_{1n} - m_{2n} - m_{3n} - \ldots + m_{nn} = m_{sn} \tag{3-18}$$

Considering that all of the m_{ij} are the unknown factors in this system, we include all of the m_{ij} into every equation. If in zone i there is no mass flow m_{ij}, m_{ij} gets a coefficient of zero. Consequently, the mass balance equation systems should be written as this:

$$m_{11} + m_{12} + m_{13} + \ldots + m_{1n} + 0 \times m_{22} + 0 \times m_{23} + \ldots + 0 \times m_{2n} + 0 \times m_{33} + \ldots + 0 \times m_{3n} + \ldots + 0 \times m_{nn} = m_{s1}$$

$$0 \times m_{11} - m_{12} + 0 \times m_{13} + \ldots + 0 \times m_{1n} + m_{22} + m_{23} + \ldots + m_{2n} + 0 \times m_{33} + \ldots + 0 \times m_{3n} + \ldots + 0 \times m_{nn} = m_{s2}$$

$$0 \times m_{11} + 0 \times m_{12} - m_{13} + \ldots + 0 \times m_{1n} + 0 \times m_{22} - m_{23} + \ldots + 0 \times m_{2n} + m_{33} + \ldots + m_{3n} + \ldots + 0 \times m_{nn} = m_{s3}$$

....

$$0 \times m_{11} + 0 \times m_{12} + 0 \times m_{13} + \ldots - 1 \times m_{1n} + 0 \times m_{22} + 0 \times m_{23} + \ldots - m_{2n} + 0 \times m_{33} + \ldots - m_{3n} + \ldots + m_{nn} = m_{sn}$$

We can write down the coefficient matrix as:

$$\begin{bmatrix} 1 & 1 & 1 & \ldots & 1 & 0 & 0 & \ldots & 0 & 0 & \ldots & 0 & \ldots & 0 & m_{s1} \\ 0 & -1 & 0 & \ldots & 0 & 1 & 1 & \ldots & 1 & 0 & \ldots & 0 & \ldots & 0 & m_{s2} \\ 0 & 0 & -1 & \ldots & 0 & 0 & -1 & \ldots & 0 & 1 & \ldots & 1 & \ldots & 0 & m_{s3} \\ \ldots & \ldots & \ldots & \ldots & & & & & & & & & & & \\ 0 & 0 & 0 & \ldots & -1 & 0 & 0 & \ldots & -1 & 0 & \ldots & -1 & \ldots & 1 & m_{sn} \end{bmatrix} \tag{3-19}$$

Since $m_{ii} = 0$, the coefficient matrix turn to be.

$$\begin{bmatrix} 0 & 1 & 1 & \ldots & 1 & 0 & 0 & \ldots & 0 & 0 & \ldots & 0 & \ldots & 0 & m_{s1} \\ 0 & -1 & 0 & \ldots & 0 & 0 & 1 & \ldots & 1 & 0 & \ldots & 0 & \ldots & 0 & m_{s2} \\ 0 & 0 & -1 & \ldots & 0 & 0 & -1 & \ldots & 0 & 0 & \ldots & 1 & \ldots & 0 & m_{s3} \\ \ldots & \ldots & \ldots & \ldots & & & & & & & & & & & \\ 0 & 0 & 0 & \ldots & -1 & 0 & 0 & \ldots & -1 & 0 & \ldots & -1 & \ldots & 0 & m_{sn} \end{bmatrix} \tag{3-20}$$

Executing:

$$row(1) = \sum_{i=1}^{n} row(i) \tag{3-21}$$

The coefficient matrix turns to be.

$$\begin{bmatrix} 0 & 0 & 0 & \ldots & 0 & 0 & 0 & \ldots & 0 & 0 & \ldots & 0 & \ldots & 0 & \sum_{i=1}^{n} m_{si} \\ 0 & -1 & 0 & \ldots & 0 & 0 & 1 & \ldots & 1 & 0 & \ldots & 0 & \ldots & 0 & m_{s2} \\ 0 & 0 & -1 & \ldots & 0 & 0 & -1 & \ldots & 0 & 0 & \ldots & 1 & \ldots & 0 & m_{s3} \\ \ldots & \ldots & \ldots & \ldots & & & & & & & & & & & \\ 0 & 0 & 0 & \ldots & -1 & 0 & 0 & \ldots & -1 & 0 & \ldots & -1 & \ldots & 0 & m_{sn} \end{bmatrix} \tag{3-22}$$

In steady state,

$$\sum_{i=1}^{n} m_{si} = 0 \tag{3-23}$$

So that the coefficient matrix is,

$$\begin{bmatrix} 0 & 0 & 0 & \dots & 0 & 0 & 0 & \dots & 0 & 0 & \dots & 0 & \dots & 0 & 0 \\ 0 & -1 & 0 & \dots & 0 & 0 & 1 & \dots & 1 & 0 & \dots & 0 & \dots & 0 & m_{s2} \\ 0 & 0 & -1 & \dots & 0 & 0 & -1 & \dots & 0 & 0 & \dots & 1 & \dots & 0 & m_{s3} \\ \dots & \dots & \dots & \dots & & & & & & & & & & & \\ 0 & 0 & 0 & \dots & -1 & 0 & 0 & \dots & -1 & 0 & \dots & -1 & \dots & 0 & m_{sn} \end{bmatrix} \tag{3-24}$$

This means that there are only (n-1) independent equations in the mass balance equation systems. The lose of the number of independent equations is due to the global mass conservation in n zones.

As to the energy balance equations, since in general cases the heat flow is composed not only of heat carried by mass flow but also by convection, there should be n independent energy balance equations in n zones, as discussed in section 3.1.1. Therefore. there should be (n-1) independent mass balance equations and n independent energy balance equations for n zones. There are totally 2n-1 balance equations.

But generally speaking, if the convective heat fluxes on the wall surfaces can be modeled as a function of air temperatures of adjacent zones, since all the zones are related by interzonal airflow rates, the number of unknowns should be n unknown temperatures and $n*(n-1)/2$ unknown mass flows. In POMA, we take advantage of the power law equation to represent the mass flow in terms of reference pressure in each zone. Thus the unknown factors are n temperatures and n reference pressures in n zones.

Since the power law equation is only concerned with the pressure drop in the path of flow, airflow is only determined by the pressure difference across the boundary. We do not need to know what the absolute pressures are. Thus we can consider the reference pressure difference as unknowns. There are n-1 reference pressure differences in n zones.

In sum, we have 2n-1 independent equations, i.e. n-1 mass balances and n energy balances, for 2n-1 unknown factors. i.e. n temperatures and n-1 reference pressure differences. The number of equations is the same as that of unknowns so that we can apply Newton-Raphson iterative technique to solve the problem.

3.2 Mathematical Solver

The steady-state indoor pattern analysis for POMA requires the simultaneous solution of mass balance equation (2-4) and energy balance equation (2-5) for all zones. Since the functions in Equation (2-4) and Equation (2-5) are nonlinear, a method is needed for the solution of simultaneous nonlinear algebraic equations.

In other zonal models, different numerical methods were applied to solve the nonlinear equations. For example, Broyden's method was used in Inard's pressure zonal model (Inard et al, 1996), Gear-Adams method was used for the resolution in BTHEBES model (Gschwind et al, 1996) and Newton-Raphson was used in Rodriguez's pressure zonal models (Rodriguez and Allard, 1995).

In the two most popular multizone models, COMIS and CONTAM, Newton-Raphson method was used to solve the nonlinear systems (Haghighat and Megri. 1996). The successful performances of these two models demonstrate that Newton-Raphson is a suitable numerical technique for nonlinear systems.

In POMA, the Newton-Raphson global convergence technique was selected to solve the nonlinear equation systems mentioned above. Newton-Raphson method solves the nonlinear problem by an iteration of the solutions of linear equations.

Illustrated in (Press et al, 1992), Newton-Raphson method is as follow. A typical problem gives N functional relations to be zero, involving variables x_i, i=1, 2, ..., N:

$$F_i(x_1, x_2, ..., x_N) = 0 \qquad i = 1,2,...,N. \tag{3-25}$$

In the neighborhood of x, each of the functions F_i can be expanded in Taylor series

$$F_i(\mathbf{X}+\delta\mathbf{X}) = F_i(\mathbf{X}) + \sum_{j=1}^{N} \frac{\partial F_i}{\partial x_j}\delta x_j + O(\delta\mathbf{X}^2) \tag{3-26}$$

Where, **X** is the entire vector of values x_i,

In matrix notation, Equation (3-26) is expressed as:

$$\mathbf{F}(\mathbf{X}+\delta\mathbf{X}) = \mathbf{F}(\mathbf{X}) + \mathbf{J}\cdot\delta\mathbf{X} + O(\delta\mathbf{X}^2) \tag{3-27}$$

Where, **F** is the entire vector of functions F_i, and

J is the Jacobian matrix:

$$J_{ij} = \frac{\partial F_i}{\partial x_j} \tag{3-28}$$

By neglecting terms of order δx^2 and higher, and by setting $\mathbf{F}(\mathbf{x}+\delta\mathbf{x})=0$. a full Newton step, which moves each function closer to zero, can be obtained as:

$$\delta\mathbf{X} = -\mathbf{J}^{-1}\cdot\mathbf{F} \tag{3-29}$$

The corrections are then added to the solution vector,

$$\mathbf{X}_{new} = \mathbf{X}_{old} + \delta\mathbf{X} \tag{3-30}$$

and the process is iterated to convergence. However, as well-known, this general Newton-Raphson method will fail if the initial guess is not sufficiently close to the root. Moreover, numerical tests of the Newton-Raphson method solution indicated occasional instances of very slow convergence as the iterations almost oscillate between two different sets of values (Walton, 1993)

Thus, a line searches and backtracking method was selected to find a proper step of variations.

$$\mathbf{X}_{new} = \mathbf{X}_{old} + \lambda\delta\mathbf{X}, \qquad 0 < \lambda \le 1 \tag{3-31}$$

Where, λ is the coefficient for the acceptable step.

The aim is to find λ so that $F_i(\mathbf{X}_{old}+\lambda\delta\mathbf{X})$ has decreased sufficiently. Until the early 1970s, standard practice was to choose λ so that x_{new} exactly minimizes F_i in the direction $\delta\mathbf{X}$. The multizone model, CONTAM, uses this technique (Walton, 1993). However, it is extremely wasteful of function evaluations to do so. A new improved strategy in (Press et al, 1992) is: First try the full Newton step, $\lambda=1$. This will lead to quadratic convergence when $\mathbf{X}$ is sufficiently close to the roots. If $F_i(\mathbf{X}_{new})$ does not meet the acceptance criteria, we backtrack along the Newton direction, trying a smaller value of λ, until a suitable point is found. Here, the criterion for the acceptable step is:

$$f(\mathbf{X}_{new}) \le f(\mathbf{X}_{old}) + \alpha \nabla f \cdot (\mathbf{X}_{new} - \mathbf{X}_{old}) \qquad (3\text{-}32)$$

The choice of λ is based on the following rules. First, try λ = 1, if this step is not acceptable, try

$$\lambda = -\frac{g^{'}(0)}{2[g(1) - g(0) - g^{'}(0)]} \qquad (3\text{-}32)$$

Where:

$$g(\lambda) = f(\mathbf{X}_{old} + \lambda \delta \mathbf{X}) \qquad (3\text{-}33)$$

On the second and subsequent backtracks,

$$\lambda = \frac{-b + \sqrt{b^2 - 3ag^{'}(0)}}{3a} \qquad (3\text{-}34)$$

Where,

$$\begin{bmatrix} a \\ b \end{bmatrix} = \frac{1}{\lambda_1 - \lambda_2} \begin{bmatrix} 1/\lambda_1^2 & -1/\lambda_2^2 \\ -\lambda_2/\lambda_1^2 & \lambda_1/\lambda_2^2 \end{bmatrix} \bullet \begin{bmatrix} g(\lambda_1) - g^{'}(0)\lambda_1 - g(0) \\ g(\lambda_2) - g^{'}(0)\lambda_2 - g(0) \end{bmatrix} \qquad (3\text{-}35)$$

Where,

λ_1 and λ_2 are the previous and recent value from Equation (3-32)

More detail of linear searches and backtracking of λ can be found in (Press et al. 1992).

Chapter 4

Simulation Results and Validations

4.1 Case Studies Selection

In the previous two chapters, a detailed illustration of POMA including the modeling approach and solution techniques has been given. In this chapter, POMA was applied to simulate rooms under different ventilation strategies, i.e. natural and forced ventilation. POMA predictions were then compared with measurement and/or CFD model prediction.

In natural ventilation, two cases were selected. The first is a window problem to predict the stratification pattern. A CFD simulation result was provided to validate the zonal model prediction. The second case was a MINIBAT test cell used by Inard to validate his zonal model (Inard et al, 1996). We compared POMA prediction with his zonal model prediction, CFD prediction and measurement data. In both cases, the CFD prediction was carried out using FLOVENT (CFD model) (Jiang, 1998).

In forced ventilation, there are three cases for the validation. The first one is the cross ventilation with isothermal jet used by Rodriguez to validate his zonal model (Rodriguez and Allard, 1995). A comparison with CFD model was presented. The second one is the same cross ventilation but with non-isothermal jet, in order to demonstrate POMA's capability of predicting the influence of the thermal buoyancy. The third case study is a 2D room with isothermal ceiling-jet. This case was used by Huo to validate his refined CFD model (Huo, 1997).

4.2 Natural Ventilation

4.2.1 Window Problem

The first case study is a window problem for stratification prediction in a steady state condition. The test room is a two dimensional rectangular room with the dimension of 6.0×2.4m(L×H). Each wall is assumed to have a uniform temperature on the inside surface. There are cold and hot vertical walls opposite to each other. The temperature of the ceiling and floor is the same. The thermal parameters of the walls are listed in Table 4-1.

Wall	Length (m)	Surface Temperature (°C)	Convection coefficient (W/m^2K)
Top	6.0	15	5.7
Bottom	6.0	15	1.0
Left	2.4	12	4.2
Right	2.4	20	4.2

Table 4-1 Input Data for the Window Problem

The room is simulated with different sizes of uniform meshes, from 4×4 to 8×8. The convergence error of mass balance and heat balance is set to 1.0 ×E-05. In fact, the energy balance is made up of two parts, convection on the wall surfaces and heat flows carried by mass flows. The heat flows carried by mass flows are very sensitive to the mass flows since the specific heat of air, C_p, is equal to 1005W/kg K. Hence, if the energy balance satisfies the convergence criteria, 1.0E-05, the convergent error of mass balance will usually reach 1.0E-09.

4.2.1.1 Temperature Distribution

Figures 4.1 to 4.3 are the temperature distribution results simulated by POMA. The CFD prediction is presented in Figure 4.4. A temperature stratification in the room is demonstrated in these figures. The highest and the lowest temperatures are detected in the upper-right and lower-left corner, respectively, predicted by both POMA and CFD, though the values are not exactly the same.

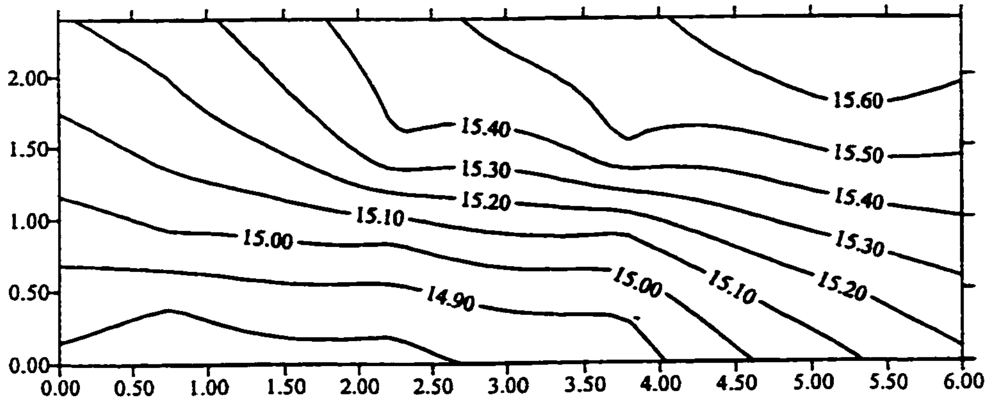

Figure 4.1 Temperature (°C) Distribution Simulated by POMA for Window Problem, 4×4 zones

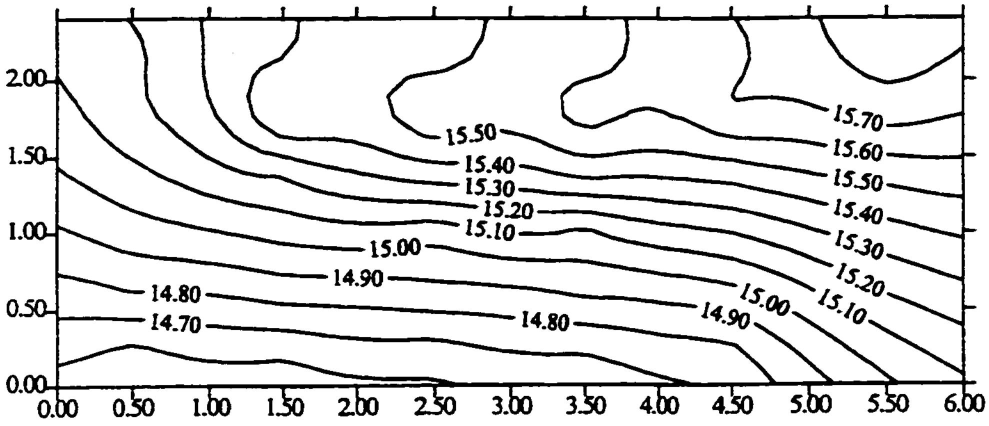

Figure 4.2 Temperature (°C) Distribution Simulated by POMA for Window Problem, 6×6 zones

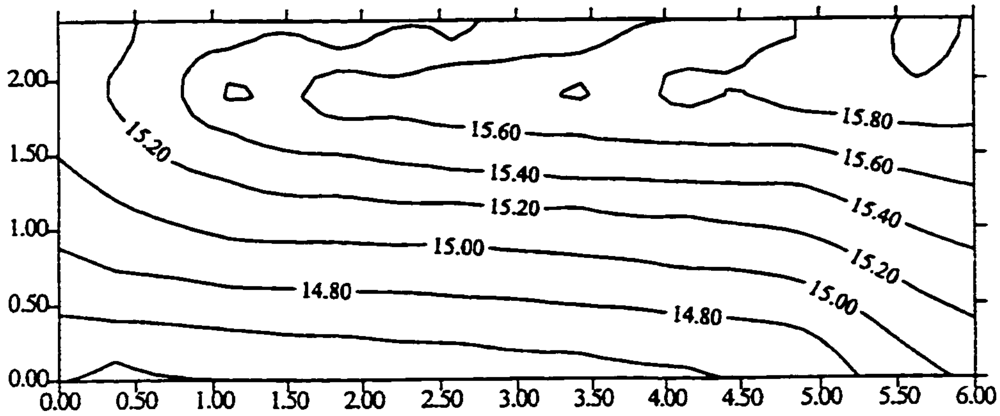

Figure 4.3 Temperature (°C) Distribution Simulated by POMA for Window Problem, 8×8 zones

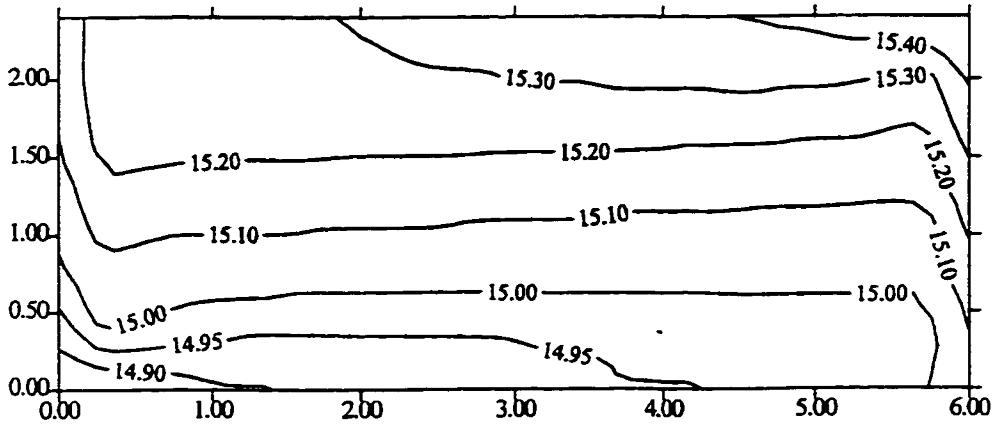

Figure 4.4 Temperature (°C) Distribution Simulated by CFD Model for Window Problem, 36×36 zones, (Jiang, 1998)

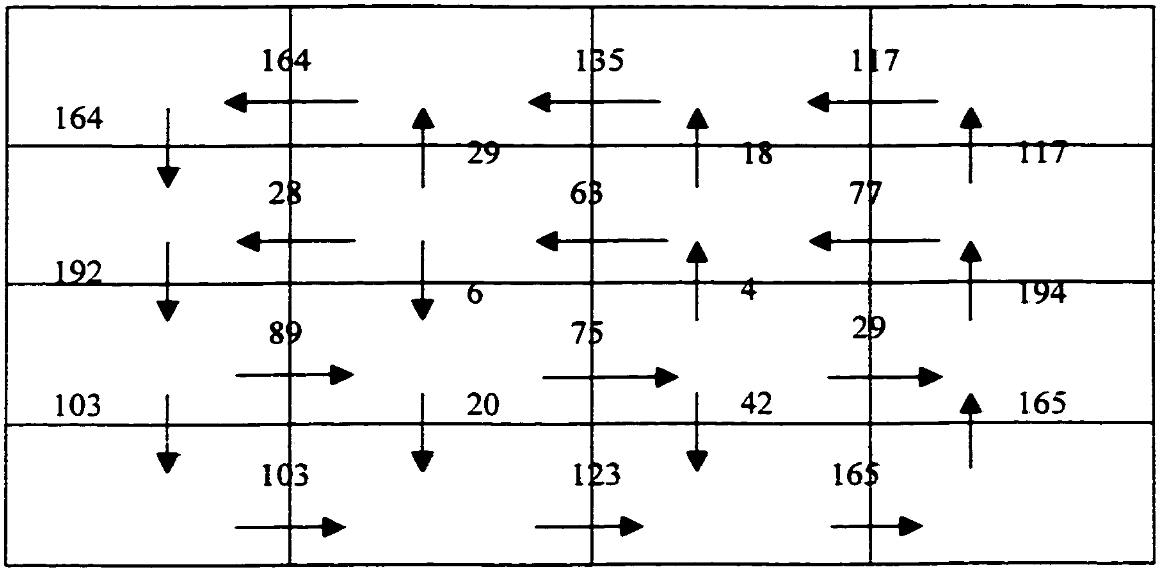

Figure 4.5 Airflow (kg/h) Distribution Simulated by POMA for the Window Problem, 4×4 zones

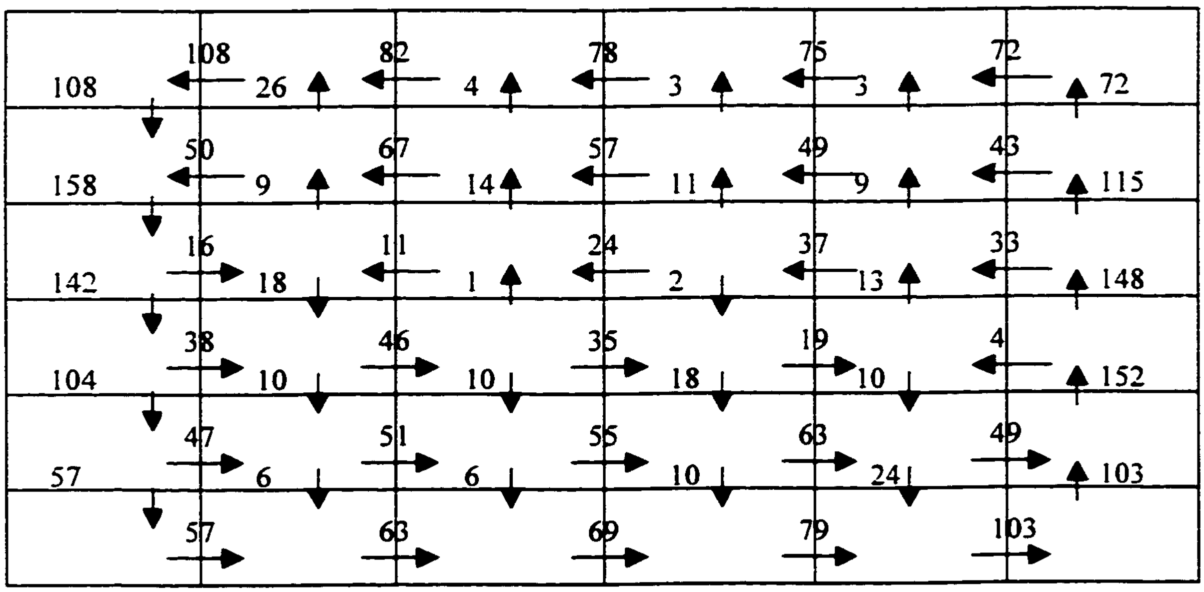

Figure 4.6 Airflow (kg/h) Distribution Simulated by POMA for the Window Problem, 6×6 zones

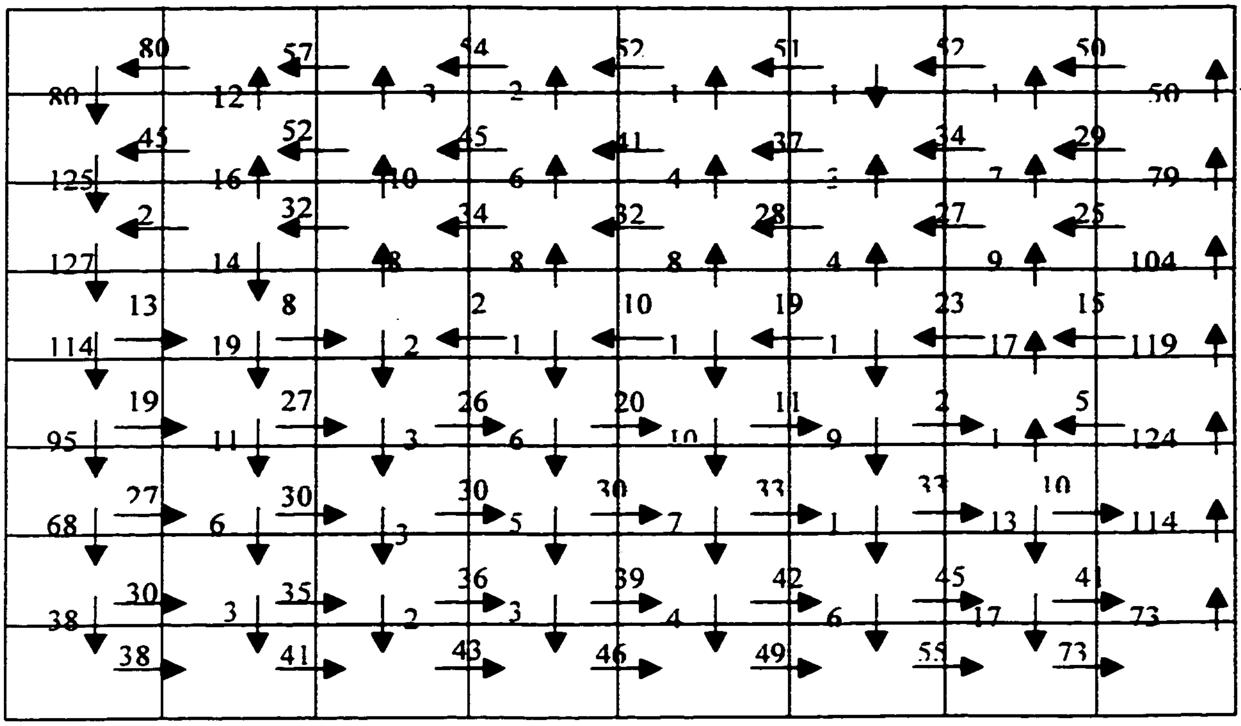

Figure 4.7 Airflow (kg/h) Distribution Simulated by POMA for the Window Problem, 8×8 zones

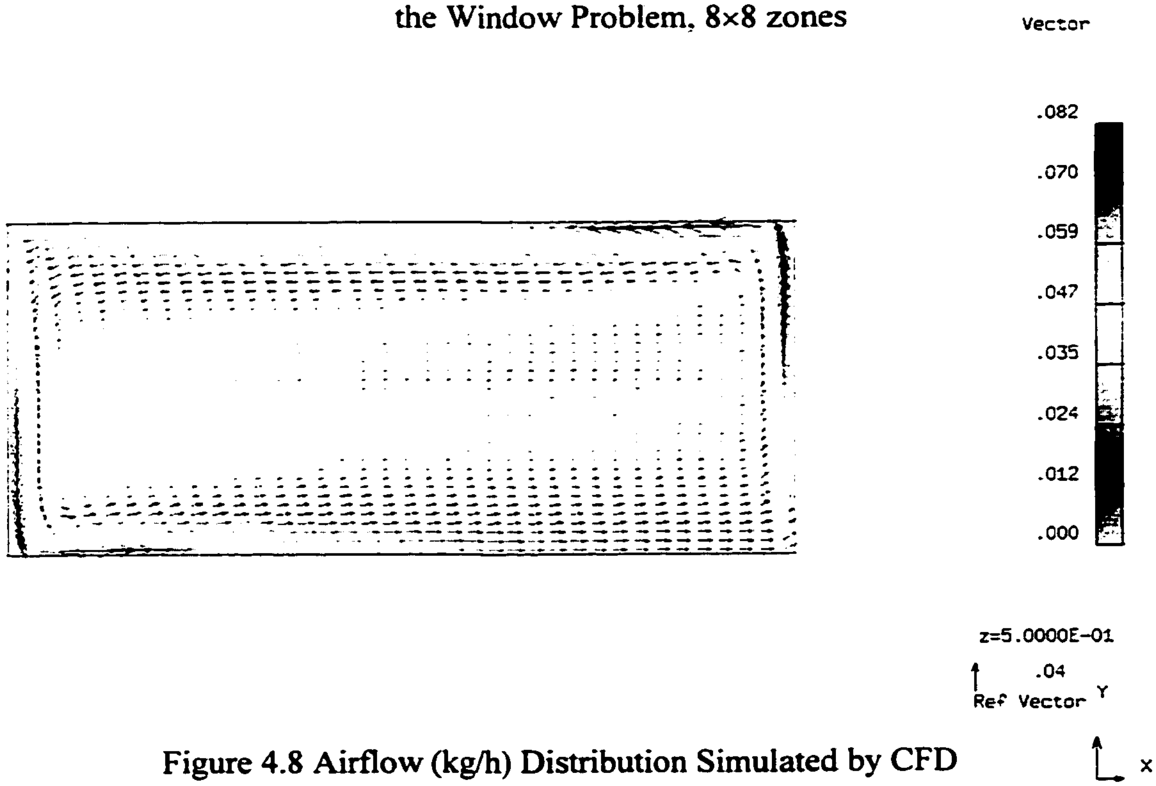

Figure 4.8 Airflow (kg/h) Distribution Simulated by CFD Model for the Window Problem, 36×36 zones, (Jiang, 1998)

4.2.1.2 Airflow Distribution.

The airflow distribution results simulated by POMA are presented in Figures 4.5 to 4.7, with the uniform mesh from 4×4 to 8×8. The arrow direction indicates the airflow direction. The prediction made by a CFD model, with 36×36 uniform mesh, is also presented in Figure 4.8. It is detected that, in these figures, an upward flow along the hot wall and a downward flow along the cold wall generate a large circulation along the walls. Moreover, in all of these figures, it is shown that the amount of airflow near the wall surface is much larger than the amount of airflow in the middle of the room. From these figures, we can see that the airflow pattern predicted by POMA agrees well with the prediction of CFD model (Jiang, 1998).

The comparison above indicates that, in the window problem, the airflow and temperature distributions predicted by POMA are similar to those predicted by CFD model.

4.2.1.3 Predicted Mean Vote (PMV) Distribution.

To demonstrate the application of POMA, we apply POMA in the evaluation of thermal comfort. It is noted that some researchers, such as Wurtz (1995), Inard et al (1994) and (Chao et al, 1998), have used PMV or PPD (Predicted Percent of Dissatisfied), which is related to PMV, to evaluate the thermal comfort in different zones. For the purpose of comparison and consistence with previous works, we choice PMV as an index to evaluate the thermal comfort.

The PMV index predicts the mean response of a large group of people according to the ASHRAE thermal sensation scale. The scale of PMV is from –3 (cold) to +3 (hot). It can be calculated based on Fanger's model (ASHRAE Fundamental, 1993):

$$PMV = [0.303\exp(-0.036M) + 0.028]L \qquad (4\text{-}1)$$

Where,

$$\begin{aligned} L = {} & (M-W) - 3.96\times10^{-8} f_{cl}[(t_{cl}+273)^4 - (t_r+273)^4] \\ & - f_{cl}h_c(t_{cl}-t_a) - 3.05[5.73 - 0.007(M-W) - P_a] \\ & - 0.42[(M-W) - 58.15] - 0.0173M(5.87 - P_a) \\ & - 0.0014M(34 - t_a) \end{aligned} \qquad (4\text{-}2)$$

Where,

M : rate of metabolic heat production, W/m^2

W : rate of mechanical work accomplished, W/m^2

f_{cl} : clothing area factor, dimensionless

h_c : heat transfer coefficient of convection at surface, $W/(m^2K)$

P_a : vapour pressure, kPa

t_{cl} : temperature of clothing surface, °C

t_r : mean radiant temperature, °C

t_a : air temperature, °C

Iclo: thermal resistance of clothes, (clo)

-0.807	-0.851	-0.811	-0.560
-1.069	-1.115	-1.070	-0.830
-1.099	-1.193	-1.155	-0.871
-0.910	-0.982	-0.947	-0.702

Figure 4.9 PMV Distribution Simulated by POMA for the Window Problem, 4×4 zones

-0.656	-0.753	-0.760	-0.728	-0.649	-0.388
-0.910	-0.990	-0.993	-0.969	-0.899	-0.594
-1.012	-1.148	-1.134	-1.104	-1.037	-0.696
-1.040	-1.186	-1.204	-1.181	-1.089	-0.732
-0.999	-1.139	-1.149	-1.125	-1.055	-0.704
-0.810	-0.921	-0.927	-0.905	-0.838	-0.536

Figure 4.10 PMV Distribution Simulated by POMA for the Window Problem, 6×6 zones

Figures 4.9 and 4.10 present the PMV predictions of POMA, for a seated person involving in light office activity (M=120W/m^2, W=0), dressing trouser, long-sleeve shirt, long-sleeve sweater, T-shirt (Iclo=1.01clo), in an environment with 50% humidity. It was shown that the average person under this circumstance would feel neutral to slightly cool at different locations of the room.

4.2.2 MINIBAT Test Cell

The second case study is a MINIBAT test cell in CETHIL (Centre de Thermique de l'INSA de Lyon) which was used to collect data for natural convection and mixed convection in a steady state condition (Inard et al, 1996) and (Allard et al, 1987). Inard used these experimental data to validate his Pressure Zonal Model, which has been illustrated in section 2.4.3. The experimental results, prediction of Inard's zonal model with 2D (6×1×10) mesh and prediction of CFD with 3D (41×51×41) mesh are presented in Figures 4.12 to 4.15 for the purpose of comparison with the prediction of POMA.

The MINIBAT test cell consists of a 24m^3 (3.1×3.1×2.5m) single volume in which the temperature is kept constant on five faces owing to another volume used as a thermal guard. The sixth face (facing south) is in contact with a climatic caisson which allows us to obtain air temperatures ranging from –10 to +40°C with a stability ±0.2°C. (Inard et al, 1996)

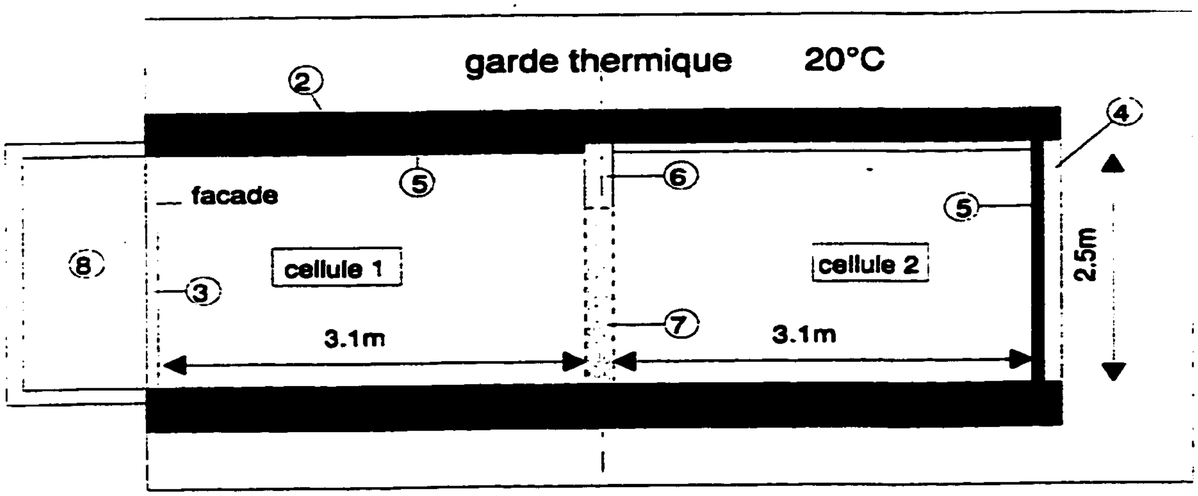

Figure 4.11 Configuration of MINIBAT Cell (Inard, 1996)

Figure 4.11 shows the configuration of MINIBAT Cell in 2D. The experiment was conducted in only one cell.

4.2.2.1 Four Cases without Heat Sources in the Room.

With 2D ($6\times1\times10$) mesh, POMA was applied to four cases of natural Ventilation:

Case 1: one cold active vertical face;

Case 2: one cold active vertical face, the face opposite being heated;

Case 3: one cold active vertical face, the floor being heated;

Case 4: one cold active vertical face, the ceiling being heated.

The measured values of inside wall surface temperature are listed in Table 4-2.

Wall	South	North	East	West	Ceiling	Floor
Case 1	6.0	13.9	14.1	14.1	13.5	11.8
Case 2	16.9	33.0	26.9	27.3	28.5	25.9
Case 3	15.3	29.1	26.1	26.2	26.0	27.6
Case 4	11.2	23.8	23.5	23.7	42.1	21.1

Table 4-2 Wall Surface Temperature (°C) of Four Cases of Natural Ventilation for MINIBAT Test Cell

4.2.2.1.1 Temperature Distribution

Figures 4.12 to 4.15 present the temperature results of four methods, i.e. POMA, Inard's zonal model, CFD model and the experimental results. The CFD results are the temperature distribution on a plane in the middle of east and west direction. In these figures, it is shown that temperature prediction of POMA fits other results very well.

In case 1, it is detected by POMA that there is temperature stratification in the middle of the room and temperature gradient near the wall. These observations agree with the prediction of CFD and measurement data. Moreover, the ranges of temperature distribution in these four figures are similar, from 11 to 13.5 °C.

In case 2, the similar temperature distribution in the room is also detected in the four figures.

In case 3, experimental data show that it is almost isothermal in the room while in both of the zonal models and CFD model the temperature gradients are detected.

In case 4, all of the four results indicate that there is a very high thermal gradient at the top of the room. Compared with Inard's model, POMA can reflect the temperature gradient near the walls, which is similar to the experimental results and CFD prediction.

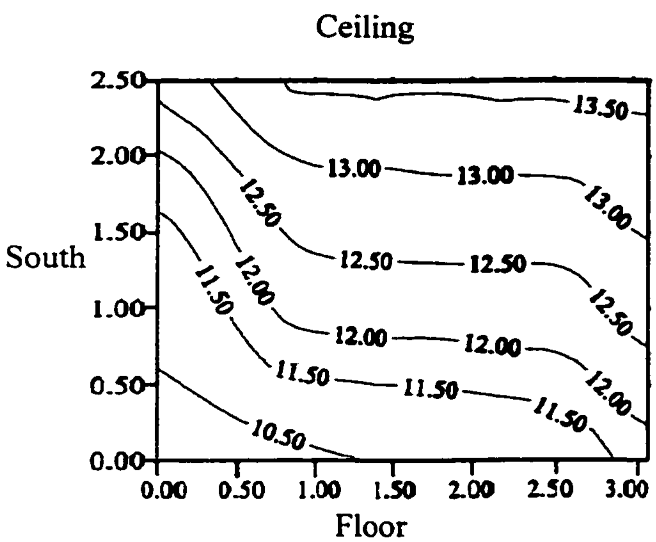

POMA (6×1×10 zones)

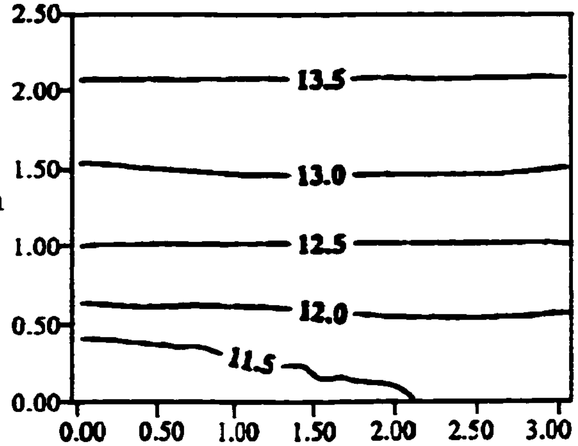

Inard's Zonal Model(6×1×10 zones)

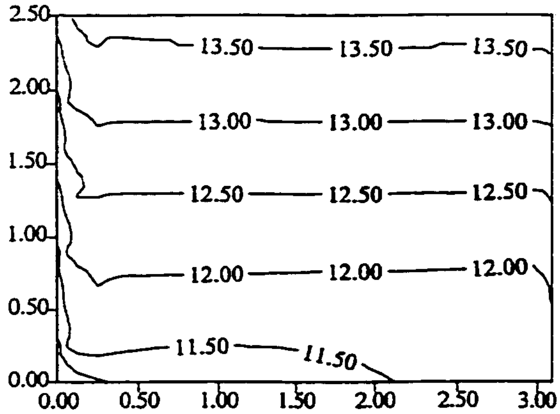

CFD Model (41×51×41 zones)
by Jiang

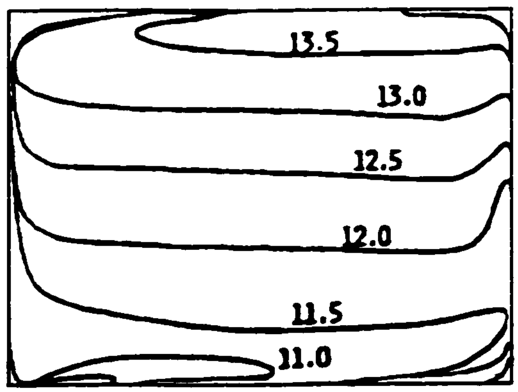

Experiment Results by Allard

Figure 4.12 Temperature (°C) Distribution of Case 1 in MINIBAT Cell

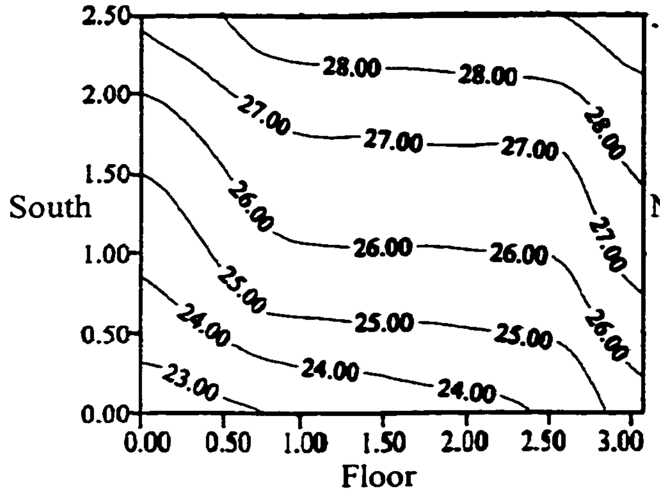

POMA (6×1×10 zones)

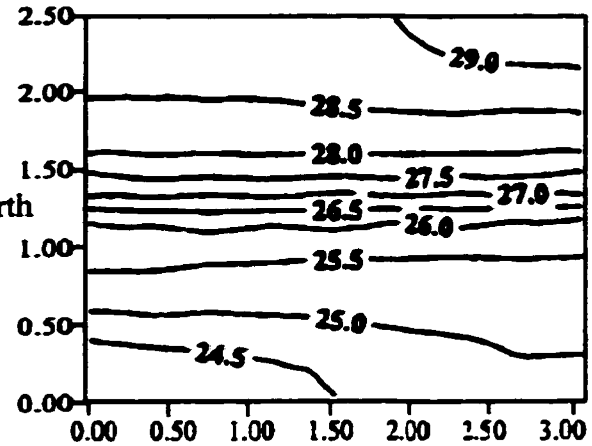

Inard's Zonal Model (6×1×10 zones)

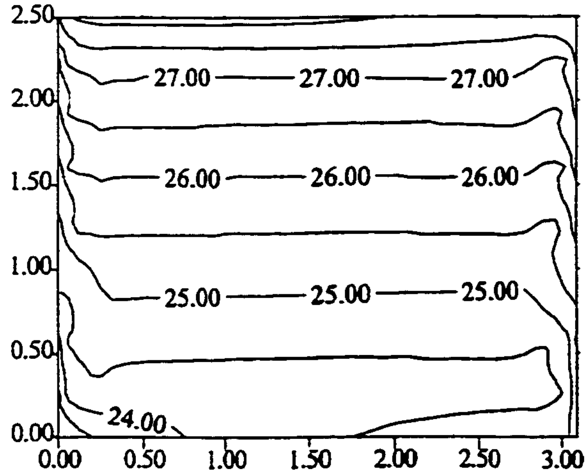

CFD Model (41×51×41 zones)
by Jiang

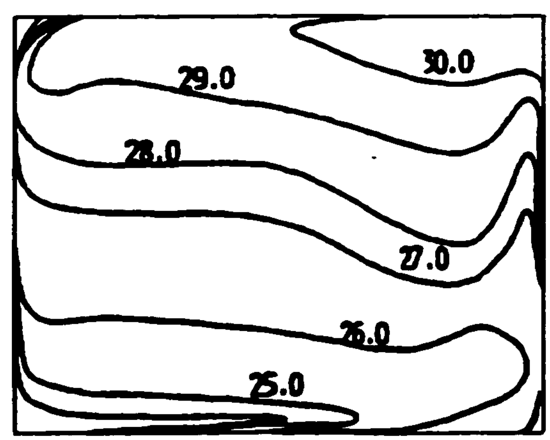

Experimental Results by Allard

Figure 4.13 Temperature (°C) Distribution of Case 2 in MINIBAT Cell

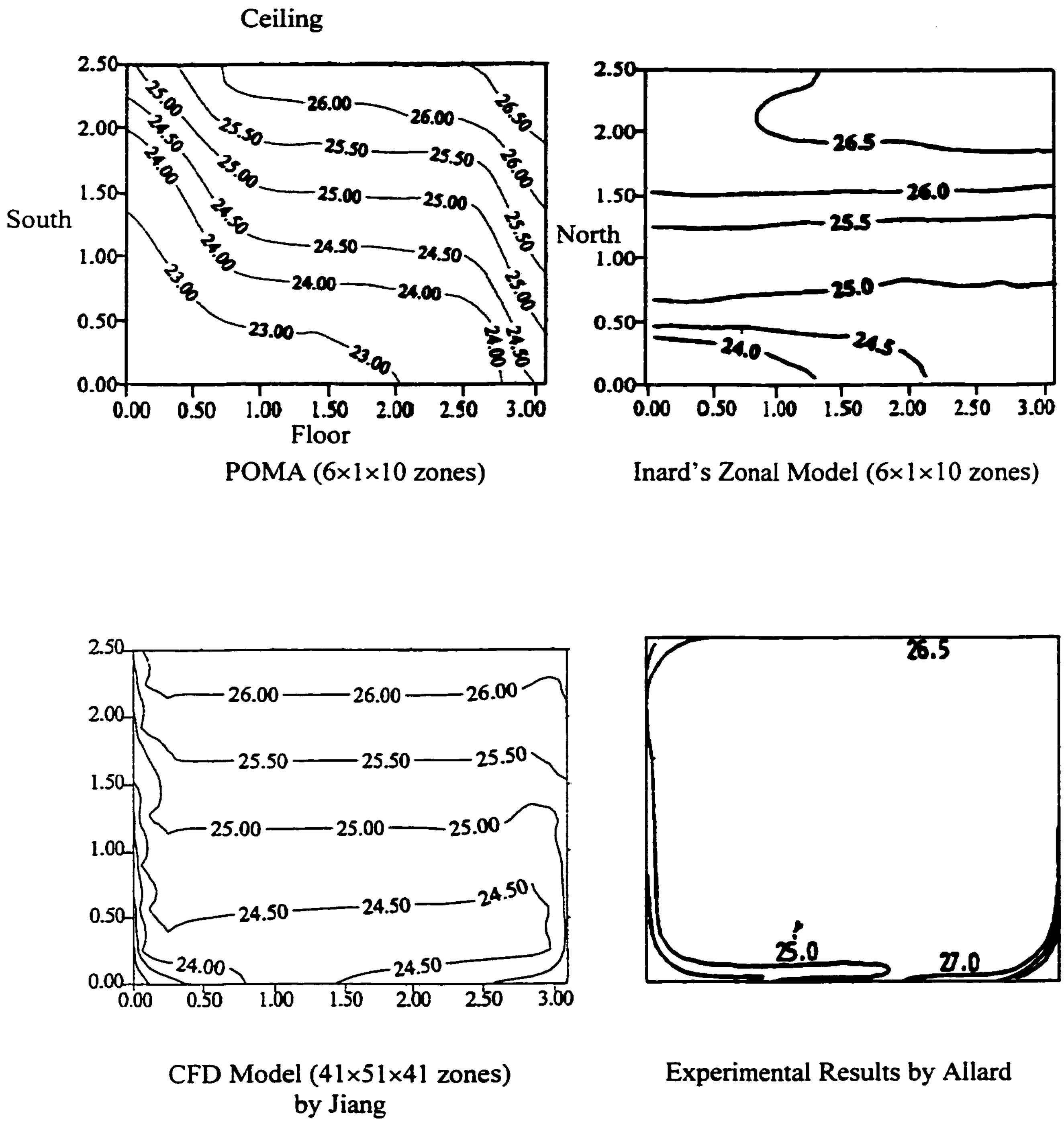

POMA (6×1×10 zones)

Inard's Zonal Model (6×1×10 zones)

CFD Model (41×51×41 zones) by Jiang

Experimental Results by Allard

Figure 4.14 Temperature (°C) Distribution of Case 3 in MINIBAT Cell

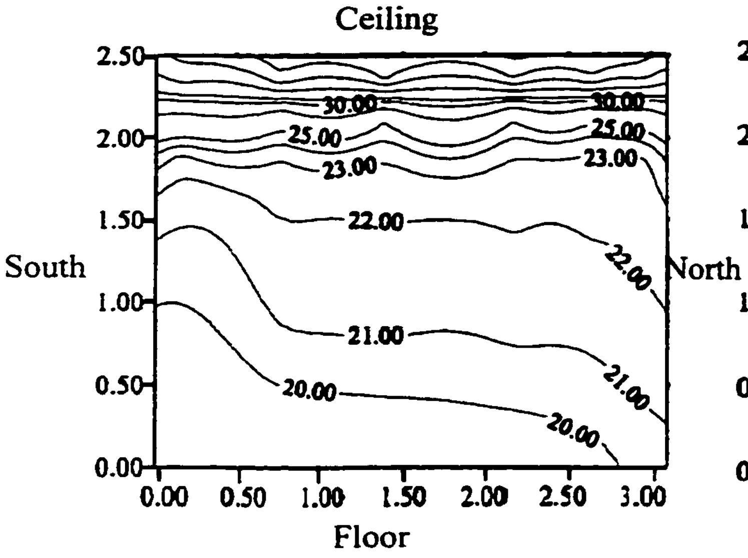

POMA (6×1×10 zones)

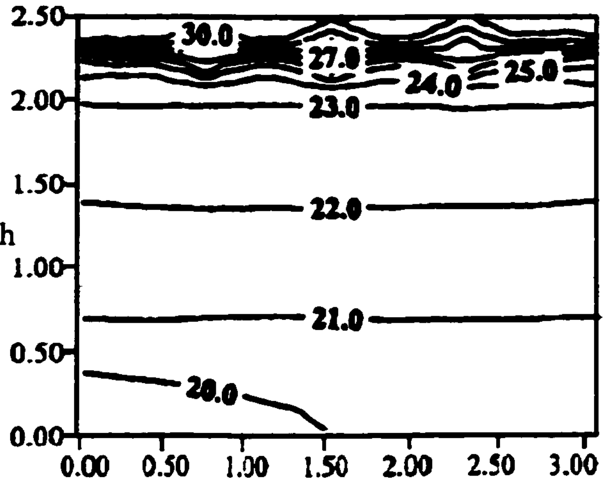

Inard's Zonal Model (6×1×10 zones)

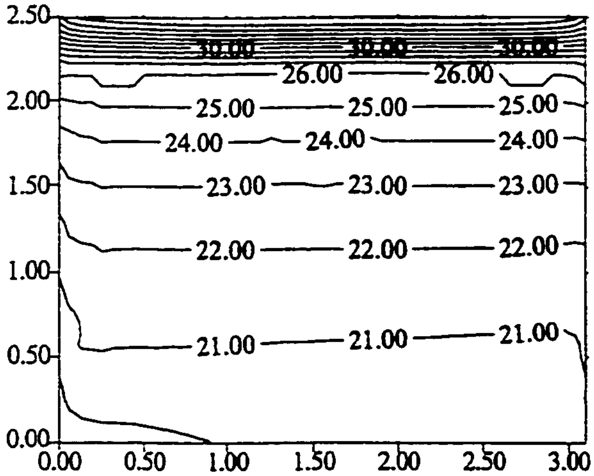

CFD Model (41×51×41 zones)
by Jiang

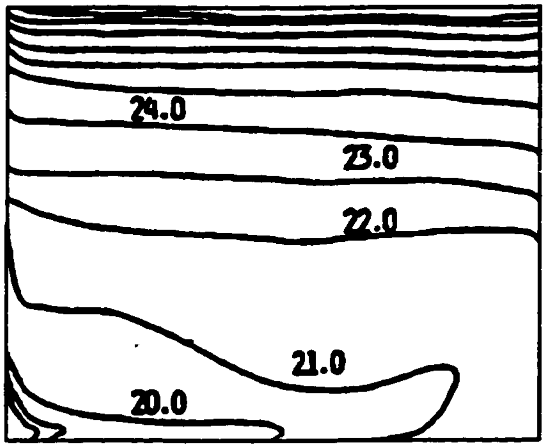

Experiment Results by Allard

Figure 4.15 Temperature (°C) Distribution of Case 4 in MINIBAT Cell

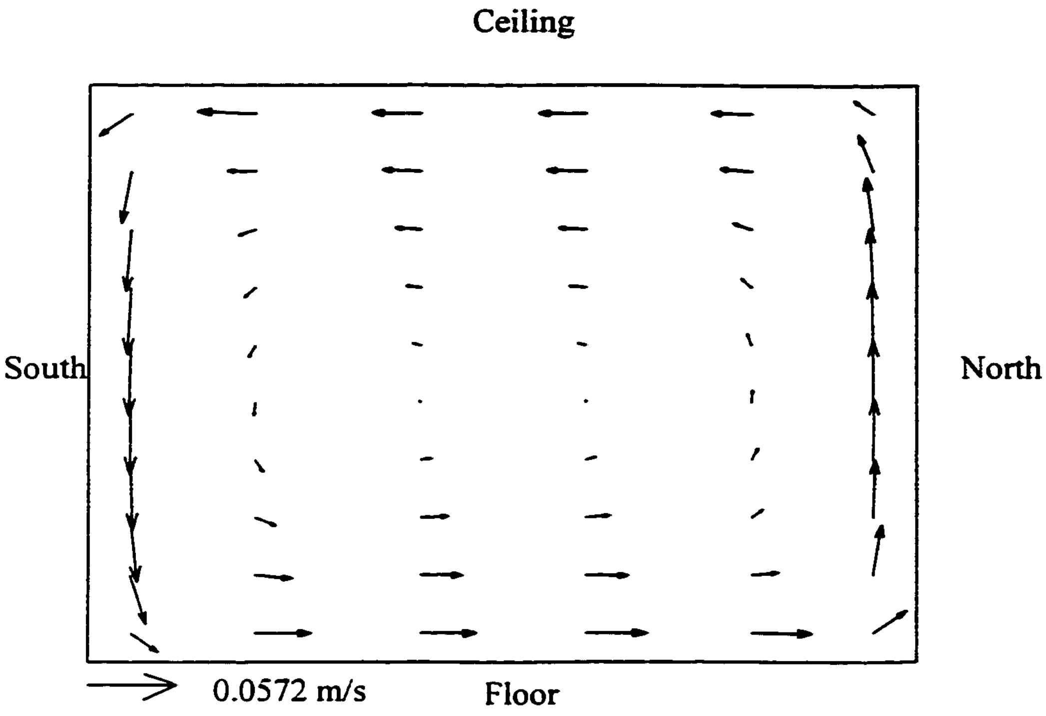

Prediction of POMA

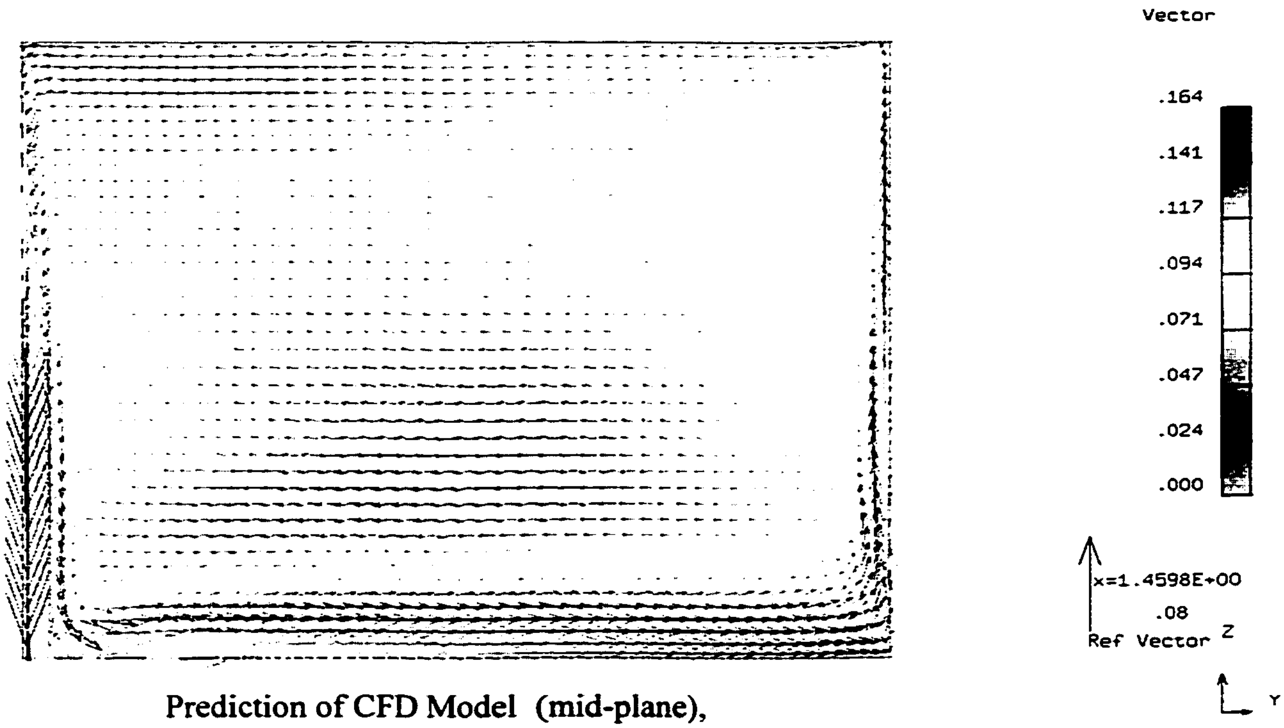

Prediction of CFD Model (mid-plane),
(Jiang, 1998)

Figure 4.16 Airflow Pattern of Case 1 in MINIBAT Cell

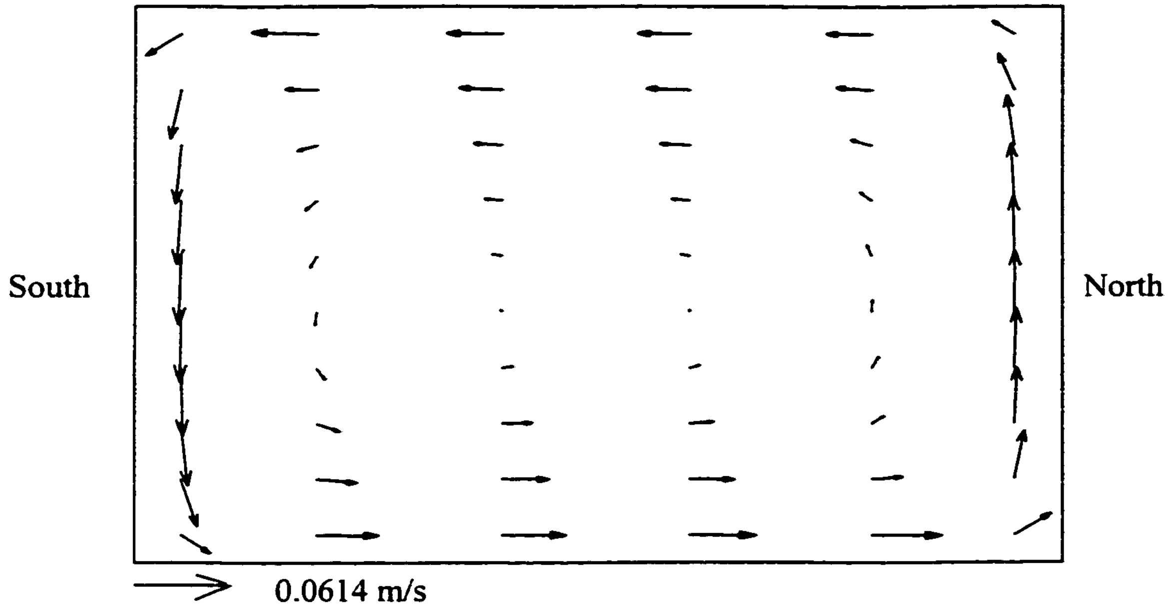

Prediction of POMA

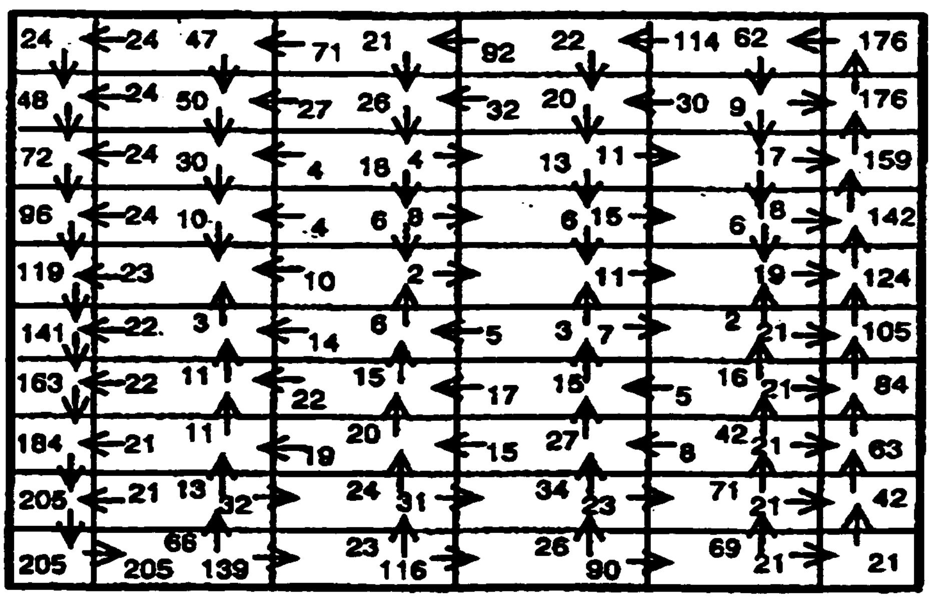

Prediction of Inard's Zonal Model

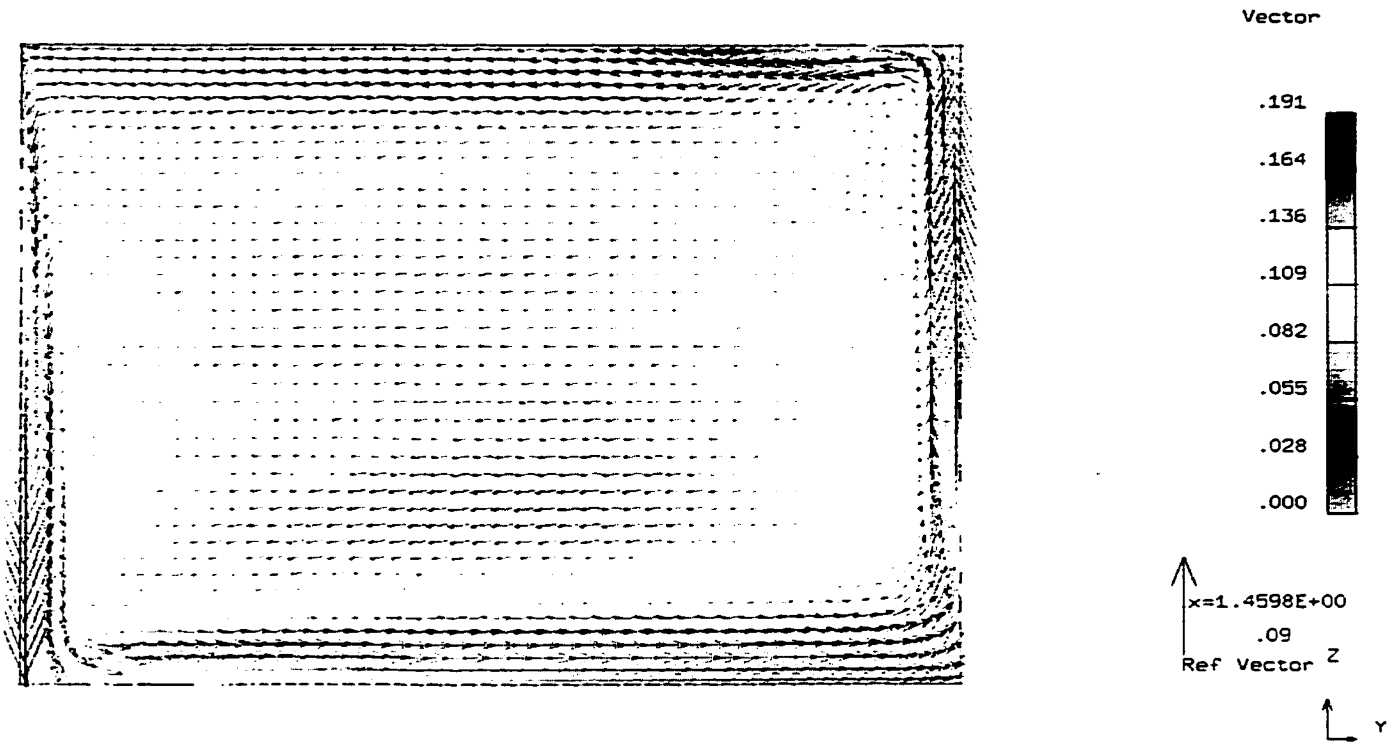

Prediction of CFD Model (Jiang, 1998)

Figure 4.17 Airflow pattern of Case 2 in MINIBAT Cell

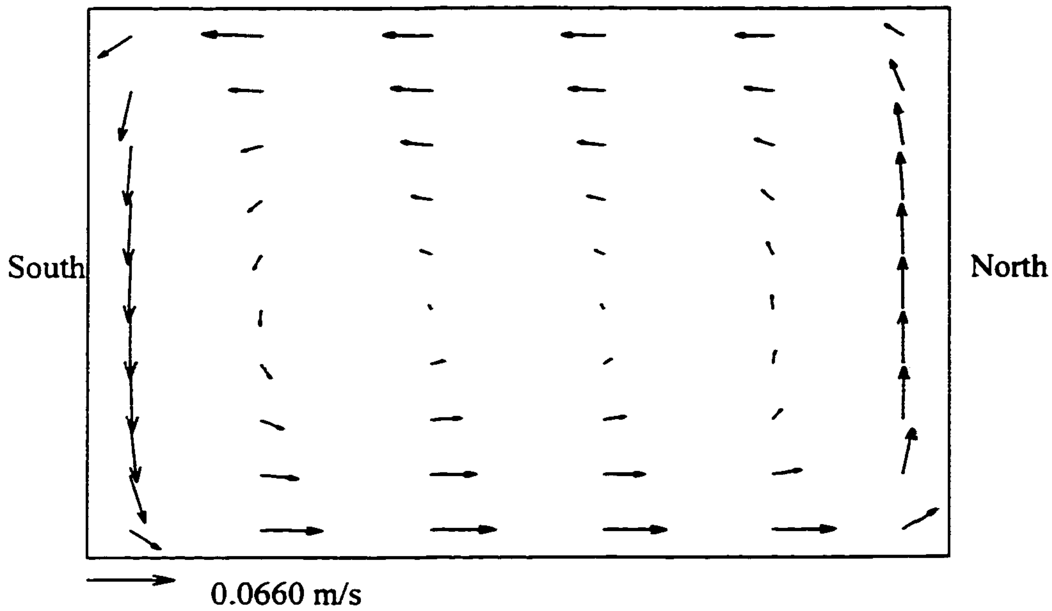

Prediction of POMA

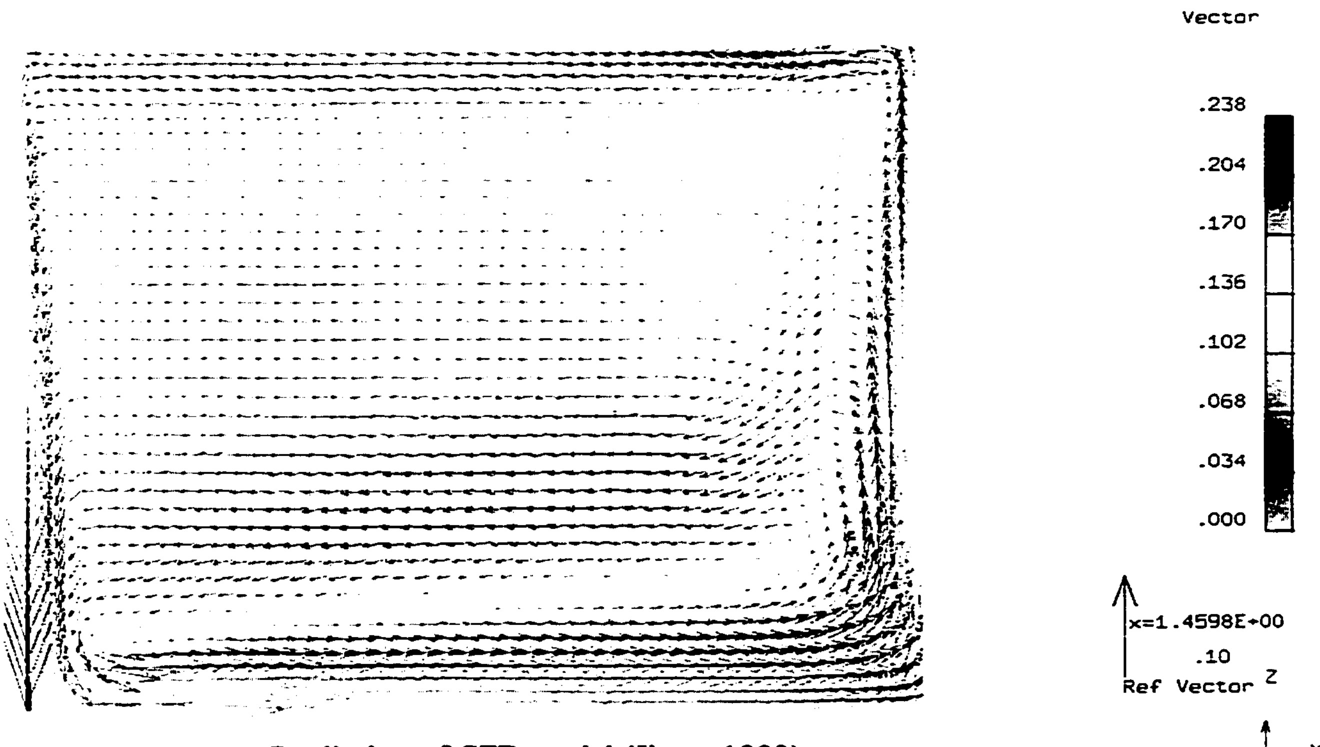

Prediction of CFD model (Jiang, 1998)

Figure 4.18 Airflow pattern of Case 3 in MINIBAT Cell

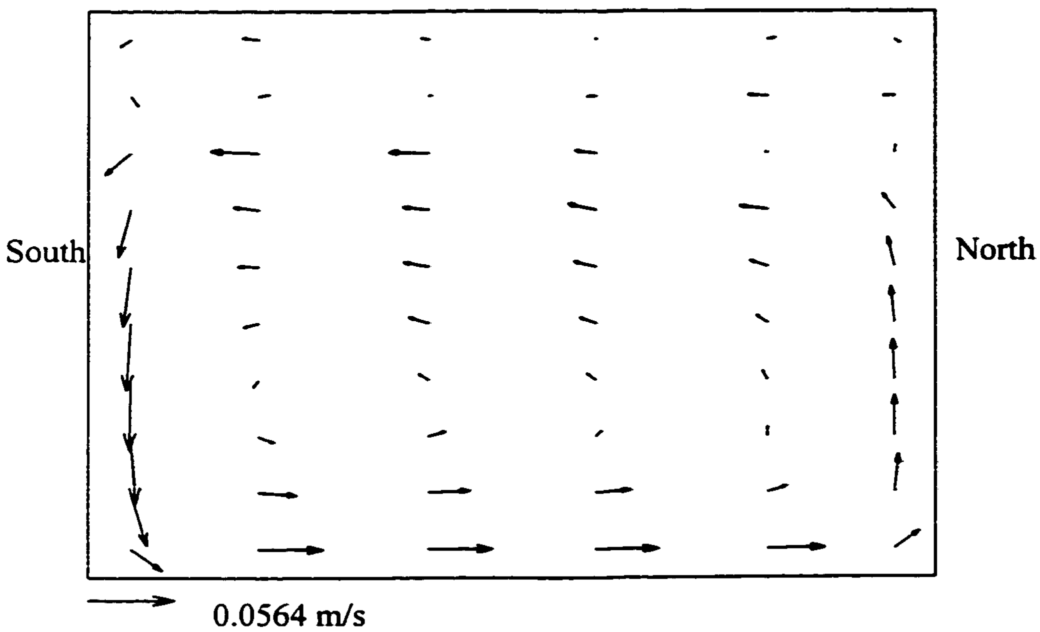

Prediction of POMA

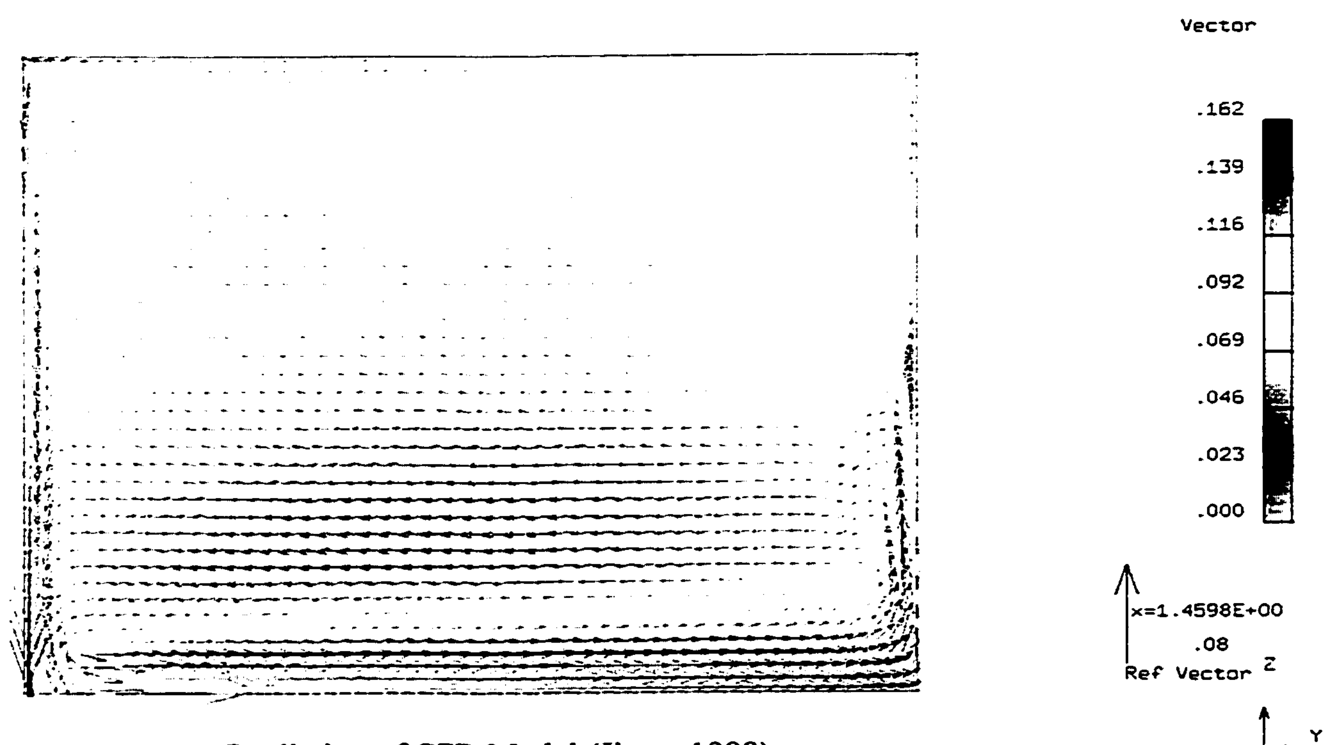

Prediction of CFD Model (Jiang, 1998)

Figure 4.19 Airflow pattern of Case 4 in MINIBAT Cell

4.2.2.1.2 Airflow Distribution

Figures 4.16 to 4.19 are the airflow pattern predicted by POMA and CFD model (Jiang, 1998). For the convenience of comparison, we presented the airflow in velocity vectors, as in CFD figures. The velocity was calculated using the following rules:

$$zone\_v = \frac{\sqrt{(top\_v + bottom\_v)^2 + (west\_v + east\_v)^2 + (south\_v + north\_v)^2}}{2} \tag{4-3}$$

Where,

zone_v : velocity of zone (m/s), as shown in the Figure 4.16 to Figure 4.19.

top_v : velocity across the top boundary of zone, (m/s)

bottom_v : velocity across the bottom boundary of zone, (m/s)

west_v : velocity across the west boundary of zone, (m/s)

east_v : velocity across the east boundary of zone, (m/s)

south_v : velocity across the south boundary of zone, (m/s)

north_v : velocity across the north boundary of zone, (m/s)

These velocities across the boundary can be calculated based on the mass flow across the boundary:

$$v = \frac{m}{\rho A} \tag{4-4}$$

Where, v : velocity across boundary, (m/s). It is a vector whose positive direction is consistent with the coordinators, m : mass flow rate across the boundary, (kg/s)

ρ : density of zone from which air flow in, (kg/m^3)

A : area of boundary, (m^2)

Comparing the predictions of POMA and CFD model, we can see a global prediction of airflow pattern similar to that of CFD can be achieved in POMA.

In Figure 4.16 for Case 1, it was detected in both models that there was an anti-clockwise circulation in the room. The main streams of flow are always near the walls in both models.

In Figure 4.17 for Case 2, the predictions of POMA and CFD are similar to each other. Figure 4.17 also lists the airflow pattern predicted by Inard's zonal model. In his model, the airflow pattern was detected to be two circles. One is near the wall surface in anti-clockwise direction, and the other is in the middle of the room in the other direction. It did not agree with prediction of CFD or POMA.

In Figure 4.18 for Case 3, as in Figure 4.16 and 4.17, an anti-clockwise circulation was detected in both of models.

In Figure 4.19 for Case 4, it was shown that in POMA and CFD the airflow volume near the ceiling was very small. The main flow was located near the walls and floor.

South | North

-0.816	-0.565	-0.466	-0.413	-0.381	-0.367
-0.972	-0.716	-0.596	-0.526	-0.481	-0.447
-1.047	-0.802	-0.660	-0.581	-0.531	-0.488
-1.098	-0.854	-0.710	-0.627	-0.574	-0.524
-1.139	-0.896	-0.753	-0.669	-0.614	-0.559
-1.176	-0.932	-0.791	-0.709	-0.653	-0.594
-1.211	-0.966	-0.830	-0.749	-0.694	-0.633
-1.248	-1.011	-0.878	-0.796	-0.741	-0.676
-1.291	-1.075	-0.953	-0.871	-0.802	-0.727
-1.310	-1.152	-1.047	-0.970	-0.908	-0.804

Figure 4.20. PMV Distribution of Case 1

South | North

0.701	1.579	2.144	2.555	2.941	3
0.321	1.277	1.947	2.419	2.878	3
0.165	1.096	1.832	2.340	2.838	3
0.078	0.988	1.744	2.273	2.784	3
0.017	0.909	1.663	2.193	2.701	3
-0.030	0.847	1.579	2.091	2.584	3
-0.069	0.796	1.492	1.964	2.424	2.949
-0.100	0.745	1.373	1.806	2.207	2.731
-0.112	0.665	1.184	1.537	1.896	2.432
0.018	0.572	0.965	1.256	1.492	1.935

Figure 4.21. PMV Distribution of Case 2

South	-0.268	0.568	1.099	1.476	1.809	2.159	North
	-0.610	0.349	0.983	1.409	1.787	2.240	
	-0.731	0.199	0.907	1.363	1.772	2.230	
	-0.790	0.129	0.861	1.336	1.748	2.190	
	-0.823	0.091	0.826	1.301	1.706	2.126	
	-0.841	0.072	0.797	1.252	1.636	2.038	
	-0.850	0.067	0.762	1.187	1.534	1.920	
	-0.848	0.069	0.699	1.088	1.388	1.765	
	-0.815	0.054	0.576	0.896	1.174	1.560	
	-0.564	0.084	0.502	1.793	1.000	1.270	

Figure 4.22. PMV Distribution of Case 3

South	2.314	3	3	3	3	3	North
	0.088	1.848	2.498	2.821	3	2.987	
	-1.352	-0.072	0.856	1.303	1.414	1.341	
	-1.752	-0.656	0.232	0.677	0.877	0.933	
	-2.006	-0.973	-0.118	0.334	0.551	0.670	
	-2.196	-1.221	-0.412	0.027	0.255	0.421	
	-2.345	-1.398	-0.656	-0.256	-0.029	0.168	
	-2.467	-1.550	-0.883	-0.521	-0.322	-0.102	
	-2.563	-1.724	-1.164	-0.841	-0.638	-0.408	
	-2.519	-1.910	-1.474	-1.200	-1.045	-0.818	

Figure 4.23. PMV Distribution of Case 4

4.2.2.1.3 PMV Distribution

We applied POMA to the prediction of PMV in the four cases. Figure 4.20 shows the result of Case 1 for a standing person with $M=120W/m^2$, $W=0$, $Icl=1.01clo$ and Humidity=50%. Figure 4.21 to 4.23 present the results of the other three cases for a seated person with light activity ($M=70W/m^2$, $W=0$), with trousers and long-sleeve shirt ($Icl=0.61clo$) in an environment with 50% relative humidity.

It was shown that in Figure 4.20 for Case 1, the person would feel cool in the room. The coolest locations were near the coldest wall in the south.

In Figure 4.21 and Figure 4.22 for Case 2 and Case 3 respectively, the person would feel warmer and warmer when he moved toward the hottest wall in the north.

In Figure 4.23 for Case 4, the PMV distribution varied greatly in the room due to the fact that the temperature of the ceiling was much higher than that of the floor. We can see the temperature distribution in Figure 4.15 also varied greatly. In the locations near the ceiling, the person would feel hot and uncomfortable since the temperature is high. However, in the lower part of the room, the person would feel cool, corresponding to the low temperature distribution.

4.2.2.2 Case with Heat Source in the Room

To study the influence of heat source to the indoor climate, Case 5 in MINIBAT cell was selected. The heat source with 1159W power was located at the lower corner of the south wall. The surface temperatures of the walls except west wall were uniform and listed in Table 4-3. The surface temperature distribution of the south wall is shown in Figure 4.24.

Wall	Temperature (°C)
North	21.8
Ceiling	22.4
Floor	21.4
West	21.9
East	22.0

Table 4-3. Wall surface temperatures in Case 5

8.6	9.7	8.4
11.1	11.9	11.0
20.5	21.1	20.5
26.3	27.3	26.3

Figure 4.24. Surface Temperature (°C) of the south wall in Case 5

A 6×3×6 grid was applied in POMA to simulate the temperature distribution within the room. Figure 4.25 presents the simulation results of POMA, Inard's model, and experimental results for the mid-plane of the grid. A similar temperature distribution was detected in all of these results. POMA's results show that the temperature of the air around the heat source, especially above the heat source, is higher than that of the air away from the heat source. POMA's results agree well with the experimental results.

In conclusion, POMA gave a consistent prediction of airflow pattern and temperature distribution with CFD and measurement in the five natural convection cases of MINIBAT Cell. Compared with Inard's zonal model, POMA's prediction of airflow pattern is similar to the prediction of CFD. However, there is some difference between the prediction of Inard's zonal model and CFD model.

POMA
(6×3×6)

Experimental
Results

South

North

Inard's Model
(6×1×10)

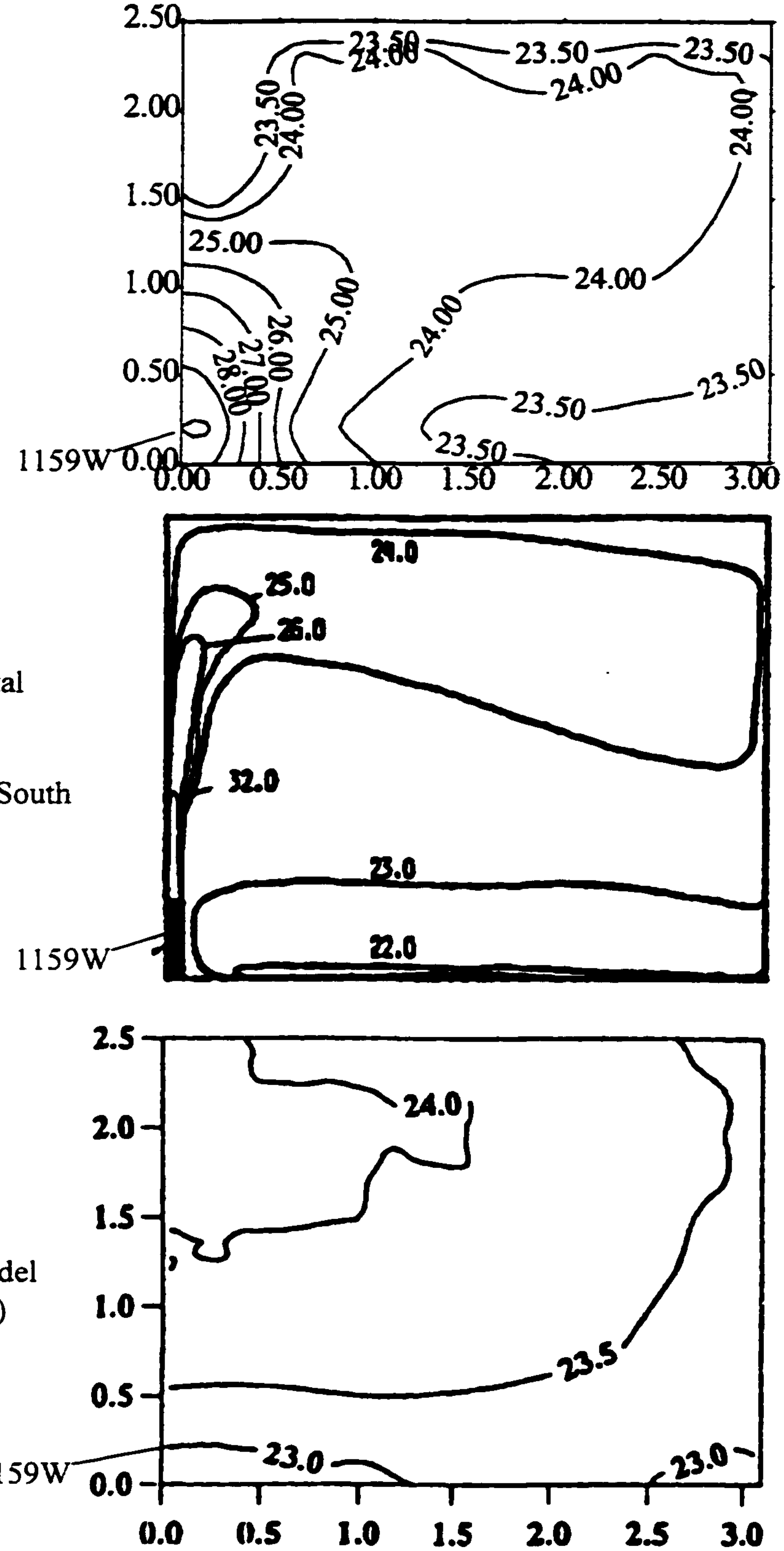

Figure 4.25. Temperature distribution in Case 5

4.3 Forced Ventilation

4.3.1 Cross Ventilation

The cross ventilation case study is a two dimensional cell with a dimension of 3×3 m^2. It was used by Rogriduez to validate his zonal models in PASCOOL (Rogriduez and Allard, 1995). There are two openings 0.5m high on opposite walls. The inlet air velocity is 0.5m/s. The room is simulated with 2D (3×5 zones) mesh. The configuration of the mesh is shown in Figure 4.26.

We simulated the room for two situations: 1). with isothermal jet; 2). with non-isothermal jet.

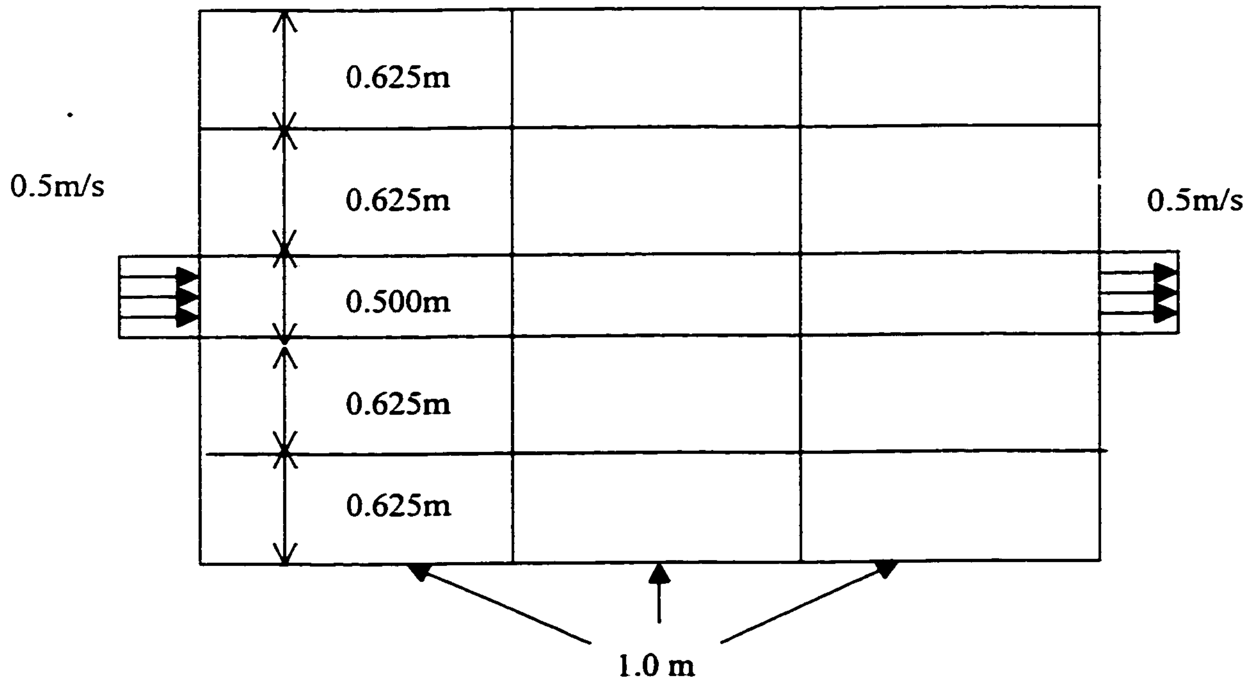

Figure 4.26 Configuration of Zones in Cross Ventilation Case

4.3.1.1 Isothermal Jet

In isothermal situation, the airflow pattern simulated by POMA is shown in Figure 4.27. Comparing CFD results, shown in Figure 4.28, with the simulation results of POMA, we can see that the flow patterns are similar. Recirculating flows near the top and bottom walls are detected and the airflow patterns are symmetrical in the two figures. Moreover, these figures also show that there is some agreement between the prediction of the flow volume in the two models.

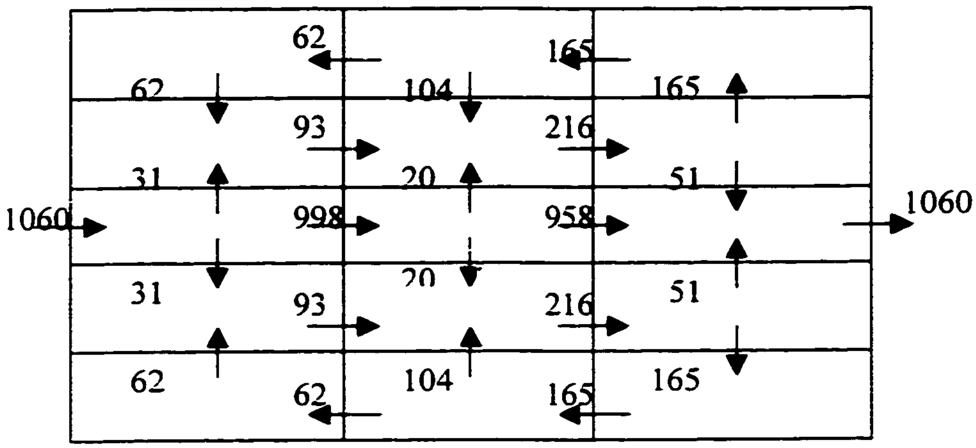

Figure 4.27 Airflow (kg/h) Pattern in Isothermal Situation Simulated by POMA

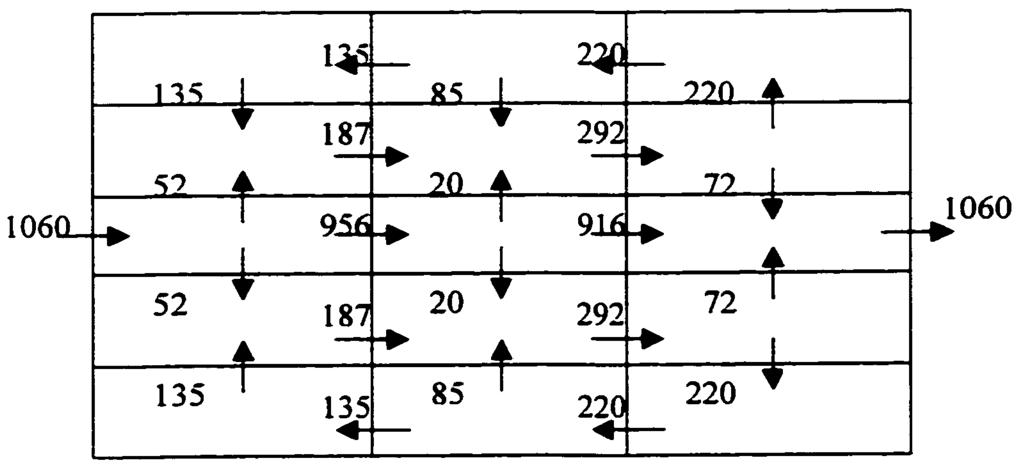

Figure 4.28 Airflow (kg/h) Pattern in Isothermal Situation Simulated by CFD

4.3.1.2 Non-isothermal Jet

In non-isothermal situation, the behavior of the diffuser air jet is affected by the thermal buoyancy due to the difference on air density. The centerline velocity of a non-isothermal jet introduced vertically and the trajectory of a non-isothermal jet introduced horizontally will be influenced by the thermal buoyancy. Since in this cross ventilation case the jet is horizontally discharged, we assume the buoyancy factor does not influence the centerline velocity. As to the drop of trajectory of the non-isothermal jet, since the length of the room (3m) is short, compared to the width of the jet (0.5m), we ignored the drop of the trajectory due to buoyancy. Thus the characteristic equations of isothermal jet can be still applicable to this situation.

In our case study, the inlet air temperature is 20°C while the wall surface temperatures are 18°C. Figures 4.29 and 4.30 show the results of airflow pattern and temperature distribution simulated by POMA. As in isothermal situation the recirculation of the flow, due to the influence of walls, is also detected along the ceiling and the floor.

In addition, the flow pattern and temperature distributions are shown to be slightly asymmetrical due to the thermal buoyancy. It demonstrates that POMA has the capability of predicting the influence of thermal buoyancy.

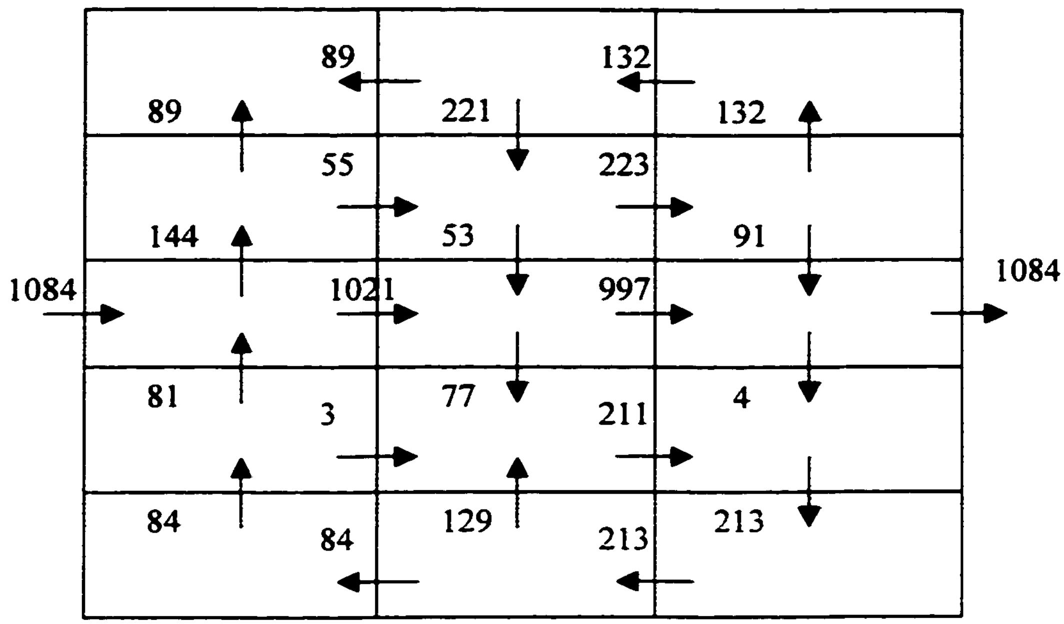

Figure 4.29 Airflow (kg/h) Pattern in Non-Isothermal Situation Simulated by POMA

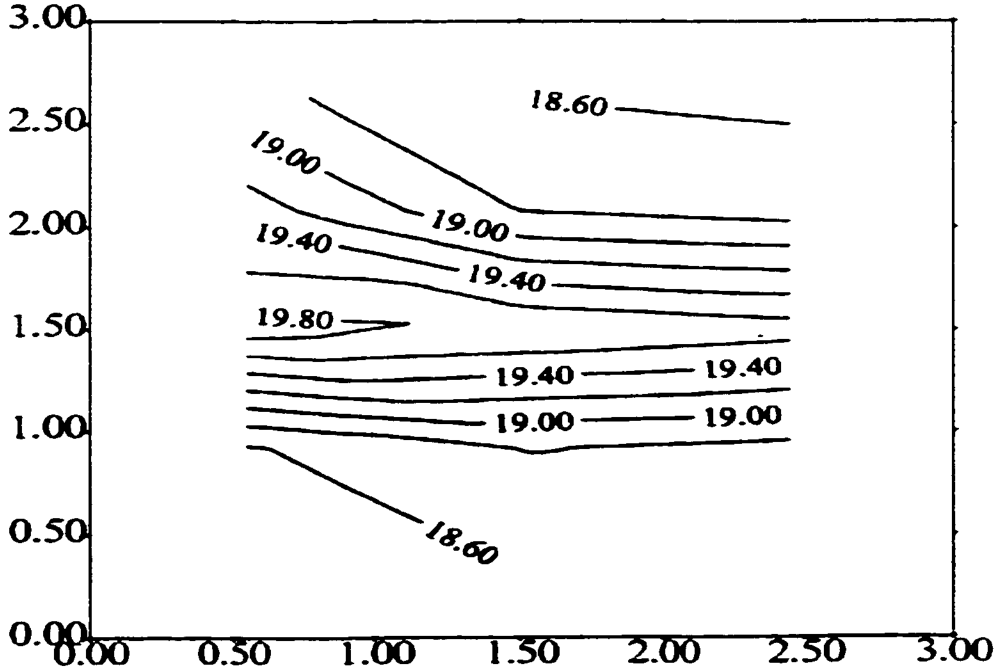

Figure 4.30 Temperature (°C) Distribution in Non-Isothermal Situation Simulated by POMA

4.3.2 Isothermal Ceiling Jet

In this case, a simple linear ceiling jet under a two dimensional isothermal condition was studied. This case is used to validate whether POMA is applicable to the room with vertically discharged jet. Huo did a thorough simulation of this case using EXACT3 (CFD) model (Huo, 1997). His results have been validated and are treated as a reference solution in this case.

In order to illustrate the influence of choice of grids in the zonal model, four kinds of grids, i.e. 10×8, 17×13, 26×13 and 37×13, were selected to simulate the pattern of the room. Figure 4.31 shows the dimension and layout of the room and linear jet.

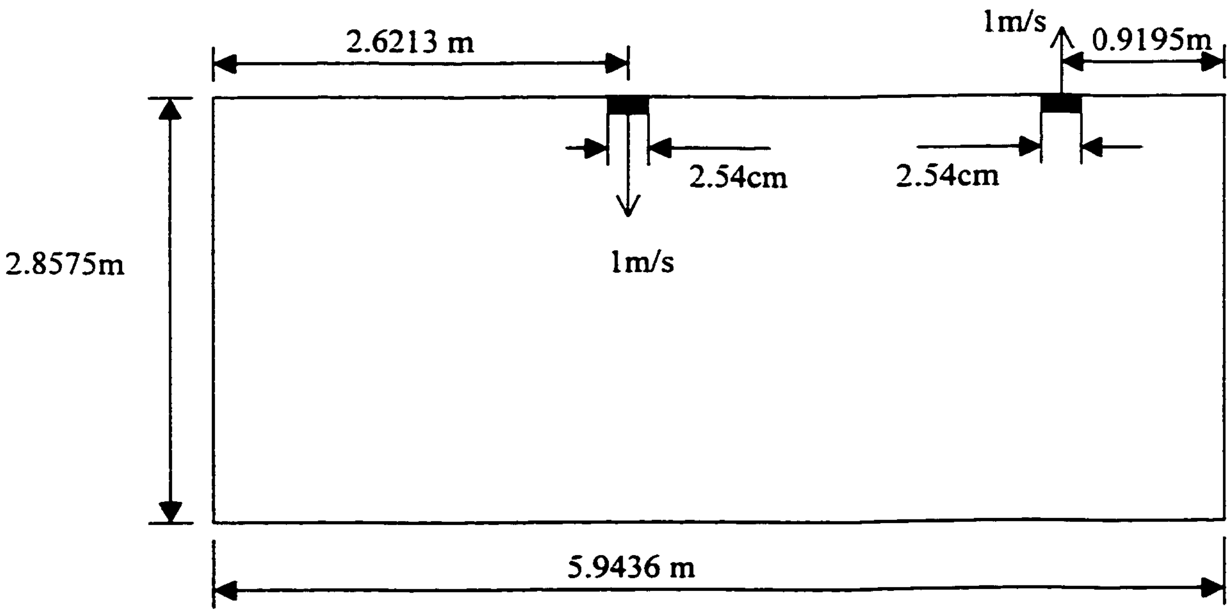

Figure 4.31 Dimension and Layout of the Room.

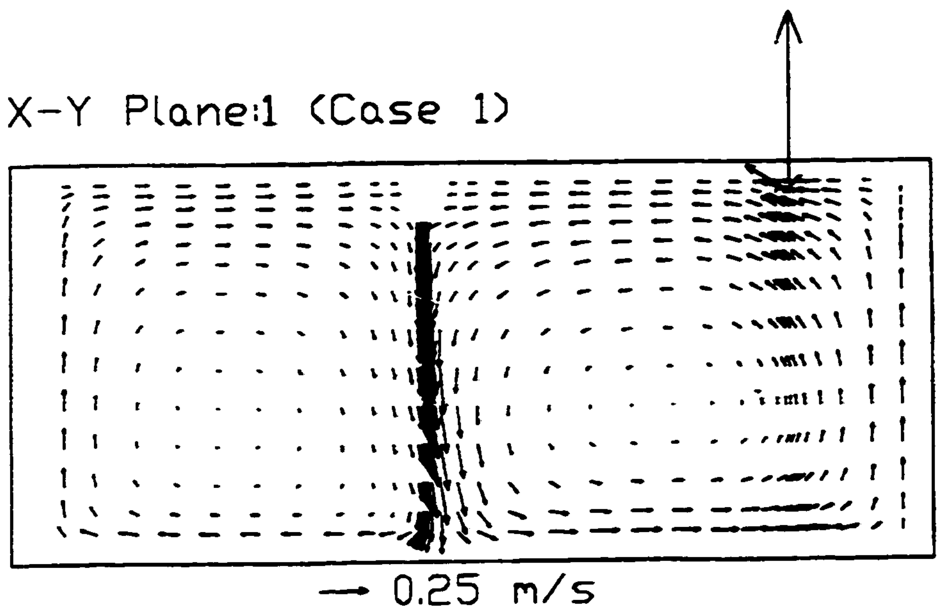

Figure 4.32 Huo's CFD Simulation of Velocity Distributions, by 38×16 Zones.

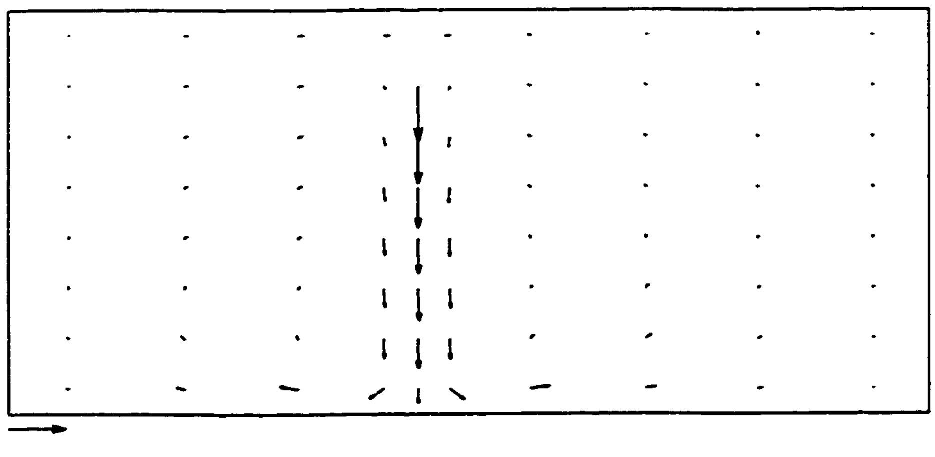

Figure 4.33 POMA Simulation of Velocity Distributions, by 10×8 Zones

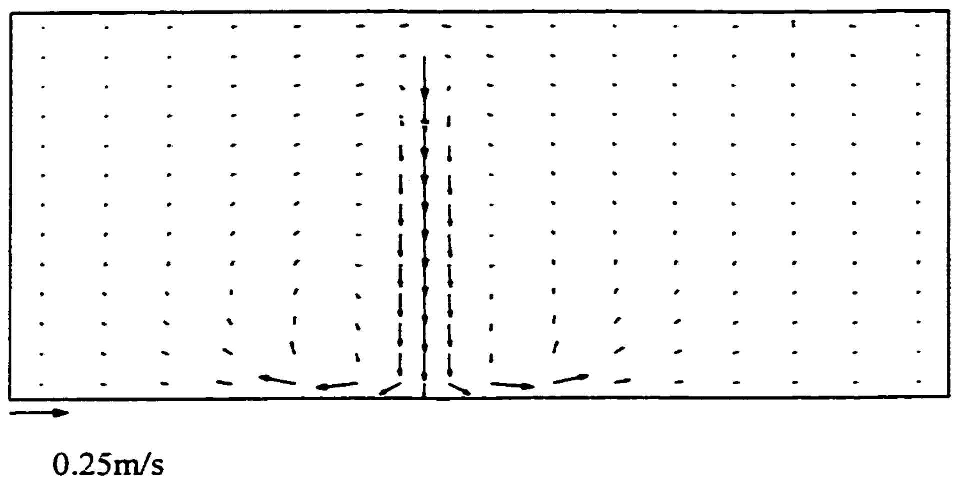

Figure 4.34 POMA Simulation of Velocity Distributions, by 17×13 Zones

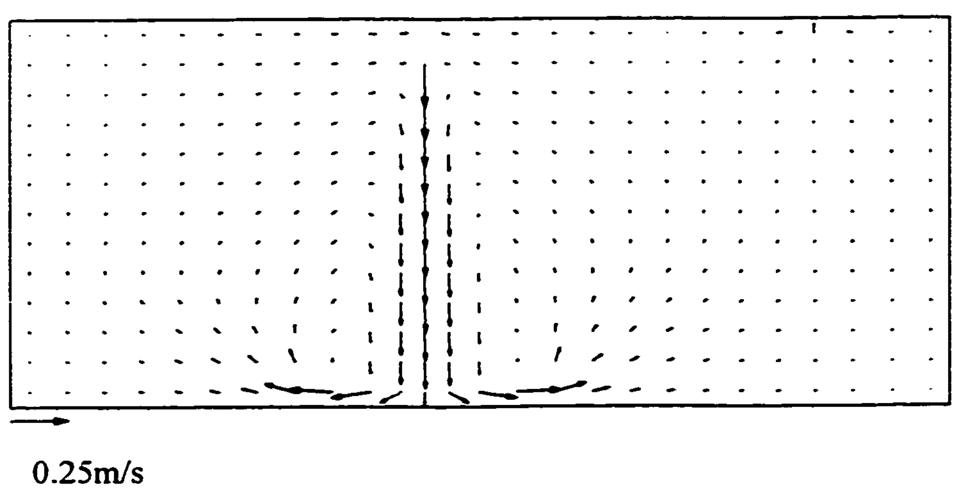

Figure 4.35 POMA Simulation of Velocity Distributions, by 26×13 Zones

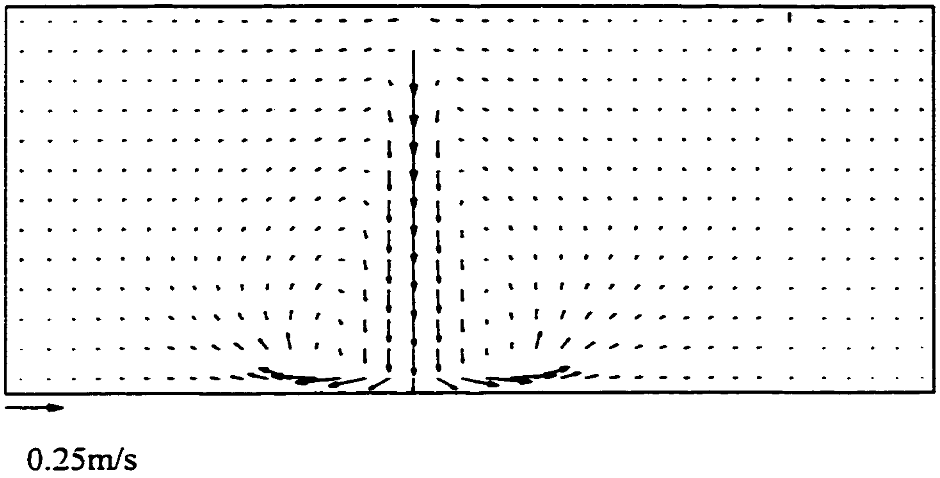

Figure 4.36 POMA Simulation of Velocity Distributions,
by 37×13 Zones

Figure 4.32 shows Huo's simulation results of velocity distribution for a 2D (16×38) mesh. It is considered to be the reference airflow pattern in the room. Figures 4.33 to 4.36 shows the results of POMA for different sizes of grids.

In Figure 4.33, with only 10×8 zones, two recirculations are shown on two sides of centerline of jet, as predicted by CFD model, though the value of velocities are not the same. It is noted that when we increase the number of zones, the airflow pattern becomes more pronounced. But it is shown that POMA does not provide the similar velocity values as expected, as shown in Figures 4.34, 4.35 and 4.36.

The largest velocities are always located in the centerline of the jet in a decay tendency in these figures. This agrees with the prediction of Huo's CFD model.

In CFD model, the main streams of the recirculations are detected to stick to the walls so that the air velocities near the walls are always larger than that far from the wall. In Figure 4.32, it is shown that when the main airflow reach the floor, it tends to turn in a right angle and flow horizontally. Nevertheless, in POMA, when the main airflow reaches the floor, it tends to flow in an upward direction, having an angle with the floor. Hence, the airflow would not remain almost the same volume in the horizontal direction but dissipate in the space. Thus in POMA's results, a perfect circulation along the wall surfaces cannot be detected as in CFD model.

This phenomenon is due to the fact that, in POMA, the momentum conservation is only implicitly taken into account in Power Law. As a consequence of that, in the zones adjacent to the floor, the velocities parallel to the floor will not necessarily remain the same in order to maintain the mass conservation. A partial velocity, which is generated by the buoyancy, vertical to the floor will compensate the mass flow volume decaying in the direction parallel to the walls. Consequently, in POMA, due to the partial velocity vertical to the wall, the main flow will move upward instead of moving in only the horizontal direction.

Suppose that we apply Bernoulli's equation,

$$\frac{P}{\rho g}+\frac{V^2}{2g}+Z=const \tag{4-5}$$

Where,

P : pressure, (Pa)

ρ : density, (kg/m^3)

g : gravitational acceleration, (m/s^2)

Z : height, (m)

V : velocity, (m/s)

In the horizontal direction along the floor, the height (z) is the same and the difference of pressure and density between two adjacent zones is small. Consequently, a consistent velocity vector can be expected along the floor.

In the zone at the corner, since the velocity on the wall should be zero. the wall boundary condition can be taken as a pressure factor.

Chapter 5

Conclusions and Future Work

5.1 POMA for Predicting Airflow Pattern and Temperature Distribution within a Room

In this thesis, a zonal model, **Pressurized zOnal Model with Air diffusers (POMA)** model, for predicting indoor airflow pattern and temperature distribution within a room was presented. The model's prediction was compared with existing information in the literature. The agreement between POMA's results and experimental and/or CFD results demonstrated that POMA is a feasible approach for the simulation of the airflow and temperature distribution in buildings.

In the case studies, it is shown that POMA has the capability to predict the indoor airflow pattern and temperature distribution within a room, which cannot be predicted by multizone models. As shown in the window problem and MINIBAT test cell, POMA can provide a good prediction of temperature stratification within a room.

In this research, simulations of POMA were executed on a Personal Computer (PC). The high capacity of computer resources, such as a workstation, required by CFD is not necessary. Large computational effort and simulation time can be saved in the zonal model with satisfying precision.

POMA has also been applied to predict the thermal comfort by means of Predicted Mean Vote (PMV). Reasonable results were acquired. It is demonstrated that POMA can be extended to some other applications, knowing two basic thermal parameters, airflow and temperature distributions.

5.2 Advantages of POMA over Other Zonal Models

In zonal models, there is a difference between the number of unknown factors and available equations. Generally there are n×(n-1) mass flow and only 2n mass and energy balance equations. Various zonal models differ from each other in the way of reducing the variables. In the development of zonal models, many zonal model developers encountered trouble in making their models general in the definition of zone geometry and in accurate description of the air diffuser, as was illustrated in the literature review.

In POMA, by representing the mass flow to reference pressure and temperature of each zone, the number of unknown factors was reduced from n×(n-1) to 2n-1, i.e. n-1 reference pressure difference and n temperature. The number of independent balance equations was proven to be only 2n-1 instead of 2n, which was taken for granted by many researchers.

The introduction of reference pressure gave POMA freedom to define the zone without prerequisite knowledge of the flow pattern. The number of zones is not longer fixed but variable in POMA. Moreover, it is noted that POMA is numerically powerful. In the case study of the Isothermal Ceiling Jet, the room can be divided into 37×13 zones. However in previous zonal models, the number of zones is limited, such as 6×1×10 in Inard's model (Inard et al, 1996) and 6×6 in Wurtz's model (Wurtz et al, 1995). This is due to the powerful Newton-Raphson Global Convergence technique used in POMA.

The air jet diffuser in POMA was described by means of characteristic equations in the ASHRAE Fundamentals. This method was proven to be applicable in the forced ventilation. In the case study of cross ventilation, it was shown that POMA could give a very good prediction of airflow pattern in the room. In the case study of isothermal ceiling jet, though the flow values are not the same as the simulation results of CFD, two large recirculations in the room can still be detected.

In other zonal models, the airflow in the jet plume was usually evaluated by empirical equations based on the experiments, such as Two-Zone Model, Analytical Model and the Five-Zone Model. The equations were only applicable to a specific jet or heat source. In POMA, the introduction of a jet description method overcomes the limitation of other zonal models in the prediction of the jet plume, since the characteristic equations in the

ASHRAE Fundamentals are applicable to all kinds of air diffusers. As to the thermal plume, POMA treats it as the normal zones so that it is not necessary to model the thermal plume specifically in POMA.

5.3 Future Work

POMA is a steady state model. Therefore, the next step of this research would be to extend its capability to the unsteady state application. This will broaden its application to naturally ventilated buildings.

The next challenging issue will also be its integration into existing building thermal analysis programs such as DOE or BLAST, and airflow models like COMIS (Feustel, 1998) or CONTAM (Walton, 1993). This would be an exciting research topic.

As explained in the section 4.3.2, in order to improve the accuracy of indoor air pattern prediction, the Bernoulli's equation is expected to integrate into POMA in the future.

Large opening models will be integrated into POMA in order to study the airflow pattern in two or more rooms connected by large openings, such as doors and windows.

REFERENCES

Abramovich, G.N. (1960) "The theory of turbulent jets." Moscow: Fizmatgiz

Allard, F., Brau, J., Inard, C., and Pallier, J.M. (1987) "Thermal experiments of full-scale dwellings cells in artificial conditions", *Energy Building,* Vol. 10, pp. 49-58

Allard, F. and Inard, C. (1992) "Natural and mixed convection in rooms: Prediction of thermal stratification and heat transfer by zonal models", *ISRACV, 1992*, pp. 335-342

ASHRAE Fundamentals 1993, Chapter 31, "Space Air Diffusion", *ASHRAE, U.S.A.*

ASHRAE Standard 55-1992 (1992) "Thermal environmental conditions for human occupancy", *ASHRAE, U.S.A.*

Byrd, R.R. (1995) "Indoor air quality frequently asked questions", *http://www.elitesoft.com/sci.hvac.*

Bouia, H. and Dalicieux, P. (1991) "Simplified modeling of air movements inside dwelling room", *Proceedings of the Building Simulation Conference,* August, 1991

Castanet, S., Bouia, H., Duta, A. and Inard, C. (1998) "Ventilation efficiency in dwelling cells: contribution to the validation of a zonal model", *ROOMVENT'98*, Vol. 3, pp.976-981

Chao, N.T., Wang,W.A. and Chiang, C.M. (1998) "A study of a control strategy utilizing outdoor air to reduce the wintertime carbon dioxide levels in a typical Taiwanese bedroom". *Energy and Buildings*, Vol. 29, 1998. pp. 93-105.

Chen, Q. and Jiang, Z. (1996) "Simulation of a complex air diffuser with CFD technique", *5th International Conference on Air Distribution in Rooms, ROOMVENT'96,* Vol. 1, pp. 227-234.

Chen, Q., Moser, A. and Huber, A. (1990) "Prediction of buoyant, turbulent flow by a low-Reynolds-number k-ε model". *ASHRAE Transactions 96*, Vol. 1.

Dalicieux, P. and Bouia, H. (1991) "Présentation d'une modélisation simplifiée desmouvements d'air à l'intérieur d'une pièce d'habitation." EDF rep. HE 12 W 3269

During, H. (1994) "Consommations energetiques et Comfort Thermique de Locaux Chauffes: approche par les Modeles Zonaux", *Ph.D. Thesis, INSA de Lyon, France*. 229 pages

Feustel, H.E. and Dieris, J. (1992) "A survey on air flow models for multizone structures", Energy and Building, Vol. 18

Feustel, H.E. and Smith, B.V. (1989) "A simplified model for predicting air glow in multizone structures", Energy and Buildings, Vol.13, No.3, Lawrence Berkeley Laboratory Report, LBL-22325

Feustel, H.E. (1996) "Annex 23—An international effort in multizone air flow modeling", *ROOMVENT'96*, Vol.2, pp.1-8

Feustel, H.E. (1998) "COMIS—An international multizone air flow and contaminant transport model", *Report from LNBL, Berkeley*, U.S.A.

Gagneau, S., Allard, F., Beghein, C. and Wurtz, E. (1998) "Construction of an automatic simulation tool based on the zonal model approach", *ROOMVENT'98*, Vol. 3, pp.39-44

Gschwind, M., Bezian, J.J., Hasebe, T., Fonzes, G., Fujita, S., Loiseau, P. and Takeda, I. (1996) "A zonal model to simulate a room heated by a gas heat pump (GHP) BTHEBES", *ROOMVENT'96*, Vol. 1, pp. 61-68

Haghighat, F., and Megri, A.C. (1996) "A comprehensive validation of two airflow models—COMIS and CONTAM", *Indoor Air, March 1996*, pp. 278-288

Haghighat, F. (1989) "Air infiltration and indoor air quality models—a review", *International Journal of Ambient Energy*, Vol.10, pp. 115-122.

Hager, W.W. (1988) "Applied numerical linear algebra", *Prentice Hall, ISBN 0-13-041294-5*

Heiselberg, P. (1997) "Simplified method for room air distribution design", *ASHRAE seminar on simplified models for room air and air contaminat distribution*, Boston, June 1997. ISSN 1395-7953-R9747

Heiselberg, P. (1994) "Interaction between flow elements in large enclosures", *ROOMVENT'94*. ISSN 0902-7513 R9427

Herrlin, M. (1987) "Luftstromning I byggnader - en berakningsmodell", *Division of Building Services Engineering, Royal Institute of Technology, Stockholm, Sweden*

Howarth, A.T. (1980) "Temperature distributions and air movements in rooms with a convective heat source", *Ph.D. Thesis, University of Manchester*.

Howarth, A.T. (1985) "The prediction of air temperature variations in naturally ventilated rooms with a convective heating", *Build. Serv. Eng. Res. Technol.*, 6 (1985) pp. 169-175

Huo, Y. (1997) "Ventilation impact on indoor air quality problems in partitioned offices", *Ph.D. thesis, Concordia University, Montreal, Canada.*

Huthcheon, N.B. and Handegord, G.O.P. (1989) "Building science for a cold climate", second edition, *NRCC, ISBN-09694366-0-2*

International Energy Agency, IEA, (1989) "Air flow pattern within buildings, -- Annex XX of the IEA implementing agreement on energy conservation in buildings and community systems", Legal text with description of project objectives, means, and responsibilities, etc., drafted by the IEA R&D staff, reviewed by the IEA office of the legal counsel, and adopted by the executive committee. No. 0633R/13.6.89.

Inard, C. (1988) "Contribution à l'étude du couplage thermique entre une source de chaleur et un local". *Ph.D. thesis, INSA de Lyon, France*

Inard, C. (1996) "Les Modèles Zonaux en Thermique du Batiment", *Habilitation à Diriger Les Recherches en Sciences, INSA de Lyon, France*

Inard, C. and Buty, D. (1991) "Simulation of thermal coupling between a radiator and a room with zonal models", *Proceeding of 12th AIVC Conference*, Ottawa, Canada, 1991, Vol. 2, pp. 125-131.

Inard, C., Bousia, H. and Dalicieux, P. (1996) "Prediction of air temperature distribution in buildings with a zonal model", *Energy and Buildings*, Vol. 24, pp. 125-132

Inard, C. and During, H. (1994) "Energy consumption and thermal comfort in buildings: an approach with zonal models", *ROOMVENT'94*, Vol. 2, pp. 131-146

Inard, C., Meslem, A. and Depecker, P. (1994) "Energy Consumption and Thermal Comfort in Dwelling-cells: A Zonal-model Approach", *Centre Thermique de Lyon*, INSA, France.

Inard, C., Meslem, A. and Depecker, P. (1996) "Use of a zonal model for the prediction of air temperature distributing in large enclosures", *ROOMVENT'96*, Vol.2, pp.177-184

Jackman, P.J. (1970) "A study of natural ventilation of tall office buildings", *Inst. Heat Vent. Eng., Vol.38*

Jiang, Z. (1998) Private Communication.

Kimura, K. (1995) " Acceptable Indoor Air Quality and Energy Consumption", Proceedings of Indoor Air Quality, Ventilation and Energy Conservation in Buildings, 2nd International Conference, Montreal, Canada, pp. 819-828

Kreith, F. and Bohn, M.S. (1986) "Principles of heat transfer, Fourth edition", *Haper & Row Publisher Inc.* 1986

Kronvall, J. (1991) "Buildings, Health and Energy", *Proceedings of 12th AIVC conference*, Vol. 1, pp. 221-239

Laret, L. (1980) "Contribution au développement de modèles mathématiques du comportement thermique transitoire de structures d'habitation", *Ph.D. Thesis, University of Liège.*

Lebrun, J. and Ngendakumana, J. (1987) "Air circulation induced by heating emitters and corresponding heat exchanges along the wall: test room results and modeling", *Proceeding of ROOMVENT'87*, Stockholm, Sweden, Session 2a, Paper 6

Lebrun, J. (1970) "Exigences physiologiques et modalités physiques de la climatisation par source statique concentrée". *Ph.D. thesis, University of Liège*,

Li, Y. and Holmberg, S. (1994) "General flow and thermal condition in indoor airflow simulation", *Building Environment*, Vol. 29, pp. 275-281

Manzoni, D. and Rongere, F.X. (1996) "Simplified models of displacement ventilation systems", *ROOMVENT'96*, Vol.2, pp.443-448

Megri, A.C. (1993) "Air flow modeling in multizone buildings equipped with a ventilation system: Prediction of pollutant transport", published in French, *Ph.D. thesis, 303 pages, INSA of Lyon, France*

Megri, A.C., Krauss, G. and ACHARD, G. (1994) "Airflow modeling of ventilation systems and their interface with the building envelope", published in French, *Revue Générale de Thermique*, N°396, December 1994, pp701-716

Megri, A.C. (1995) "Prediction and evaluation of indoor air quality in Multi-zone buildings equipped with a ventilation system", published in French, *Anales de l'ITBTP September 1995, N°536, Série Equipement technique 119*, pp.114-131

Moser, A., et al (1992) "A new method for linking results of detail air flow pattern calculation with multizone models", *13th AIVC conference*, Nice, France pp. 63-77

Moser, A. (1991) "The message of Annex 20: Air flow pattern within buildings", *Proceedings of 12th AIVC conference*, Vol. 1, pp. 1-26

Murakami S., Kato, S., Akabayashi, S., Mizutami, M. and Kim, Y.D. (1991) "Wind tunnel test on velocity pressure field of cross ventilation with open windows", *ASHRAE Transaction*, 1991, pp. 525-538

Nielsen, P.V. (1989) "Airflow simulation techniques – progress and trends", *Proceeding of 10th AIVC conference*, Dipoli, Finland, Paper 10, pp. 203-223

Press, W.H., Teukolsky, S.A., Vetterling, W.T. and Flannery, B.P. (1992) "Numerical recipes in C: the art of scientific computating", *Cambridge University Press*, *ISBN 0-521-43108-5*

Rodriguez, E. and Allard, F. (1995) "Zonal modeling for natural ventilation", *Final report of ventilation thermal mass subtask in PASCOOL, chapter 7*

Schalin, A., Dorer, A., Van der Mass, J. and Moser, A. (1992) "A new method for linking results of detailed airflow pattern calculation with multizone models", 13th AIVC Conference, Nice, France, 15-18 Sep. 1992.

Shikrot, E.O. and Zhivov, A.M. (1996) "Zonal model for displacement ventilation design", *ROOMVENT'96*, Vol.2, pp.449-458

Shepelev, I. (1961) "Air supply ventilation jets and air fountains", *Proceedings of the academy of construction and architecture of the USSR 4.*

Stroustrup, B. (1998) "The C++ programming language 3rd edition", *Addison-Wesley, ISBN 0201539926.*

Valbjorn O. et al (1990) " Indoor climate and air quality problems – investigation and remedy", SBI Report 212, Danish Building Research Institute

Togari, S., Arai, Y. and Miura, K. (1993) "A simplified model for predicting vertical temperature distribution in a large space", *ASHRAE Transactions 99(1),* pp. 88-99

Walton, G.N. (1989) "AIRNET – A computer program for building airflow network modeling", *United States Department of Commerce, National Institute of Standards and Technology*

Walton, G.N. (1993) "CONTAM93 – Users Manual", *United States Department of Commerce, National Institute of Standards and Technology*

Wurtz, E., Nataf, J. and Winkelmann, F.C. (1996) "Two and three – Dimensional natural and mixed convection simulation using modular zonal model". *LBNL report, 1996.7.*

Wurtz, E. (1995) "Modélisation tridimensionnelle des transferts thermiques of aéraauliques dans le bâtiment en environnement orienté object", Ph.D. thesis, *Ecole Nationale des Ponts et Chausseés,* 1995